WHITE PAPER ON FORWARD PHYSICS, BFKL, SATURATION PHYSICS AND DIFFRACTION*

Martin Hentschinski[a,†], Christophe Royon[b,†]
Marco Alcazar Peredo[a], Cristian Baldenegro[c]
Andrea Bellora[d], Renaud Boussarie[e]
Francesco Giovanni Celiberto[f,g,h], Salim Cerci[i]
Grigorios Chachamis[j], J.G. Contreras[k], Sylvain Fichet[l]
Michael Fucilla[m,n,o], Gero von Gersdorff[p], Pablo González[q]
Andreas van Hameren[r], Jamal Jalilian-Marian[s,t]
Mats Kampshoff[q], Valery Khoze[u], Michael Klasen[q]
Spencer Robert Klein[v], Georgios Krintiras[b], Piotr Kotko[w]
Krzysztof Kutak[r], Jean-Philippe Lansberg[o], Emilie Li[o]
Constanin Loizides[x], Mohammed M.A. Mohammed[m,n]
Maxim Nefedov[y], Melih A. Ozcelik[z], Alessandro Papa[m,n]
Michael Pitt[α], Agustin Sabio Vera[β,γ], Jens Salomon[β]
Sebastian Sapeta[r], Gustavo Gil da Silveira[δ]
Victor Paulo Gonçalves[ϵ], Mark Strikman[ζ], Deniz Sunar Cerci[i]
Lech Szymanowski[y], Daniel Tapia Takaki[b], Marek Taševský[η]
Samuel Wallon[o]

[a]Departamento de Actuaria, Física y Matemáticas, Universidad de las Américas Puebla
Ex-Hacienda Santa Catarina Martir S/N, San Andrés Cholula 72820 Puebla, Mexico
[b]The University of Kansas, Department of Physics and Astronomy
1251 Wescoe Hall Dr. Lawrence, KS 66045, USA
[c]LLR, CNRS, Ecole Polytechnique, Institut Polytechnique de Paris
91128 Palaiseau, France
[d]INFN Sezione di Torino, 10125 Torino, Italy
[e]CPHT, CNRS, Ecole Polytechnique, Institut Polytechnique de Paris
91128 Palaiseau, France
[f]European Centre for Theoretical Studies in Nuclear Physics and Related Areas (ECT*)
38123 Villazzano, Trento, Italy
[g]Fondazione Bruno Kessler (FBK), 38123 Povo, Trento, Italy
[h]INFN-TIFPA Trento Institute of Fundamental Physics and Applications
38123 Povo, Trento, Italy
[i]Adiyaman University, Faculty of Arts and Sciences, Department of Physics
02040-Adiyaman, Turkey
[j]Laboratório de Instrumentação e Física Experimental de Partículas (LIP)
Av. Prof. Gama Pinto, 2, 1649-003 Lisboa, Portugal
[k]Faculty of Nuclear Sciences and Physical Engineering
Czech Technical University in Prague, Prague, Czech Republic
[l]CTP South American Institute for Fundamental Research & IFT-UNESP
R. Dr. Bento Teobaldo Ferraz 271, São Paulo, Brazil
[m]Dipartimento di Fisica, Università della Calabria
87036 Arcavacata di Rende, Cosenza, Italy

[n]Istituto Nazionale di Fisica Nucleare, Gruppo collegato di Cosenza
87036 Arcavacata di Rende, Cosenza, Italy
[o]Université Paris-Saclay, CNRS, IJCLab, 91405 Orsay, France
[p]Department of Physics, PUC-Rio, 22451-900 Rio de Janeiro, Brazil
[q]University of Münster, Institute for Theoretical Physics
Wilhelm-Klemm-Str. 9, 48149 Münster, Germany
[r]Institute of Nuclear Physics Polish Academy of Sciences
Radzikowskiego 152, 31-342 Kraków, Poland
[s]Department of Natural Sciences, Baruch College
17 Lexington Ave, New York, NY 10010, USA
[t]City University of New York Graduate Center
365 Fifth Ave, New York, NY 10016, USA
[u]IPPP, Durham University, Durham DH1 3LF, UK
[v]Lawrence Berkeley National Laboratory, Berkeley CA 94720, USA
[w]AGH University of Science and Technology
Faculty of Physics and Applied Computer Science
Mickiewicza 30, 30-059 Kraków, Poland
[x]ORNL, Physics Division, Oak Ridge, TN, USA
[y]National Centre for Nuclear Research (NCBJ), Pasteura 7, 02-093 Warsaw, Poland
[z]Institute for Theoretical Particle Physics, KIT, 76128 Karlsruhe, Germany
[α]CERN, CH-1211, Geneva 23, Switzerland
[β]Instituto de Física Teórica UAM/CSIC, Nicolás Cabrera 15, 28049 Madrid, Spain
[γ]Theoretical Physics Department, Universidad Autónoma de Madrid
28049 Madrid, Spain
[δ]Universidade Federal do Rio Grande do Sul, Porto Alegre-RS, 91501-970, Brazil
[ϵ]Universidade Federal de Pelotas, Pelotas-RS, 96010-610, Brazil
[ζ]Pennsylvania State University, University Park, PA, 16802, USA
[η]Institute of Physics of the Czech Academy of Sciences
Na Slovance 2, 18221 Prague, Czech Republic

Received 30 March 2023, accepted 3 April 2023,
published online 27 April 2023

The goal of this white paper is to give a comprehensive overview of the rich field of forward physics. We discuss the occurrences of BFKL re-summation effects in special final states, such as Mueller–Navelet jets, jet–gap–jets, and heavy quarkonium production. It further addresses TMD factorization at low x and the manifestation of a semi-hard saturation scale in (generalized) TMD PDFs. More theoretical aspects of low-x physics, probes of the quark–gluon plasma, as well as the possibility to use photon–hadron collisions at the LHC to constrain hadronic structure at low x, and the resulting complementarity between LHC and the EIC are also presented. We also briefly discuss diffraction at colliders as well as the possibility to explore further the electroweak theory in central exclusive events using the LHC as a photon–photon collider.

DOI:10.5506/APhysPolB.54.3-A2

† Editor

1. Introduction

For successful runs at any colliders, such as the LHC at CERN or the incoming EIC at BNL, and future projects such as FCC at CERN, it is fundamental to fully understand the complete final states. This obviously includes the central part of the detector that is used in searches for Beyond the Standard Model (BSM) physics but also the forward part of the detector, the kinematic region close to the outgoing particles after collision. The detailed understanding of final states with high forward multiplicities, as well as those with the absence of energy in the forward region (the so-called rapidity gap), in elastic, diffractive, and central exclusive processes is of greatest importance. Some of these configurations originate from purely non-perturbative reactions, while others can be explained in terms of multi-parton chains or other extensions of the perturbative QCD parton picture such as the Balitsky–Fadin–Kuraev–Lipatov (BFKL) formalism. Future progress in this fundamental area in high-energy physics requires the combination of experimental measurements and theoretical work.

Forward Physics addresses physics that takes place in the forward region of detectors, which at first is defined as the region complementary to the central region. The latter is the region dominantly employed in the search for new physics at *e.g.* the Large Hadron Collider. It is then also the central region where colinear factorization of hard processes in terms of a partonic cross section, convoluted with corresponding colinear parton distribution functions, is well defined. 'Hard process' refers here to a certain reaction subject to strong interactions, which is characterized by the presence of a hard scale M with $M \gg \Lambda_{\rm QCD}$ with $\Lambda_{\rm QCD}$ the characteristic scale of Quantum Chromodynamics (QCD) of the order of a few hundred MeV. Physics in the forward region is, on the other hand, at first characterized by production at large values of rapidity with respect to the central region. For hard reactions, where the underlying partonic sub-process is resolved, one, therefore, deals with the interplay of partons with a relative large proton momentum fraction x_1, with $x_1 \sim 0.1 \ldots 1$, and partons with very small proton momentum fractions x_2 down to 10^{-6} in the most extreme scenario. Such small momentum fractions lead generally to a breakdown of the convergence of the perturbative expansion and require re-summation, which is achieved by the Balitsky–Kuraev–Fadin–Lipatov (BFKL) evolution. The latter gives rise to the so-called hard or BFKL Pomeron, which predicts a strong and power-like rise of the gluon distribution in the proton in the region where $x_2 \to 0$. While such a rise is clearly seen in data, unitarity bounds prohibit such a rise to continue forever: at a certain value of x_2, this rise must slow down and eventually come to hold. The latter is strongly related with the formation of an over-occupied system of gluons, known as the Color Glass Condensate, whose exploration is one of the physics central goals of a fu-

ture Electron Ion Collider (EIC). While at an EIC a dense QCD state will be achieved through scattering of electrons on heavy ions, forward physics at the LHC allows here for a complementary exploration, since high gluon densities are here at first produced through the low-x evolution of the gluon distribution in the proton. Forward physics allows, therefore, for the exploration of both the BFKL evolution (perturbative evolution toward the low-x region) as well as to search and investigate effects related to the on-set of gluon saturation.

Besides the direct interaction of partons at very low proton momentum fraction, forward physics also allows for the observation of a different class of events, so-called diffractive events. The latter are characterized through the presence of large rapidity gaps and, therefore, probe physics beyond conventional colinear factorization. In the case of hard events, they give access to complementary information on the physics of high gluon densities as well as corrections due to soft re-scattering. At the same time, such processes are themselves of direct interest for the exploration of electroweak physics and BSM physics: due to the presence of rapidity gaps, such events are characterized through a very few numbers of particles in the final state and allow therefore for very clean measurements with a strongly reduced background, in comparison to conventional LHC measurements. Closely related to such diffractive events are photon-induced reactions which can be observed at the LHC. While such reactions can produce final states both in the central and forward region, control of the forward region is of particular importance for those reactions, since it allows us to control whether in a certain event the scattering proton stayed indeed intact and acts in this way as the photon source. In such events, either one or both of the two scattering protons or ions at the LHC act as a photon source. The former allows for the study of exclusive photon–hadron interaction at the highest center-of-mass energies and yields, therefore, another tool for the study of highest gluon densities, with high precision; as for inclusive reactions, such exclusive reactions are complementary to measurements at the future Electron Ion Collider, since at the LHC high parton densities are predominately generated due to high-energy evolution, while an EIC relies due to its lower center-of-mass energy on the nuclear enhancement. Photon–photon interactions are on the other hand of high interest since they provide very clear probes of electroweak and BSM physics. With both scattering hadrons intact after the interaction, the QCD background is suppressed to a minimum in such a reaction and complements in this way the LHC searches for new physics based on inclusive events in the central region.

The outline of this white paper is as follows: Section 2 is dedicated to attempts to pin down the BFKL evolution at the LHC as well as its actual use for phenomenology. Section 3 deals with high gluon densities, saturation as well as their relation to TMD PDFs. Section 4 deals with the investigation of high gluon densities at the LHC and their phenomenological consequences. Section 5 is dedicated to ultra-peripheral collisions and Section 6 to the recent Odderon discovery as well as diffractive jets. Section 7 deals with electroweak physics. In Section 8, we draw our conclusions.

2. Manifestations of BFKL evolution

Main Contributors: C. Baldenegro, F.G. Celiberto, S. Cerci, G. Chachamis, M. Fucilla, P. González, M. Kampshoff, M. Klasen, J.-P. Lansberg, M.M.A. Mohammed, M. Nefedov, M.A. Ozcelik, A. Papa, Ch. Royon, D. Sunar Cerci, A. Sabio Vera, J. Salomon

In the following section, we describe both attempts to pin down the BFKL evolution and the underlying multi-Regge kinematics in multi-jet events, Section 2.1, as well as reactions characterized by two events widely separated in rapidity, Section 2.2. While in those cases the BFKL evolution takes place within a hard event which extends over several units of rapidity, Section 2.3 addresses the case where the BFKL evolution is absorbed into the gluon distribution, resulting in an unintegrated gluon distribution. Section 2.4 addresses, finally, the case where BFKL evolution is matched with colinear factorization and used to re-sum large logarithms curing an instability of the latter in the limit of large partonic center-of-mass energies.

2.1. Mueller–Navelet jets

An active area of research in QCD phenomenology at high energies is to pin down novel observables where the dominant contributions stem from the Balitsky–Fadin–Kuraev–Lipatov (BFKL) domain [1–8]. This is a challenging task, since for typical observables, calculations based on matrix elements computed at fixed order (together with the Dokshitzer–Gribov–Lipatov–Altarelli–Parisi (DGLAP) evolution [9–13] to account for the scale dependence of PDFs) tend to describe the bulk of the data adequately. It is then needed to move toward corners of the phase space to isolate the BFKL effects. This can be done by studying the structure of final states in the Mueller–Navelet (MN) jets events [14], namely events that have two jets with similar and large enough transverse momentum $p_\perp$ that can serve as a hard scale, $\Lambda^2_{\rm QCD} \ll p_\perp^2 \ll s$, where s is the c.o.m. energy squared. The two tagged jets should also be separated by a large rapidity interval Y while there is a rich mini-jet activity in between. Numerous studies took place on the

MN jets both at leading-order (LO) BFKL as well as at next-to-leading order (NLO). The main quantity of interest in most studies was the azimuthal decorrelation between the two outermost jets, for a non-exhaustive list of theoretical works see Refs. [15–34] while relevant experimental analyses by ATLAS and CMS can be found in Refs. [35–38].

The CMS Collaboration reported a measurement of azimuthal angle decorrelation between the most forward and the most backward jets (so-called Mueller–Navelet jets) in proton–proton collisions at $\sqrt{s} = 7$ TeV [38]. In the analysis, jets with transverse momentum, $p_\perp > 35$ GeV and absolute rapidity, $|y| < 4.7$ are considered. The normalized cross sections are compared with various Monte Carlo generators and analytical predictions based on the DGLAP and BFKL parton evolution equations. In Fig. 1, the azimuthal angle decorrelation of dijets and the ratio of its average cosines ($C_n = \langle \cos(n(\pi - \phi_{\text{dijet}})) \rangle$) are shown as a function of rapidity separation between the jets, Δy, reaching up to $\Delta y = 9.4$ for the first time. At higher centre-of-mass energies, new measurements of azimuthal angular decorrelations in the MN jet events need to be defined and performed. It will be fundamental to test the dependence of the $\Delta\phi$ correlations as a function of the outermost jets $p_\perp$, in addition to the Δy scan. The region of applicability of the BFKL formalism is expected to occur in cases where the outermost jets have similar $p_\perp$. At the same time, we are interested in studying the radiation pattern between the jets presented in the form of "mini-jets" between the outermost jets. Indeed, as the rapidity interval increases, there is more phase space available for extra radiation to be emitted, so it is natural for the average jet multiplicity to increase. The number of mini-jets as well

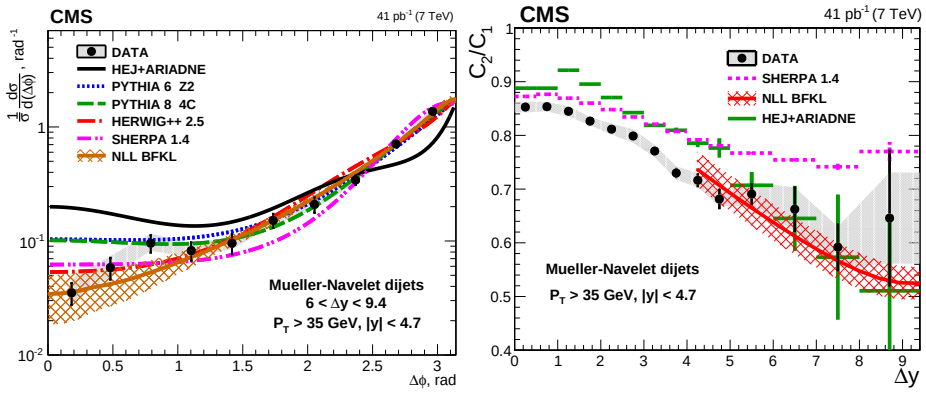

Fig. 1. Left: The azimuthal-angle difference distribution measured for Mueller–Navelet jets in the rapidity interval $6.0 < \Delta y < 9.4$. Right: Comparison of the measured ratio C_2/C_1 as a function of rapidity difference Δy to SHERPA, HEJ+ARIADNE, and analytical NLL BFKL calculations at the parton level [38].

as the emission pattern in y–ϕ space could potentially be used in addition to the azimuthal angular decorrelation to further characterize MN dijet events. The main focus will be given on the definition of more "exclusive" observables that exploit the two-jet angular correlations between the mini-jets and the outermost jets in y–ϕ space, together with a measurement of $\langle\cos(\Delta\phi)\rangle$ between the outermost jets.

From the phenomenological studies so far, it became apparent that more precise theoretical work is needed (*e.g.* see [38]). In Refs. [39, 40], new observables were proposed aiming at probing novel multi-Regge kinematics signatures.

In order to define properly the proposed observables, we assume that a MN event is characterized by:

$$\begin{aligned} & k_a\,, \quad k_b && : \text{ transverse momenta of the MN jets}\,, \\ y_0 = y_a = Y\,, \quad & y_{N+1} = y_b = 0 && : \text{ rapidities of the MN jets}\,, \\ & k_1, k_2, \ldots, k_N && : \text{ transverse momenta of the mini-jets}\,, \\ & y_1, y_2, \ldots, y_N && : \text{ rapidities of the mini-jets with } y_{i-1} > y_i\,. \end{aligned} \tag{1}$$

Then the observables are

$$\langle p_\perp \rangle \;=\; \frac{1}{N}\sum_{i=1}^{N} p_{\perp,i}\,, \tag{2}$$

$$\langle \mathcal{R}_y \rangle \;=\; \frac{1}{N-1}\sum_{i=1}^{N-1} \frac{y_i}{y_{i-1}}\,, \tag{3}$$

and

$$\langle \mathcal{R}_{ky} \rangle = \frac{1}{N-1}\sum_{i=1}^{N-1} \frac{k_i \mathrm{e}^{y_i}}{k_{i-1}\mathrm{e}^{y_{i-1}}}\,. \tag{4}$$

Equation (3) differs from the original definition in [39] since now i runs over the mini-jets and excludes the leading MN jets. $\langle \mathcal{R}_{ky} \rangle$ incorporates a $p_\perp$ dependence which carries information related to the decoupling between transverse and longitudinal components of the emitted gluons. For the proposed observables, one can see that events where the mini-jets have relatively low $p_\perp$, contrary to what one would naively expect, give a very significant contribution to the gluon Green's function (Fig. 1 in [39]) and, consequently, to the cross section. The experimental analyses however (mainly to deal with jet energy reconstruction uncertainties) impose a veto on the $p_\perp$ of any resolved mini-jet. Usually, the $p_\perp$ veto value for ATLAS and CMS is $Q_0 = 20$ GeV which is rather large if we compare it to the $Q_0 = 1$ GeV value which was the jet $p_\perp$ infrared cutoff for the plots in [39].

Here, we are performing a first comparison between the predictions from a fixed order calculation and a BFKL-based computation for the observables described in Eqs. (2), (3), and (4). We focus on events where two jets with rapidities y_a in the forward direction and y_b in the backward direction can be clearly identified. In order for the BFKL dynamics to be relevant, the difference $Y = y_a - y_b$ needs to be large enough so that terms of the form of $\alpha_{\mathrm{s}}^n Y^n$ be important order-by-order to get a good description of the partonic cross section which can be written in the factorized form

$$\hat{\sigma}\left(Q_1, Q_2, Y\right) = \int \mathrm{d}^2 k_{\perp A}\, \mathrm{d}^2 k_{\perp B}\, \phi_A\left(Q_1, k_{\perp a}\right)\, \phi_B\left(Q_2, k_{\perp b}\right) f\left(k_{\perp a}, k_{\perp b}, Y\right). \tag{5}$$

In this expression, $\phi_{A,B}$ are impact factors depending on the external scales, $Q_{1,2}$, and the off-shell reggeized gluon momenta, $k_{\perp a,b}$. The gluon Green function f depends on $k_{\perp a,b}$ and the center-of-mass energy in the scattering $\sim \mathrm{e}^{Y/2}$.

Here, we will work at leading order (LO) with respect to an expansion in the strong coupling constant α_{s}, however, for the BFKL phenomenology at the LHC, it is mandatory to work within the next-to-leading order (NLO) approximation for both the impact factors and the gluon Green's function which introduces the dependence on physical scales such as the one associated to the running of the coupling and the one related to the choice of energy scale in the re-summed logarithms [41–44]. It is possible to write the gluon Green function in an iterative way in transverse momentum and rapidity space at LO [45] and NLO [46, 47]. The iterative solution at LO has the form of (for the NLO expressions see Refs. [46, 47])

$$f = \mathrm{e}^{\omega(k_{\perp A})Y}\left\{\delta^{(2)}\left(k_{\perp A} - k_{\perp B}\right) + \sum_{N=1}^{\infty}\prod_{i=1}^{N}\frac{\alpha_{\mathrm{s}} N_{\mathrm{c}}}{\pi}\int \mathrm{d}^2 k_{\perp i}\,\frac{\theta\left(k_i^2 - \lambda^2\right)}{\pi k_i^2}\right.$$
$$\left.\times \int_0^{y_{i-1}} \mathrm{d}y_i \mathrm{e}^{\left(\omega\left(k_{\perp A}+\sum_{l=1}^{i} k_{\perp l}\right)-\omega\left(k_{\perp A}+\sum_{l=1}^{i-1} k_{\perp l}\right)\right)y_i}\delta^{(2)}\left(k_{\perp A}+\sum_{l=1}^{n} k_{\perp l}-k_{\perp B}\right)\right\}, \tag{6}$$

where

$$\omega\left(q_\perp\right) = -\frac{\alpha_{\mathrm{s}} N_{\mathrm{c}}}{\pi}\ln\frac{q^2}{\lambda^2} \tag{7}$$

corresponds to the gluon Regge trajectory which carries a regulator, λ, of infrared divergences. All these expressions have been implemented in the Monte Carlo code BFKLex which has already been used for different applications ranging from collider phenomenology to more formal studies in the calculation of scattering amplitudes in supersymmetric theories [48–53].

For the fixed order QCD computation of the observables in Eqs. (2), (3), and (4), we use POWHEG [54–56] and PYTHIA 8 [57]. In both the BFKL-based computation and the fixed order one, the anti-$k_\perp$ jet clustering algorithm has been used as implemented in FastJet [58, 59]. We use the following kinematic cuts:

$$\begin{aligned} p_{\perp 0} &\in [30; 40]\,\text{GeV}\,, \\ p_{\perp n-1} &\in [20; 30]\,\text{GeV}\,, \\ p_{\perp \text{min}} &\geq 20\,\text{GeV}\,, \\ Y &\in [-4.7; 4.7]\,, \end{aligned} \tag{8}$$

whereas the jet radius was taken to be $R = 0.5$ and the NNPDF31 [60] PDF sets were used.

In Figs. 2 and 3, we present some preliminary plots of the observables defined in Eqs. (2), (3), and (4). At the moment, there are no clear conclusions to draw here, this is still work in progress and the final results will be reported elsewhere.

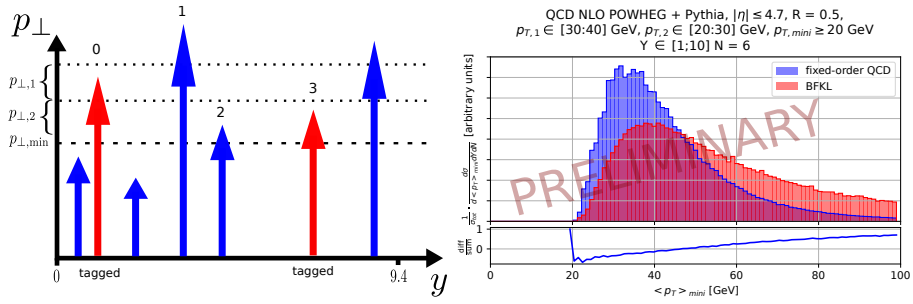

Fig. 2. Left: Minijets below $p_{\perp,\text{min}} = 20$ GeV are ignored for the calculation of the observables. Right: The observable from Eqs. (2).

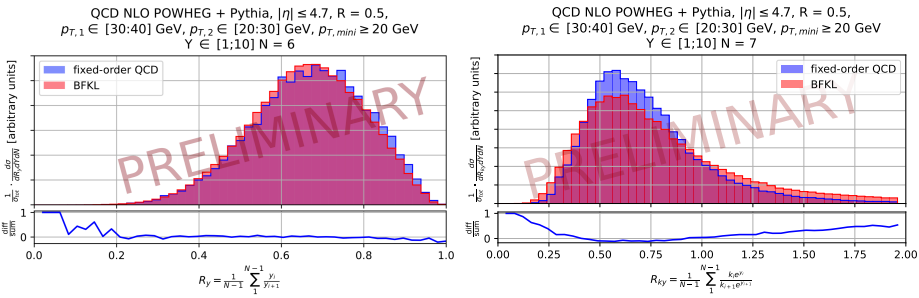

Fig. 3. Left: The observable from Eq. (3). Right: The observable from Eq. (4).

2.2. Toward precision studies of BFKL dynamics

Over the last decade, predictions for a large number of semi-hard observables in unpolarized hadronic collisions have been obtained. Among them, azimuthal correlations between two jets emitted with high transverse momenta and large separation in rapidity (Mueller–Navelet dijet channel [14]) have been identified as promising observables whereby discriminating between BFKL-resummed and fixed-order-inspired calculations [31, 61]. Several phenomenological studies have been conducted so far [23, 26, 28–30, 32, 62–67], which are in fair agreement with the only set of data available, *i.e.* the one collected by the CMS Collaboration for *symmetric* ranges of the jet transverse momenta [68]. In Ref. [69] (see also Refs. [70–77]), clear evidence was provided that the high-energy re-summed dynamics can be sharply disengaged from the fixed-order pattern at LHC energies when *asymmetric* cuts for transverse momenta are imposed both in dijet and in jet plus light-hadron final states. A wealth of inclusive hadronic semi-hard reactions have been considered as test-fields for the BFKL re-summation: di-hadron correlations [78–80], multi-jet emissions [81–94], J/ψ-plus-jet [95, 96], heavy-quark pair [97–99], and forward Drell–Yan di-lepton production with backward-jet detection [100] and more.

One well-known issue in the BFKL approach is that NLO corrections to Green's function turn out to be large and with the opposite sign with respect to the LO contribution. This is generally true also for the impact factors, depicting the transition in the fragmentation region of the colliding particles, all that resulting is a strong instability of the high-energy series. A notable example in this respect is represented by the Mueller–Navelet reaction, where instabilities can be dumped by unnaturally large values of the renormalization and factorization scales [29, 30, 69], chosen within suitable optimization schemes, such as the Brodsky–Lepage–Mackenzie (BLM) method [101–104]. This brings to a substantial lowering of cross sections and hampers any chance of making precision studies.

Recently, however, a set of semi-hard reactions was singled out exhibiting a first, clear stability, in the typical BFKL observables, under higher-order corrections calculated at *natural* scales. It is the case of forward emission of objects with a large transverse mass, such as Higgs bosons [105–108] and heavy-flavored jets [109–111], studied with partial NLO accuracy. Strong stabilizing effects in full NLO emerged in recent studies on inclusive emissions of Λ_c baryons [108, 112] and bottom-flavored hadrons [113]. Here, corroborating evidence was provided that the characteristic behavior of variable-flavor-number-scheme (VFNS) colinear fragmentation functions (FFs) describing the production of those heavy-flavored bound states at large transverse momentum [114–116] acts as a fair stabilizer of high-energy dynamics. We refer to this property, namely the existence of semi-hard re-

actions that can be studied in the BFKL approach without applying any optimization scheme nor artificial improvements of the analytic structure of cross section, as *natural stability* of the high-energy re-summation. Figure 4 (left) summarizes the key features of a well-behaved perturbative series in the case of the $p_\perp$-distribution of a forward Higgs inclusively produced together with a backward jet (rapidity difference $\Delta Y = 5$) in proton–proton collisions at $\sqrt{s} = 14$ TeV: Born and NLO fixed order predictions are clearly separated from LO and NLO BFKL, and the latter shows a very moderate dependence on scale variation. Similar features are seen if a bottom-flavored hadron is detected instead of a Higgs boson in the forward region — see Fig. 4 (right). This supports the statement that high-energy emissions in forward regions of rapidities bring along a high discovery potential and a concrete opportunity to widen our understanding of the hadronic structure and, more general, of strong interactions at new-generation colliders, such as the EIC [117–119], HL-LHC [120], the International Linear Collider (ILC) [121], the Forward Physics Facility (FPF) [122, 123], and NICA-SPD [124, 125].

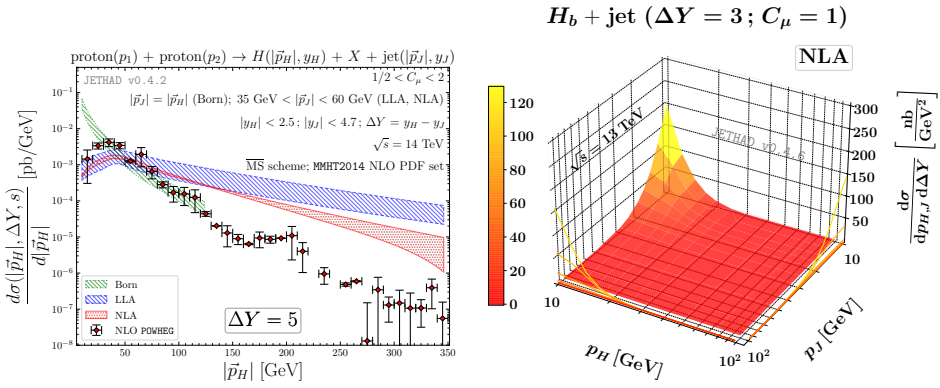

Fig. 4. Left: $p_\perp$-dependence of the NLA cross section for the inclusive hadroproduction of a Higgs + jet system at $\Delta Y = 5$ and $\sqrt{s} = 14$ TeV. Shaded bands give the uncertainty effect of coming from $\mu_{\text{R,F}}$ scale variation. Right: NLA doubly differential $p_\perp$-distribution for the inclusive emission of a H_b + jet system at $\Delta Y = 3$ and $\sqrt{s} = 13$ TeV. Calculations are done at natural scales. Figures from Refs. [105, 113].

2.3. Unintegrated gluon distribution (UGD)

Inclusive emissions of single forward particles represent a golden channel to access the proton content at low-x via an unintegrated gluon distribution. The original definition of the unintegrated gluon distribution relies on high-energy factorization and the Balitsky–Fadin–Kuraev–Lipatov (BFKL)

evolution [1–3, 5]. It takes the form of convolution in transverse momentum space between BFKL Green's function and the proton impact factor. Green's function is process-independent and accounts for the re-summation of small-x logarithms, while the proton impact factor represents the non-evolved part of the density and is of non-perturbative nature. Our knowledge of the proton impact factor is very limited and different models for it and for the unintegrated gluon distribution itself have been proposed so far. First analyses of unintegrated gluon distributions were performed in the context of deep-inelastic-scattering (DIS) structure functions [126, 127]. Subsequently, the unintegrated gluon distribution was probed via the exclusive electro- or photoproduction of vector mesons at HERA [128–138] and the EIC [139–141], the single inclusive heavy-quark emission at the LHC [142], and the forward Drell–Yan production at the LHCb [143–146].

The connection between the unintegrated gluon distribution and the colinear gluon PDF was investigated through a high-energy factorization framework set-up in Refs. [147–149], and via the Catani–Ciafaloni–Fiorani–Marchesini (CCFM) *branching* scheme [150–154]. Then, first determinations of small-x improved PDFs *à la* Altarelli–Ball–Forte (ABF) [155–161] were recently achieved [162–164]. A first connection between the unintegrated gluon distribution and the unpolarized and the linearly-polarized gluon TMDs, f_1^g and $h_1^{\perp g}$, was investigated in Refs. [165–167]. Recent studies [168–170] on the hadronic structure in the *saturation* regime have highlighted the significance of the interplay between the Color Glass Condensate (CGC), the low-x improved TMD (iTMD) framework [171, 172], and the BFKL dynamics, see also the discussion in Section 3. Here, both the genuine and the kinematic twists play a key role in shedding light on the transition regions among these approaches.

In Fig. 5, we show the dependence on the hard scale Q^2 of seven different unintegrated gluon distributions, presented in Section 3 of Ref. [139]. To be specific, we single exclusive production of a ρ-meson in lepton–proton collisions via the sub-process

$$\gamma^*_{\lambda_\mathrm{i}}\left(Q^2\right)\, p \;\to\; \rho_{\lambda_\mathrm{f}} p\,, \tag{9}$$

where a photon with virtuality Q^2 and polarization λ_i is absorbed by a proton and a ρ-meson with polarization λ_f is detected in the final state. The two spin states $\lambda_{\mathrm{i,f}}$ can be longitudinal (0) or transverse (1). The (00) combination gives rise to the longitudinal cross section, $\sigma_\mathrm{L}(Q^2)$, while the (11) one to the transverse cross section, $\sigma_\perp(Q^2)$. Here, the semi-hard scale ordering, $W^2 \gg Q^2 \gg \Lambda^2_\mathrm{QCD}$ (with W the hard-scattering center-of-mass energy), is stringently preserved, and the small-x regime, $x = Q^2/W^2$, is accessed. We further present new results for the EIC [117–119] at the reference energy of

$W = 30$ GeV (right panel). We make use of the twist-2 (twist-3) distribution amplitudes s for the longitudinal (transverse) configuration, and we gauge the impact of the colinear evolution of the distribution amplitudes describing the exclusive emission of the ρ via a variation of the non-perturbative parameter a_2 ($\mu_0 = 1$ GeV) in the range from 0.0 to 0.6 (see Section 2 of Ref. [139] for further details).

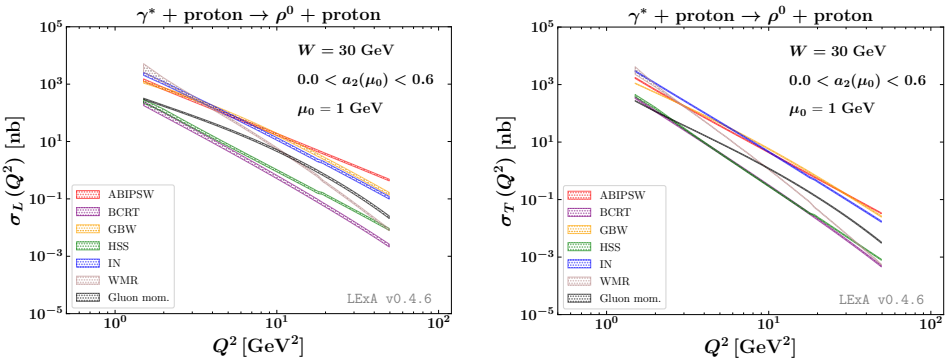

Fig. 5. Q^2-dependence of the longitudinally (left) and transversely (right) polarized cross section, $\sigma_{\mathrm{L,T}}$, for all the considered UGD models, at the EIC reference energy of $W = 30$ GeV. Uncertainty bands describe the effect of varying non-perturbative parameters inside distribution amplitudes depicting the exclusive emission of a ρ meson. Figures from Ref. [139].

We point out that our predictions are spread over a large range. This provides us with clear evidence that polarized cross sections for the exclusive production of light-vector mesons (such as the ρ particle) in lepton–proton collisions act as a discriminator for the unintegrated gluon distribution. We expect that future studies at the EIC will substantially extend our knowledge of the gluon content of the proton at small x.

2.4. BFKL re-summation of NLO colinear factorization: Heavy quarkonium production

Another way the BFKL dynamics manifests itself is within a direct re-summation of contributions enhanced by logarithms of partonic center-of-mass energy in colinear factorization. Such an approach allows to combine high-energy re-summation with theoretical fixed-order predictions which are in general available at a higher perturbative order than their counterparts obtained within high-energy factorization. In the following, we focus on the production of heavy quarkonia — bound states of $c\bar{c}$ or $b\bar{b}$ heavy-quark pairs, see [173–175] for a recent review. New quarkonium-related measurements had been proposed for the experimental programs of the High-Luminosity

LHC [120] and Spin Physics Detector at NICA [124], as well as for fixed-target program at the LHC [176, 177]. It is believed that the non-relativistic nature of these bound states should allow for the description of hadronization of the heavy quark–antiquark pair into an observed quarkonium state with a modest number of free parameters. Despite the availability of several factorization approaches such as the Color-Singlet Model [178], Non-Relativistic QCD Factorization approach [179], and more recent potential-NRQCD [180] and Soft-Gluon factorization [181, 182], none of them is yet capable to fully describe the rich phenomenology of inclusive heavy-quarkonium production observables, which includes differential cross sections and polarization observables in proton–proton, lepton–proton collisions, and e^+e^- annihilation, as described in more detail in the reviews [120, 124, 173–175] cited above.

As pointed out in Ref. [183], for the case of $p_\perp$-integrated prompt η_c hadroproduction cross section and in Ref. [184] for the total inclusive photoproduction cross section of prompt J/ψ, the colinear NLO calculations of these quantities, based on the Color-Singlet (CS) Model, become unreliable if the collision energy $\sqrt{s}$ significantly exceeds the heavy-quarkonium mass M, see Fig. 6 leading to negative cross sections for reasonable values of factorization scale such as $\mu_F = 2M$. A careful analysis of the perturbative partonic cross section and the convolution integral of the former with parton distribution functions allows to trace this instability back to the behavior of the NLO partonic coefficient function at the large partonic center-of-mass energy $\hat{s} \gg M^2$. Beyond NLO, the high-energy logarithmic corrections $\sim \alpha_s^n \ln^{n-1}(\hat{s}/M^2)$ arise in this limit. The necessary re-summation can be addressed using the BFKL re-summation in a form of High-Energy Factor-

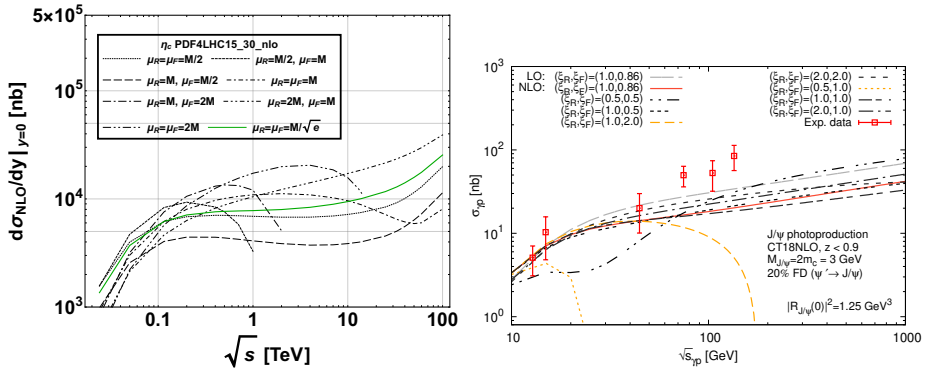

Fig. 6. Collision energy dependence of $p_\perp$-integrated prompt inclusive η_c hadroproduction cross section (left panel, adopted form Ref. [183]) and prompt inclusive J/ψ photoproduction cross section (right panel, adopted from Ref. [184]) at NLO in α_s in the Color-Singlet Model for various choices of factorization ($\mu_F = \xi_F M$) and renormalization ($\mu_R = \xi_R M$) scales.

ization (HEF), provided by Refs. [147–149, 185]. The formalism described in these papers allows one to perform a re-summation of Leading Logarithmic (LL) corrections $\sim \alpha_s^n \ln^{n-1}(\hat{s}/M^2)$ to the partonic cross section in all orders in α_s. As shown in [186], in order for this re-summation to be consistent with the factorization-scale dependence of colinear PDFs, subject to standard NLO DGLAP evolution, it is needed to truncate the full LL $(\ln \hat{s}/M^2)$ re-summation for the partonic cross section by taking into account only Doubly-Logarithmic (DL) terms $\sim \alpha_s^n \ln^{n-1}(\hat{s}/M^2) \ln^n(\boldsymbol{q}_\perp^2/\mu_F^2)$ in the re-summation functions of high-energy logarithms. This allows to obtain the double logarithmic re-summed expression — $\hat{\sigma}_{ij}^{(HEF)}(\hat{s}, \mu_F, \mu_R)$ $(i, j = q, \bar{q}, g)$, which is guaranteed to reproduce the leading logarithmic terms in the $\hat{s} \gg M^2$ asymptotics of the exact partonic cross section up to NNLO in α_s; it serves, therefore, for an approximation for the latter one in the Regge limit. In Ref. [186], the re-summed expression was then combined with the exact colinear NLO result, through introducing a smooth weight functions $0 < w_{ij}^{(CF)}(\hat{s}) < 1$

$$\hat{\sigma}_{ij}(\hat{s}) = \sigma_{ij}^{(CF,LO)}(\hat{s}) + \alpha_s w_{ij}^{(CF)}(\hat{s}) \hat{\sigma}_{ij}^{(CF,NLO)}(\hat{s}) + \left(1 - w_{ij}^{(CF)}(\hat{s})\right) \hat{\sigma}_{ij}^{(HEF)}(\hat{s}) \,, \tag{10}$$

which we construct by suitably adapting the Inverse Squared Errors Weighting (InEW) matching method of Ref. [187] in such a way that the NLO CF term is suppressed when $\hat{s} \gg M^2$ and the re-summation term is suppressed outside of the Regge limit.

The numerical results of such a matching calculation are illustrated by plots in Fig. 7. The left panel shows how the InEW matching of NLO colinear factorization and the re-summed contributions works. In the right panel, the plot of the InEW-matched total cross section (red line) is shown together with its μ_F and μ_R scale-variation uncertainty (shaded band). One can see that the scale uncertainty of the matched prediction does not show any pathological behavior at high energy, unlike the scale-variation plots in Fig. 6, and it is reduced compared to the scale uncertainty of the LO cross section.

Thus, we conclude that problems with high-energy behavior of $p_\perp$-integrated cross sections of quarkonium production described in Refs. [183, 184] are manifestations of the *necessity* to perform the BFKL-type re-summation of high-energy logarithms in the partonic coefficient function of these processes. Nevertheless, such re-summed partonic cross section is only part of the full answer, and at realistic energies $\sqrt{s}$, the region of $M^2/\hat{s} \sim 1$ gives comparably large contribution, as it is clear from the left plot in Fig. 7, so both contributions should be matched. Interestingly, at high energies,

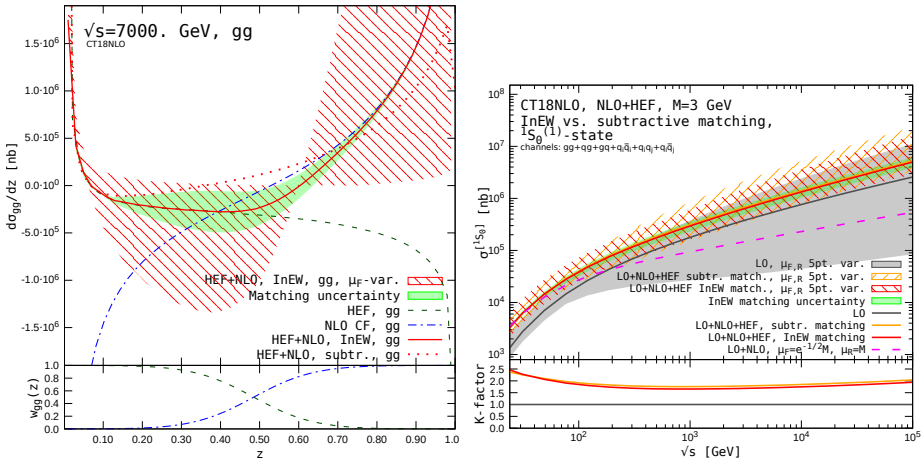

Fig. 7. Left: the integrand of the total η_c hadroproduction cross section as a function of $z = M^2/\hat{s}$ in the gg-channel. Dashed line — DL HEF contribution, dash-dotted line — NLO CF contribution, solid line — their matching, according to Eq. (10), the weight function is shown in the inset. Right: The total cross section of hadroproduction production of the $c\bar{c}\left[{}^1S_0^{(1)}\right]$-state as a function of $\sqrt{s_{pp}}$. Plots adopted from Ref. [186].

the $\hat{\mu}_{\rm F}$-prescription of Refs. [183, 184] predicts a much lower cross section[1] (dashed line in the right panel of Fig. 7) than the matched NLO+ re-summed calculation, which shows the importance of systematic re-summation formalism, see Section 2.5 of Ref. [186] for a more detailed discussion.

In the future, these calculations based on a double logarithmic re-summation of high-energy logarithms matched with NLO colinear factorization in the scheme described above need to be extended to the J/ψ photoproduction case, studied in Ref. [184], as well as to the case of rapidity and $p_\perp$-differential hadroproduction cross sections of prompt η_c and $\chi_{c0,1,2}$ mesons, including the Color-Octet contributions for the latter ones. Another important intermediate-term goal is to study how the DL HEF+NLO CF calculation changes the prompt J/ψ $p_\perp$-spectrum in the Color-Singlet Model. And crucially, we must find the way to extend out formalism beyond the double logarithmic approximation to be able to reduce scale-variation uncertainties of our results to make them useful *e.g.* for determination of the gluon PDFs at low scales and small x. Experimentally, the inclusive J/ψ photoproduction in a wider range of $\sqrt{s_{\gamma p}}$ than was available at HERA could be

[1] This happens for pseudo-scalar quarkonia because of the low value of $\hat{\mu}_{\rm F} < M$ which leads to less evolved gluon PDFs and therefore smaller cross sections. In contrast to this, for other processes such as Higgs production, one may encounter larger $\hat{\mu}_{\rm F} > M$ values and consequently larger cross sections due to PDF evolution [183].

accessed using ultra-peripheral collisions at the LHC, as well as future EIC data which will lie at lower energies but will be more precise due to the increased luminosity. The $\chi_{c0,1,2}$ production cross section in a wide range of energies could be studied by the fixed-target experiments using the LHC beams [176, 177, 188].

2.5. Diffraction: Gaps between jets

Another jet probe of the BFKL dynamics at the LHC is the production of two high-$p_\perp$ jets separated by a large (pseudo)rapidity interval void of particle activity, as proposed by Mueller and Tang nearly 30 years ago [189]. The rapidity gap signature between the jets is indicative of an underlying t-channel color-singlet exchange mechanism. The hard scale of the process, justified by the high jet $p_\perp$, allows for a treatment of this exchange in terms of perturbation theory. A natural mechanism in QCD to explain this process is the BFKL Pomeron exchange between partons. This description is expected to be more justified as the jets become more separated in rapidity. Contributions based on DGLAP evolution are expected to be strongly suppressed in dijet events with a central rapidity gap by virtue of a Sudakov form factor that needs to be supplemented to the calculation. Thus, the jet–gap–jet process may allow us to directly access the small-x dynamics of interest, complementary to other standard probes of this regime of QCD interactions.

Measurements of the jet–gap–jet events have been presented by the CDF, D0, and CMS at $\sqrt{s} = 0.63$, 1.8, 7, and 13 TeV [190–193]. At the Tevatron and at the LHC, the pseudo-rapidity gap between the jets is defined as the absence of particles in $|\eta| < 1$ with $p_\perp > 200$ MeV (or 300 MeV in some cases) between the highest $p_\perp$ jets. The threshold is constrained by the capability of the detectors to reconstruct charged-particle tracks and by the calorimeter noise energy threshold. Experimentally, these events are very clean and can be separated from the overwhelming color-octet exchange dijet background using data-driven methods or Monte Carlo generators. The observable that is extracted in these measurements is the fraction of color-singlet exchange dijet events in the inclusive dijet sample

$$f_{\mathrm{CSE}} \equiv \frac{\mathrm{d}\sigma_{\mathrm{CSE}}}{\mathrm{d}\sigma_{\mathrm{inclusive}}} \,. \tag{11}$$

The f_{CSE} fraction is measured as a function of the second-leading jet $p_\perp^{\mathrm{jet2}}$, the pseudo-rapidity separation between the jets $\Delta\eta_{jj} \equiv |\eta_{\mathrm{jet1}} - \eta_{\mathrm{jet2}}|$, and in some cases, a measure of momentum imbalance between the jets, such as $\Delta\phi_{jj} \equiv |\phi_{\mathrm{jet1}} - \phi_{\mathrm{jet2}}|$. Theoretical uncertainties related to the choice of PDF and the variation of renormalization and factorization scales partially cancel in f_{CSE}. Correlated experimental uncertainties related to jet-energy corrections, luminosity, acceptance, and efficiency effects cancel in the ratio.

The f_{CSE} fractions are of the order of 0.5–1%, depending on the collision energy and dijet kinematics. This means that about 0.5–1% of the inclusive dijet cross section is due to hard color-singlet exchange.

Previous phenomenological studies of the jet–gap–jet process were based on PYTHIA 6 and Herwig 6 Monte Carlo generator [194–198]. This is a good motivation to re-visit the phenomenological predictions in light of the recent developments on the event generator tuning at the LHC and with the advent of NLO+PS generators for the calculation of the cross section for inclusive dijet production. This helps us assess the possible theoretical shortcomings and ideas for future experimental measurements.

To understand these measurements in the context of BFKL dynamics, we have embedded the BFKL Pomeron exchange amplitudes at NLL with LO impact factors in the PYTHIA 8 event generator. We use a recent CP1 tune of PYTHIA 8, which has an improved phenomenology of initial- and final-state radiation, multiple-parton interactions, and hadronization for a wide range of energies and collision systems, including 13 TeV pp collisions [199]. We use POWHEG+PYTHIA 8 for the NLO+PS calculation of the inclusive dijet cross section using the CP5 tune of PYTHIA 8. We compared our calculations to the measurements by the Tevatron and LHC experiments using the same rapidity gap selection as the experiments ($p_\perp > 200$ MeV in $|\eta| < 1$) and with a rapidity gap definition that is closer to the theoretical expectation ($|\eta| < 1$, no $p_\perp$ requirement). In Fig. 8, we show a few predictions for 13 TeV together on top of the measurement by CMS. While conducting these studies, we discovered that there is an important role of initial-state radiation effects in the destruction of central gaps as one goes to larger $\sqrt{s}$. We find that the description using a theoretical-like gap and the experimental gap agree with each other, modulo a global normalization factor, at 1.8 TeV and 7 TeV, but a clear disagreement is observed at 13 TeV. The theoretical gap prediction gives a better description of the data at 13 TeV.

In investigating the source behind the phenomenological differences between the gap definitions, we find that there is sensitivity in the modeling of fragmentation with the additional production of color charges with ISR in PYTHIA 8. The Run 2 tunes of CMS were fit to reproduce charged particle spectra measurements in minimum-bias events split into single-diffractive (forward rapidity gap), non-diffractive, or inelastic topologies [200]. For a better phenomenological interpretation of the jet–gap–jet process, additional experimental input on measurements of minimum-bias events with central rapidity gap topologies, similar to the ones used for the jet–gap–jet process but without the requirement of high-$p_\perp$ jets, will be necessary to further tune ISR and fragmentation modeling effects. To get more insight into this aspect, future phenomenological calculations should be done by embedding the BFKL calculations in the Herwig 7 generator, which has a different evolution variable in the parton shower and a different fragmentation model.

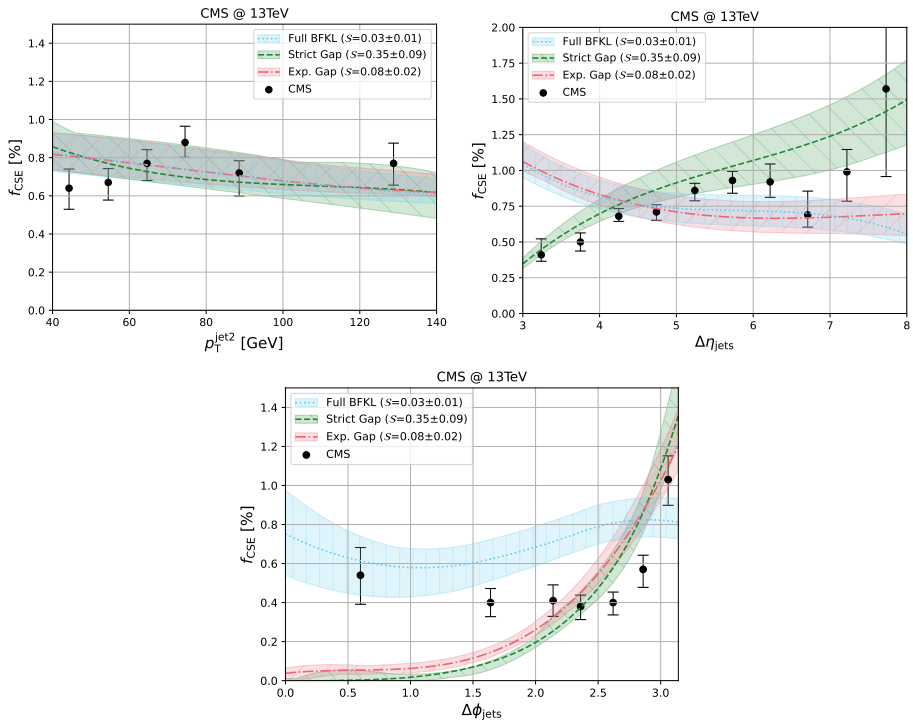

Fig. 8. Measurement of the color-singlet exchange fraction f_{CSE} at 13 TeV by the CMS Collaboration [193]. Theoretical predictions based on the BFKL calculations at next-to-leading logarithmic accuracy assuming an experimental gap ("exp gap"), a theoretical-like gap ("strict gap"), and no gap requirement ("full BFKL") are presented. The bands represent uncertainties related to factorization and renormalization scale variations. The gap survival probabilities, indicated in the legend, were fit with a χ^2 scan.

The present BFKL calculations for the jet–gap–jet process account for the re-summation of logarithms of energy at NLL accuracy using LO impact factors. The NLO impact factors were calculated in recent years [201, 202], but they have not been incorporated into the phenomenological analysis yet. In addition, to improve the phenomenological description, it will be important to take into account the effect of wide angle, soft gluon emissions into the gap region. These lead to so-called non-global logarithms, which are not re-summed in the BFKL framework. The re-summation is known exactly in the large-N_c limit, and is described by the Banfi–Marchesini–Smye equation [203]. The effect of these non-global logarithms for the jet–gap–jet topology is a suppression of the gluon–gluon processes relative to quark–gluon and quark–quark processes [204].

Experimentally, future measurements could benefit from exploring different definitions of the pseudo-rapidity gap between the jets. For example, by scanning the $p_\perp$ threshold used to define the pseudo-rapidity gap in order to better control the aforementioned ISR effects, or by defining a "sliding" pseudo-rapidity gap interval event-by-event. To suppress the underlying event activity, one could target hadron–hadron collisions where at least one of the colliding hadrons remains intact due to the Pomeron exchange. Such a measurement has been presented by the CMS and TOTEM [193], demonstrating the feasibility of such studies. However, the sample size was rather limited and did not allow for a differential measurement of the f_{CSE}. Special runs at the LHC at $\sqrt{s} = 14$ TeV with single proton–proton collisions with an integrated luminosity of $\mathcal{L} = 10\ \mathrm{pb}^{-1}$ would allow for a highly differential measurement in a controlled hadronic environment.

To this date, we still do not have a global and satisfactory description of the jet–gap–jet events from the point of view of QCD. In principle, given the hard scale of the process, the jet–gap–jet process should be describable in terms of perturbation theory, and potentially be a venue for understanding the BFKL dynamics. It is counter-intuitive that such a simple signature is more complicated to describe than the significantly "busier" inclusive dijet events.

According to the Tevatron and LHC measurements, about 0.5–1% of the inclusive dijet cross section is due to a t-channel hard color-singlet exchange. The sub-process for QCD hard color-singlet exchange is not currently implemented as a standard sub-process in modern Monte Carlo event generators. As the experimental precision increases for inclusive jet cross-section measurements, the absence of t-channel color-singlet exchange sub-processes becomes more important, for example for PDF or α_{s} extractions. Thus, for the next years in high-energy physics, it will be important to have a proper understanding of this process, both experimentally and theoretically.

3. Hadronic structure at low x and gluon saturation

Main Contributors: R. Boussarie, F.G. Celiberto, M. Fucilla, A. van Hameren, J. Jalilian-Marian, P. Kotko, K. Kutak, M.M.A. Mohammed, A. Papa, S. Sapeta, L. Szymanowski, S. Wallon

3.1. Color Glass Condensate and high gluon densities

Even though BFKL re-summation can stabilize collinear factorization, this approach is expected to eventually breakdown due to the resulting high gluon occupation numbers. The gluon distribution is rapidly growing at small x due to radiation of more and more small-x gluons, due to the availability of large longitudinal phase space at high energies. At some point, the

number of partons occupying the same transverse are in the target hadron or nucleus will be large. The QCD-improved parton model (where nearby partons are treated as not interacting with each other) will be therefore cease to be applicable to describe those high energy collisions. This is the phenomenon of the so-called gluon saturation. In the Color Glass Condensate formalism, one treats this state with a large gluon occupation number as a classical color field generated by the large-x color degrees of freedom generically called sources of color charge ρ. In this formalism, a high-energy hadronic or nuclear collision is then treated as a collision of two highly contracted classical color fields, *i.e.* shock waves. This a highly non-trivial and, so far, not amenable to analytic solutions in general. A somewhat easier problem is to consider scattering of a dilute system of partons on a dense system of gluons described as a saturated state of gluons. In this so-called dilute-dense collision, the relevant degrees of freedom are the Wilson lines in fundamental or adjoint representation,

$$V(x_\perp) \equiv \hat{P} \exp\left\{ ig \int_{-\infty}^{+\infty} \mathrm{d}x^+ \, A_a^- \, t_a \right\} \tag{12}$$

re-summing multiple scatterings of a quark or gluon parton projectile on the classical color field A^- describing the target dynamics in light-cone gauge $A^+ = 0$. Production cross sections in this approach involve two and four point correlation functions of Wilson lines known as dipoles and quadrupoles (these are the only two correlation functions in leading N_c approximation). Quantum loop effects are then incorporated into this formalism via a functional renormalization group equation known as the JIMWLK equation [205–215] which in the Gaussian and large-N_c approximation reduces a close equation known as the BK equation [216, 217]. While applications of the Color Glass Condensate to high-energy collisions at HERA, RHIC, and the LHC have yielded tantalizing hints of gluon saturation effects there is still no firm evidence.

3.2. Transverse-momentum-dependent parton distribution functions

Unlike colinear factorization, such an approach is based on high-energy factorization, which yields cross sections as convolutions in transverse momenta or coordinates, in contrast to convolutions in hadron momentum fraction, encountered for colinear factorization. In [165], it has been shown that by neglecting any higher twist correction, one finds in the small-x description of semi-inclusive observables the sought-after distributions which contain the information on transverse momentum in hadron: the Transverse-Momentum-Dependent (TMD) gluon distributions. These distributions allow for 3-dimensional imaging of hadrons: one accesses one longitudinal

direction and two transverse dimensions of momentum inside them. Such TMD distributions are not only of interest to characterize effects related to the presence of high gluon densities in a hadron. More generally, they allow to obtain a 3D imaging of the proton content and to answer fundamental questions of the dynamics of strong interactions, such as the origin of proton mass and spin calls, see Refs. [218, 219] and references therein. The complete list of unpolarized and polarized gluon TMDs at leading twist (twist-2) was provided for the first time in Ref. [220]. Note that this list is generic and is at first not restricted to high-energy factorization and/or the presence of high parton densities. They however provide useful tools to map the information contained in correlators of the multiple Wilson lines Eq. (12). Table 1 contains the eight twist-2 gluon TMDs for a spin-1/2 target, using the nomenclature defined in Refs. [221, 222]. The two functions on the diagonal in Table 1 respectively stand for the density of unpolarized gluons inside an unpolarized nucleon, f_1^g, and of circularly polarized gluons inside a longitudinally polarized nucleon, g_1^g. They are the counterparts to the well-known unpolarized and helicity gluon PDFs obtained within colinear factorization. According to the TMD factorization, *i.e.* factorization in the limit where a certain transverse momentum $k_\perp$ is significantly smaller than a certain hard scale M, $M \gg k_\perp$, all these densities embody the re-summation of transverse-momentum logarithms, which constitute their perturbative input. Much is known about this re-summation [223–225], but very little is known about the non-perturbative content of these TMD distribution. It is then this non-perturbative content (from the point of view of TMD factorization) which promises to give information on the Color Glass Condensate.

Table 1. A table of leading-twist gluon TMDs for spin-1/2 targets. U, L, T stand for unpolarized, longitudinally polarized, and transversely polarized hadrons, whereas U, 'circular', 'linear' depict unpolarized, circularly polarized, and linearly polarized gluons, respectively. T-even (odd) functions are given in blue (red). Black functions are T-even and survive the integration over the gluon transverse momentum.

nucleon pol. \ gluon pol.	U	circular	linear
U	f_1^g		$h_1^{\perp g}$
L		g_1^g	$h_{1\mathrm{L}}^{\perp g}$
T	$f_{1\mathrm{T}}^{\perp g}$	$g_{1\mathrm{T}}^{g}$	h_1^g, $h_{1\mathrm{T}}^{\perp g}$

The distribution of linearly polarized gluons in an unpolarized hadron, $h_1^{\perp g}$, is particularly relevant at low x since it leads to spin effects in collisions of unpolarized hadrons [226–231], whose size is expected to become more and more relevant when x diminishes. The Sivers function, $f_{1\mathrm{T}}^{\perp g}$, gives on the other hand information about unpolarized gluons in a transversely polarized nucleon, and is relevant to study transverse-spin asymmetries emerging in collisions with polarized-proton beams. Within the context of low-x physics, it is of particular interest due to its connection with the QCD Odderon [232].

First attempts at phenomenological analyses of f_1^g were done in Refs. [233–235]. The phenomenology of $f_{1\mathrm{T}}^{\perp g}$ was discussed in Refs. [236–239]. Due to the shortage of experimental data on the gluon-TMD sector, exploratory analyses of gluon TMDs via simple and flexible models are required. Pioneering analyses along this direction were conducted by the hands of the so-called *spectator framework* [220, 240, 241]. Originally employed to model quark-TMD distributions [221, 242–246], it relies on the assumption that from the struck hadron a gluon is extracted, and what remains is considered an effective on-shell spin-1/2 object. Spectator-model T-even gluon TMDs at twist-2 were recently obtained in Ref. [247] (see also Refs. [248–250]), while a preliminary calculation of the T-odd ones can be found in Refs. [251–253]. The T-even gluon correlator is taken at the tree-level and does not account for the gauge-line dependence, which appears in our model in the T-odd case.

For an unpolarized proton, we identify the unpolarized distribution

$$x\rho(x,p_x,p_y) = x f_1^g\left(x,\boldsymbol{p}_\perp^2\right) \tag{13}$$

as the probability of extracting unpolarized gluons at given x and $\boldsymbol{p}_\perp$, while the Boer–Mulder density

$$x\rho^{\leftrightarrow}(x,p_x,p_y) = \frac{1}{2}\left[x f_1^g\left(x,\boldsymbol{p}_\perp^2\right) + \frac{p_x^2-p_y^2}{2M^2}\, x h_1^{\perp g}\left(x,\boldsymbol{p}_\perp^2\right)\right] \tag{14}$$

represents the probability of extracting linearly-polarized gluons in the transverse plane at x and $\boldsymbol{p}_\perp$.

Contour plots in Fig. 9 refer to the behavior in $\boldsymbol{p}_\perp$ of the ρ-densities in Eqs. (13) and (14), respectively, obtained at $Q_0 = 1.64$ GeV and $x = 10^{-3}$ for an unpolarized proton virtually moving toward the reader. The color code is related to the size of the oscillation of each density along the p_x and p_y directions. To better catch these oscillations, ancillary 1D plots representing the corresponding density at $p_y = 0$ are shown below each contour plot. As expected, the density of Eq. (13) has a cylindrical pattern around the direction of motion of the proton. Conversely, the Boer–Mulders

ρ density in Eq. (14) presents a dipolar structure which reflects the fact that gluons are linearly polarized. The running away from the cylindrical symmetry is emphasized at small x, because the Boer–Mulders function is particularly large. From the analytic point of view, the ratio between f_1^g and $h_1^{\perp g}$ TMDs turns to a constant in the asymptotic limit of $x \to 0^+$. This is in line with the prediction coming from the linear BFKL evolution, *i.e.* that at low x, the "number" of unpolarized gluons equals the number of linearly-polarized ones, up to higher-twist effects (see, *e.g.*, Refs. [254–258]). Therefore, a connection point between our gluon TMDs and the high-energy QCD dynamics has been established.

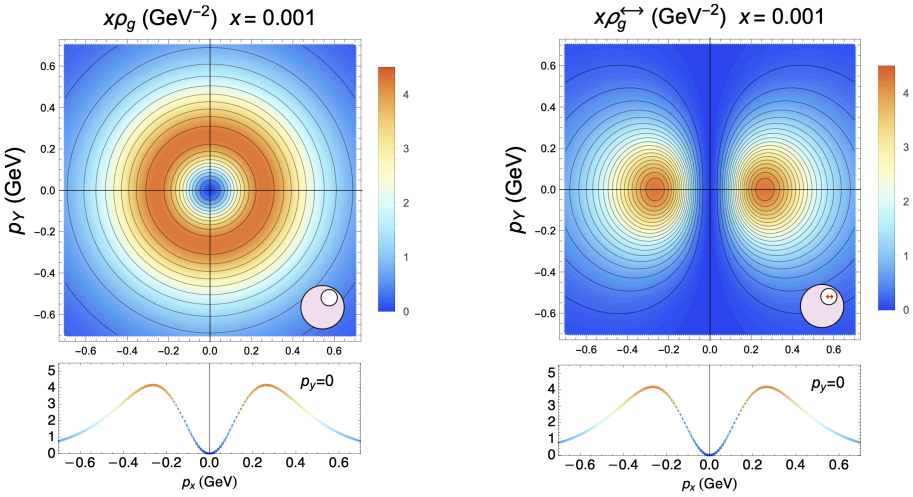

Fig. 9. 3D tomographic imaging of the proton unpolarized (left) and Boer–Mulders (right) gluon TMD densities as functions of the gluon transverse momentum, for $x = 10^{-3}$ and at the initial-energy scale, $Q_0 = 1.64$ GeV. 1D ancillary panels below the main contour plots show the density at $p_y = 0$. Figures from Ref. [247].

To access more dimensions of partonic content, exclusive processes are necessary. The richest distributions one encounters in perturbative QCD processes are the so-called Generalized TMD distributions (GTMD). They parameterize master correlators of 5 parameters $(x, \xi, \vec{k}_\perp^2, \vec{\Delta}_\perp^2, \vec{k}_\perp \cdot \vec{\Delta}_\perp)$, where $x, \vec{k}_\perp$ are, respectively, the fraction of the longitudinal target momentum and the transverse momentum carried by a parton, and ξ and $\vec{\Delta}_\perp$ are the longitudinal and transverse momentum transfer to the hadron. For $(\xi = 0, \vec{\Delta}_\perp = \vec{0}_\perp)$, the GTMD becomes a TMD. In a given process, the set of GTMD distributions which are accessed depends on the final-state kinematics, but also on the parton and hadron polarizations with repercussions on the measured final state. Multidimensional tomography of hadrons as a probe for Wigner

distributions and TMD distributions has been a major focus of theoretical and experimental efforts, and it will be an important share of the physics goals of future colliders such as the Electron Ion Collider [259]. Examples of relevant processes — which also allow, at least in principle, for an analysis at next-to-leading order in the perturbative expansion — are meson production in $\gamma^{(*)}p$ collisions [260], inclusive and diffractive dijets [170, 259, 261–264], see also [265] for a first phenomenological application to HERA data, as well as exclusive pion production in *unpolarized* electron–proton scattering in the forward region, which is a direct probe of both the gluon Sivers function and the QCD Odderon [232].

3.3. Complementarity between EIC and LHC

There exists a very nice complementarity between the EIC and LHC experiments. Indeed, it is possible to gather important input on such (G)TMD distributions from photon–hadron reactions, which at the LHC is accessible through ultra-peripheral proton–nucleus and nucleus–nucleus collisions, see Section 5 for a detailed discussion. A photoproduction process which provides the necessary hard scale for an analysis based on the perturbative QCD expansion is the production of quarkonia, in particular diffractive exclusive photoproduction of J/ψ charmonia with negative charge parity which allows to study the distribution of gluons in the target. On the other hand, the same type of production of charmonia with positive charge parity as η_c or χ_c permits studying gluonic exchanges with the negative charge parity corresponding to Odderon exchanges. A related process is exclusive diffractive meson production at large momentum transfer $|t|$, which could provide a new set of observables to reveal saturation effects. While HERA measurements are limited by statistics, UPC reactions at the LHC might allow for the observation of a different scaling in t, when passing from high-energy kinematics governed by the BFKL-like descriptions to extreme rapidities in which saturation effects are expected. Instead of using t as a hard scale, it is also possible to study diffractive states which contain at least one meson carrying a large $p_\perp$, originating from colinear fragmentation of the virtual $q\bar{q}$ pair produced by the photon. The large value of $p_\perp$ ensures that each of the q and $\bar{q}$ carries an (opposite) large $q_\perp$ through the usual ordering of colinear fragmentation. Relying on the recent results obtained for impact factors $\gamma \to q\bar{q}g$ at leading order and $\gamma \to q\bar{q}$ at next-to-leading order, which were used for the computation of the $\gamma \to$ dijet impact factor at NLO, a complete NLO study could be done in the future. Most probably, the pion channel which is the best known for fragmentation functions, would be the most promising.

Last but not least, it is worth mentioning large invariant mass systems: In the spirit of time-like Compton scattering, in which the hard scale is provided by the virtuality of the emitted virtual photon, exclusive production at the JLab of a γ-meson pair of large invariant mass is a very promising process to access to Generalized Parton Distributions (GPD) [266, 267], another particular facet of the master correlators obtained by integrating out their $\vec{k}_\perp$ dependency. It turns out that the same process in the large-s limit belongs to the class of diffractive processes, therefore furnishing another probe for studying gluonic saturation. Thus, by covering a very wide kinematical range, the same process studied at the JLab, EIC (in photoproduction), and LHC (in UPC), would allow to pass from a description based on colinear factorization involving a nucleon GPD to a high-energy description in which linear and non-linear re-summation effects are expected.

3.4. Forward dijets: from LHC to EIC

Dijets produced in the forward direction of the detectors are characterized by final states at large rapidities and hence they trigger events in which the partons from the nucleus carry a small longitudinal momentum fraction x. This kinematic setup is well-suited to investigate the properties of the dense partonic system and the phenomenon of saturation. The following study is based on the so-called small-x Improved Transverse-Momentum-Dependent factorization framework [168, 171, 268–271] which accounts for exact kinematics of the scattering process with off-shell initial-state gluons, gauge invariant formulation of the TMD gluon densities as well as off-shell partonic amplitudes, and complete kinematic twists, while neglecting genuine twists. The framework therefore covers both $k_\perp$-factorization [148, 272] in the limit of large off-shellness of the initial-state gluon from the nucleus and small-x TMD factorization [165] in the limit where momenta of the final-state jets are much larger than the momentum of the incoming off-shell gluon. Furthermore, [169, 170] demonstrate very good agreement of this approach with the full CGC result in the region dominated by hard jets *i.e.* $k_\perp, p_\perp > Q_\mathrm{s}$.

While the original Improved TMD framework includes gluon saturation effects, it does not account for the complete set of contributions proportional to the logarithms of the hard-scale set by the large transverse momenta of jets — the so-called Sudakov logarithms. As shown in Refs. [273, 274], the inclusion of the Sudakov logarithms is necessary in order to describe the LHC jet data in the region of small x. In the low-x domain, the re-summation leading to the Sudakov logarithms has been developed in Refs. [275, 276], see also [277]. In Ref. [278], it was for the first time shown that the interplay between the saturation effects and the re-summation of the Sudakov logarithms is essential to describe the small-x forward–forward dijet data.

In this section, we present two results that demonstrate the relevance of both effects, *i.e.* non-linearity, accounting for saturation, and the Sudakov effects, accounting for emissions of soft gluons. We shall consider two processes:

— the inclusive dijet production

$$p\,(P_p) + A\,(P_A) \to j_1(p_1) + j_2(p_2) + X\,, \tag{15}$$

— the dijet production in deep inelastic scattering

$$e\,(P_e) + A\,(P_A) \to e\,(p_e) + j_1(p_1) + j_2(p_2) + X\,, \tag{16}$$

where A can be either the lead nucleus or a proton.

To describe the former process, we use a hybrid approach where one assumes that the proton p is a dilute projectile, whose partons are colinear to the beam and carry momenta $p = x_p P_p$. The hadron A is probed at a dense state. The jets j_1 and j_2 originate from the hard partons produced in a collision of the probe a with a gluon belonging to the dense system A. This gluon is off-shell, with momentum $k = x_A P_A + k_\perp$ and $k^2 = -|\vec{k}_\perp|^2$. The ITMD factorization formula for the above process can be found in Ref. [171], while the formula for the e–A collision can be found in Ref. [279].

As it has been argued above, in order to provide realistic cross-section predictions, one needs to include also the Sudakov effects. For dijet production at the LHC, we used a DGLAP-based Sudakov form factor [278].

In Fig. 10, we show normalized cross sections as functions of $\Delta\phi$ in p–p and p–Pb collisions. The three panels correspond to three different cuts on the transverse momenta of the two leading jets. The points with error bars represent experimental data from Ref. [280]. The main results for the p–Pb collisions are represented by the blue solid lines. The broadening of the distributions as we go from p–p to p–Pb comes from the interplay of the non-linear evolution of the initial state and the Sudakov re-summation.

In Fig. 11, we show predictions for nuclear modification in the DIS process as one increases the energy of the collision. In particular, we present the results for three values of the energy that are relevant for the EIC, LHeC, and FCCeh. We see that for larger energies, the suppression due to saturation is larger, and that the Sudakov form factor cancels to a large degree. This result demonstrates that having results for the absolute cross sections [279] and nuclear modification ratio, one can in principle isolate effects due to saturation from the effects coming from Sudakov re-summation.

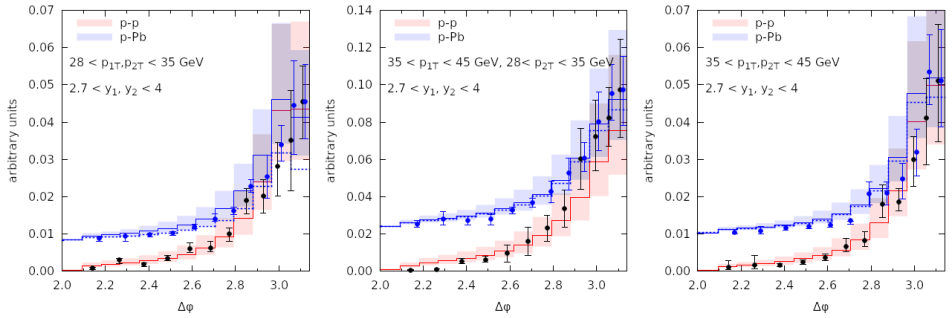

Fig. 10. Broadening of azimuthal decorrelations in p–Pb collisions *versus* p–p collisions for different sets of cuts imposed on the jets' transverse momenta. The plots show normalized cross sections as functions of the azimuthal distance between the two leading jets, $\Delta\phi$. The points show the experimental data [280] for p–p and p–Pb, where the p–Pb data were shifted by a pedestal so that the values in the bin $\Delta\phi \sim \pi$ are the same. Theoretical calculations are represented by the histograms with uncertainty bands coming from varying the scale by factors 1/2 and 2.

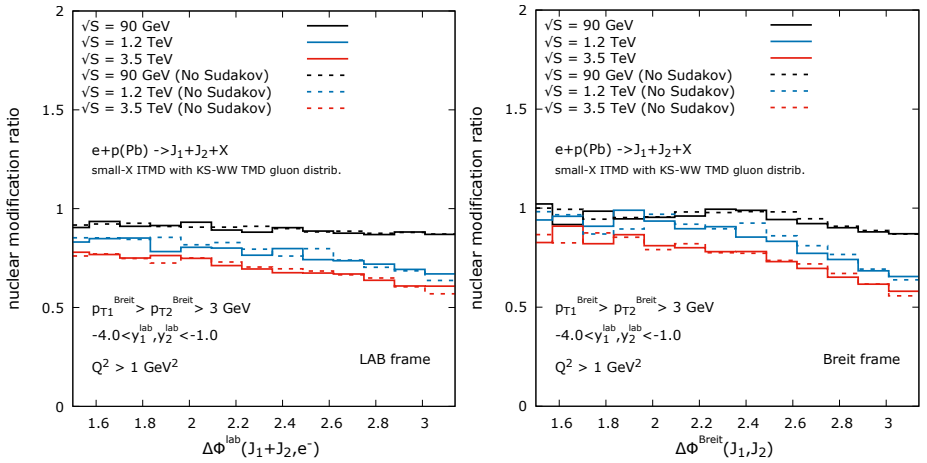

Fig. 11. Nuclear modification factor R_{pA} as a function of the azimuthal angle between the jet system and the scattered electron in the LAB frame (left) and as a function of the azimuthal angle between the jets in the Breit frame (right). The calculations are done for three different CM energies per nucleon. Solid lines correspond to calculations using the Sudakov form factor and KS-based WW gluon density.

3.5. Color Glass Condensate beyond high-energy factorization

Theory predictions for Color Glass Condensate correlators are genuinely based on high-energy factorization which can be recast as the first order of an expansion in parton momentum fraction x. However, in particular for EIC kinematics but also if descriptions are to be extended to central rapidities, there is the danger that one is leaving the regime of applicability of this expansion. This is most easily seen in the kinematics relation

$$x_{1,2} = \frac{p_\perp}{\sqrt{s}} \, \mathrm{e}^{\pm y} \,, \tag{17}$$

where $x_{1,2}$ are the projectile and target momentum fraction probed in the collision, while $p_\perp$ and y are the transverse momentum and rapidity of the produced particle. As it is seen as one looks at higher and higher transverse momenta of produced particles, one is probing larger and larger values of momentum fractions x of the target, which eventually will become too large for the CGC formalism to be a valid description of the target. Furthermore, multiple scatterings of the projectile on the target (which need to be taken into account due to the high-gluon density of the latter) are treated in the eikonal, *i.e.* recoil-less approximation, which can only accommodate a small angle deflection of the projectile. This eikonal approximation to multiple scatterings is the reason one can elegantly re-sum them into a Wilson line. As one considers particle production at higher $p_\perp$, this recoil-less approximation breaks down and partons are scattered at a large angle. This is not included in the CGC formalism. In Fig. 12, we show the difference in the target x

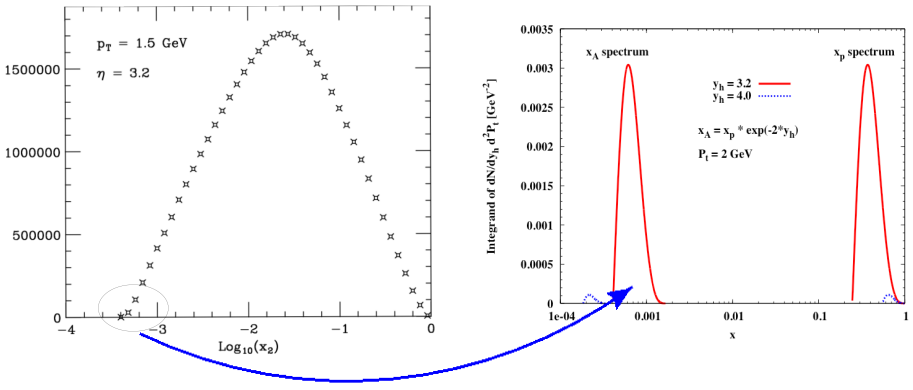

Fig. 12. A comparison of target x-range contributing to single inclusive pion production in proton–proton collisions at RHIC. The left panel is (from Ref. [281]) showing the target x-range as predicted by the colinear factorization formalism, while the right panel is the x-range obtained from the Color Glass Condensate formalism, taken from Ref. [282].

involved in the pion production in proton–proton collisions in the forward rapidity region at RHIC. Both colinear factorization and CGC approaches fit the data well and yet the physical cross section is dominated by very different target xs in the two approaches so clearly, there is a discrepancy. Both approaches cannot be correct at the same time, so at least one or both of the two must be missing some crucial physics. This demonstrates the need for a more general formalism that includes colinear factorization at high $p_\perp$ and the Color Glass Condensate formalism at small x.

In [283–285], a new approach to particle production at high energies was proposed which aims to accomplish this, including large-x (high $p_\perp$) physics as encoded in colinear factorization and gluon saturation effects at small x as described by the JIMWLK equation. A related, but different approach [286, 287] aims at first at unification of colinear factorization and low-density high-energy factorization. All these approaches imply the necessity to go beyond the eikonal approximation and allow for a large angle deflection of the projectile parton. This cannot happen if one considers scattering from small-x modes of the target as is the case in CGC. Therefore, one must include scattering from the large-x modes of the target. This work is currently in progress and will be reported elsewhere.

4. Imprints of high gluon densities at low x at the LHC

Main Contributors: G.K. Krintiras, C. Loizides, M. Strikman

4.1. Open QCD questions at a hadron–hadron collider: Parton fragmentation, mini-jets, and their interplay with high parton densities

Apart from the study of specific observables which allow to obtain information on different TMD distribution function, there exist also more global features of QCD phenomenology at a hadron–hadron collider, which allow to study and quantify the manifestation of high and potentially saturated parton distributions.

4.1.1. Evidence for non-linear QCD dynamics in the fragmentation region in pA scattering

A first region where such evidence for QCD non-linear dynamics could be found is the fragmentation region of proton–nucleus scattering. In a collision of two nucleons or nuclei, a parton with a given hadron momentum fraction x_1 resolves partons in another nucleon down to momentum fractions of the order of

$$x_2 = 4{p_\perp}^2/(x_1 s)\,, \tag{18}$$

with $p_\perp$ the transverse momentum of the parton and $\sqrt{s}$ the center-of-mass energy of the collider. At the LHC, for $x_1 = 0.3$, $|p_\perp| = 2$ GeV/c, and

$\sqrt{s} = 14$ TeV in proton–proton collisions, one is therefore sensitive down to values of approximate $x_2 \sim 3 \times 10^{-7}$. Even smaller values of x, down to $x \sim 10^{-9}$, are resolved in the collisions with cosmic rays. At such low values of x, the secondary hadron is, in general, characterized by the presence of high parton — in particular gluon — densities. A parton propagating through such a dense medium of small $x \geq x_2$ partons acquires a significant transverse momentum, due to interaction with the dense gluonic field and loses a finite fraction of its momentum [288]. This is in particular the case for central proton–nucleus collisions, where parton densities are further subject to nuclear enhancement[2].

One consequence of this is a strong suppression of the leading particle spectrum as compared to minimal bias events: Each parton fragments independently and splits into a couple of partons with comparable energies. This suppression is especially pronounced for the production of nucleons: for values of Feynman $x_{\rm F} \sim x_1$ above 0.1, the differential multiplicity of pions should exceed that of nucleons, see [289] for a study which however does not include an additional suppression due to finite fractional energy losses. Suppression of forward pion production was observed at RHIC in deuteron–gold collisions at $x_{\rm F} \geq 0.3$ [290, 291], see also the discussion in [281]. It is important to note that in this kinematic regime, perturbative QCD works pretty well. Indeed, essential values of x_2 are in these reactions of the order of ~ 0.01 [281], see Fig. 12 (left), which is still far from the phase-space region where gluon densities are so high that non-linear effects may become important in the evolution of nuclear parton distribution functions. Note that in the CGC scenario, central collisions dominate and one has to assume the existence of a mechanism for a very strong suppression of the scattering in the DGLAP $x_2 \geq -0.01$ kinematics. Nevertheless, the observed suppression of the inclusive per nucleon $d\mathrm{Au} \to \pi^0 + X$ cross section as compared to the inclusive $pp \to \pi^0 + X$ cross section, $R_{d\mathrm{Au}}$,

$$R_{d\mathrm{Au}}(x_{\rm F} = 0.5, p_\perp = 2\ \mathrm{GeV}/c) \sim 0.5\,, \tag{19}$$

is in a gross contradiction with the naive perturbative QCD prediction of $R_{d\mathrm{Au}}(\mathrm{pQCD}) = 1.0$. Moreover, the analysis of the STAR data on the multiplicity of hadrons produced in the events with a forward π^0 trigger indicates that the dominant contribution to the pion yield originates from peripheral collisions. This suggests that for central collisions, the actual suppression is much larger — about a factor of the order of five.

[2] Note that there is a moderate gain in the gluon density per unit area in such proton–nucleus collisions and hence in the average value of gained transverse momentum in comparison to scattering on a proton. Nevertheless, fluctuations of the gluon density are much smaller in the case of nuclei.

The observed pattern is consistent with the scenario of an effective fractional energy loss, which leads to a large suppression: The π inclusive cross section strongly drops with the increasing x_{F}. Leaving details aside, the observed effect is strong evidence for a break down of the perturbative QCD approximation. It is natural to suspect that this is due to effects of strong small-x gluon fields in nuclei, as the forward kinematics is sensitive to small-x effects. Overall, the generic features expected in all models in which interaction strength is comparable with a black disk limit are:

(i) Strong suppression of the large x_{F} spectra at moderate values of $p_\perp$,

(ii) Broadening of the transverse momentum distributions of leading hadrons at large x_{F}.

Both effects should become more and more pronounced with increasing collision energy and centrality of collision, and/or increase of the number of nucleons A. They should be studied as a function of A and centrality. Hence, one may expect much stronger suppression the of pion spectrum at $x_{\mathrm{F}} \gtrsim 0.4$ and a stronger $p_\perp$ broadening at the LHC as compared to RHIC. Note that these effects should be much more mild for central proton–nucleus collisions, due to weak dependence of the cross section on x_{F}. This is in line with the observation of the ALICE experiment [292], which measured the pion yield as a function of $p_\perp$ at central rapidities at the LHC and found only a small enhancement of the yield for the central collisions. Note that the rapidity interval between the pion and the initial nucleon is in this case is similar to that of the RHIC experiments. This is consistent with the scenario that at central rapidities, the only significant effect is $p_\perp$ broadening due to elastic re-scatterings, which leads to an enhancement of the cross section rather than to its suppression. It would be informative to measure a recoil gluon mini-jet from the underlying quark–gluon collision to study the effect of suppression as a function of x_g for the fixed pion x_{F}.

Further exploration of these effects in pp scattering would be possible by studying the production of the leading mesons with a centrality trigger-like dijet production at central rapidities. It would also be instructive to study these effects in the ultra-peripheral collisions at the LHC since in this case, one can reach center-of-mass energies for the photon–nucleus reaction, which are comparable to center-of-mass energies for nucleus–nucleus scattering at RHIC.

4.1.2. Mini-jet dynamics at collider energies

The leading order cross section for scattering of two partons grows within perturbative QCD rapidly with decreasing momentum transfer between the scattering partons. Combining this effect with the growth of gluon

densities at small x, one obtains an inclusive mini-jet cross section which exceeds even the inelastic proton–proton cross section. This suggests that the average mini-jet multiplicity may exceed one. To tame this mini-jet cross section, the Monte Carlo models either introduce a hard (no collisions with $p_\perp < p_0(s)$) or a soft cutoff (smoothly switching off interactions with $p_\perp$s below a few GeV/c). Interestingly, models seem to suggest that the suppression factor grows rather rapidly with collision energy. Clarifying the precise mechanism for the energy dependence of the suppression of mini-jets in both proton–proton and proton–nucleus scattering is one of the current challenges of the high energy QCD. Note that while gluon saturation generates such an effect for the small-x region, it does not explain a similar suppression for the peripheral proton–nucleus and proton–proton collisions. It also does not explain suppression for $x \sim 10^{-2} \div 10^{-3}$ far from the black disk limit [293]. A comparison of transverse momentum distributions of hadrons produced in the very forward region and central rapidities would certainly help in a better understanding of this suppression mechanism.

A direct observation of mini-jets is pretty difficult, since transverse momenta of hadrons generated in the fragmentation of mini-jets may be rather close to the soft scale. The hadron density close to the fragmentation region of protons is however much smaller than for central rapidities, which should make extraction of the mini-jet signal easier. One possible strategy is to select a hadron (a mini-jet) at $y \sim 2 \div 4$ or even higher with the fixed $p_\perp$ and measure the average transverse momentum of hadrons produced at negative rapidities. A distinctive feature of this mechanism is the presence of transverse correlations between hadrons only at small rapidity intervals, $\Delta y \leq 2$, which follow a Gaussian distribution in Δy in contrast to the power law suppression of correlations in the hard mechanism [294]. Another suggestion is to use proton–nucleus scattering to distinguish the production of two pairs of mini-jets in two-parton collisions ($2 \to 4$ mechanism) from the production of four mini-jets in two binary collisions ($4 \to 4$ mechanism) [295]. The procedure is based on the centrality dependence of two mechanisms — the production rate in the $2 \to 4$ mechanism grows linearly with the nuclear thickness, while in the $4 \to 4$ mechanism, it is quadratic in thickness [295].

4.2. Forward direct photon measurements

Prompt photons provide direct access to the parton kinematics since they couple to quarks, and unlike hadrons are not affected by the final-state effects. At leading order (LO), the photon is produced directly at the parton interaction vertex without fragmentation. At LHC collision energies, the quark–gluon Compton cross section is significantly larger than quark–anti-quark annihilation. At next-to-leading order (NLO) or higher order, photons may also be produced by bremsstrahlung or fragmentation of one

of the outgoing partons. However, fragmentation photons are accompanied by hadronic fragmentation products and the contribution of this process can be largely suppressed by application of isolation cuts. Isolation cuts ensure that the remaining particle production process is dominantly from Compton scattering, where the measured photon is directly sensitive to the gluon PDF [296].

In this paragraph, we will focus on direct photon measurements at forward rapidities, as enabled by the LHCb experiment [297, 298] and the planned forward calorimeter (FoCal) upgrade of ALICE [299]. The LHCb is a single-arm spectrometer equipped with tracking and particle-identification detectors as well as calorimeters with a forward angular coverage of about $2 < \eta < 5$. The FoCal is a calorimeter at $3.4 < \eta < 5.8$ consisting of a high-granularity, compact silicon–tungsten (Si+W) sampling electromagnetic part with longitudinal segmentation and a conventional high-granularity metal/scintillating hadronic part providing good hadronic resolution and compensation.

In fact, measurements of isolated photon spectra at forward rapidities at the LHC are sensitive to the gluon density at small Bjorken-x of up to about $x = 10^{-5}$ over a large range of momentum transfer, Q^2. By comparing measurements in p–Pb and pp collisions, one can hence extract the gluon nuclear modification at small x and Q^2. The parton structure of protons and nuclei is described by momentum distributions at an initial momentum scale, and the scale dependence of the structure can be calculated with linear QCD evolution equations, such as the DGLAP [9, 12, 13] and BFKL [3–5, 300] equations. At small x, hadronic structure is expected to evolve non-linearly due to the presence of high gluon densities, as predicted by the JIMWLK [301] and BK [302] evolution equations. These non-linear effects should affect multi-parton dynamics, resulting in phenomena beyond a reduction of inclusive yields, including for instance observable effects in coincidence measurements. Measurements of photon–jet correlations will allow to study this effect quantitatively by constraining the parton kinematics as precisely as possible in hadron interactions.

To illustrate the expected performance of future forward isolated photon measurements, the expected uncertainties of the gluon PDFs for the nNNPDF fit using either pseudo-data for the EIC (starting from nNNPDF1.0) [303] or the FoCal above 4 GeV/c based on nNNPDF2.0 [304], are presented in the left panel of Fig. 13. As expected, the higher-energy option of the EIC (which will be realized by eRHIC at BNL) will constrain the gluon PDF for x down to about 5×10^{-3}, while isolated photon measurements provided by the FoCal would lead to significantly improved uncertainties even significantly below 10^{-4}. We also note that the uncertainty on the nNNPDF2.0 parametrization is already smaller than the EIC band. The fit to EIC

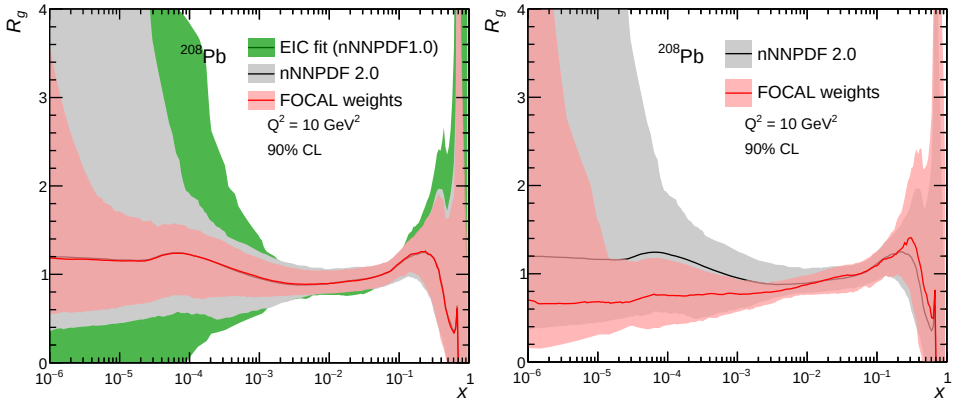

Fig. 13. The nuclear modification of the gluon distribution, R_g, for the Pb nucleus *versus* x at $Q^2 = 10$ GeV$^2/c^2$. Left: Compared are the nNNPDF2.0 parametrization [304] and fits to the FoCal pseudo-data above 4 GeV/c (red band), as well as "high energy" EIC pseudo-data (green band; starting from the nNNDPF1.0 parametrization) [303]. In all cases, 90% confidence-level uncertainty bands are drawn, and the nuclear PDFs are normalized by the proton NNPDF3.1. Right: Comparison of the original and the reweighted nNNPDF2.0 fits, where the FoCal pseudo-data were shifted by about 0.7 [304].

pseudo-data from the nNNPDF group gives a qualitatively similar result to an earlier study based on modified EPPS16 nuclear PDFs [305], although the uncertainty estimates at small x where there is no direct constraint from the pseudo-data differ. Clearly, the FoCal measurements will probe much smaller x than the existing and possible future EIC measurements, and lead to high precision results due to the excellent direct photon performance. However, in the case of the EIC, unlike at a hadron collider, the initial state is precisely known, and one can map x and Q^2, independently, and measure not only longitudinal but also generalized parton (GPDs) and transverse-momentum (TMDs) distributions [118]. Furthermore, the EIC will allow us to scan the A (nucleus) dependence using several nuclear beams.

So far, it was assumed in the re-weighting process that the central value of the FoCal measurement of the isolated photon $R_{p\mathrm{Pb}}$ would be the same as the central value of the initial baseline prediction. Instead, in the right panel of Fig. 13, we show the effect of the FoCal pseudo-data for a value of $R_{p\mathrm{Pb}}$ shifted to about 0.7. In this case, the FoCal data would add a significant amount of new information to the global fit, leading to a deviation of R_g from the expected value in almost the entire range of $10^{-5} < x < 10^{-2}$. Therefore, this analysis indicates that FoCal measurements could be sensitive either to the gluon shadowing effects or to possible non-linear QCD dynamics. To

disentangle one from the other, a dedicated analysis of the χ^2 in global pdf fits and the nPDF behavior in the small-x region would be required, following the approach of Ref. [162].

Significant suppression of R_g arises also from forward charm measurements [306] when they are included in the determination of nuclear PDFs as recently done [307]. In this case, comparing precise forward photon and charm measurements will allow us to test factorization and universality of the nuclear PDFs. Fig. 13.

4.3. Top-quark pair production as a tool to probe Quark–Gluon-Plasma formation

Past deep-inelastic-scattering (DIS) experiments provided accurate information on the partonic structure of the free proton. Notwithstanding the phenomenological success of Quantum Chromodynamics (QCD) analyses, a detailed understanding of the partonic structure modifications in bound nuclei is still lacking. Compared to the parton distribution functions (PDFs) in the proton, nuclear PDFs (nPDFs) are less constrained mainly because of the lack of data across the momentum fraction x-squared momentum transfer Q^2 plane and nuclear mass number range. The scheduled proton–lead (pPb) and lead–lead (PbPb) LHC Runs 3–4 at the LHC provide the opportunity to precisely constrain the nPDFs for the lead nucleus. This is demonstrated in Fig. 14, where a simple projected scenario of the existing CMS measurement [308] is assumed, considering improvements in the statistical and currently dominant systematic uncertainties, respectively. There is even a complementarity between the physics programs at the LHC and the planned Electron Ion Collider, allowing for stringent tests of the nPDF universality too. Top quark production (inclusively or differentially) in pPb and PbPb collisions has been suggested as a valuable probe of the high-$x$$\sim$$10^{-2}$–$10^{-1}$ gluon distribution at very high Q^2 in the Pb ions [309].

One powerful probe of the quark–gluon plasma (QGP) is "jet quenching", *i.e.*, the study of jet modifications while passing through the QGP. Processes used so far, *e.g.*, dijet or Z/γ+jet production, are only sensitive to the properties of the QGP integrated over its lifetime. Hadronically decaying W bosons can provide novel key insights into the time structure of the QGP when studied in events with a top–anti-top quark pair [313] thanks to a "time delay" between the moment of the collision and that when the W boson decay products start interacting with the QGP. Although there seems to exist limited potential to bring the first information on the time structure of the QGP considering the baseline LHC scenario of Runs 3–4, lighter ions

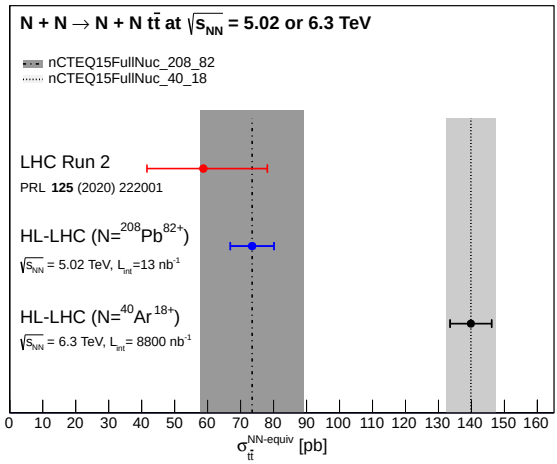

Fig. 14. Comparison of inclusive top-quark pair production cross sections measured at LHC Run 2 [308] and projected at HL-LHC with either lead–lead or argon–argon collisions. Vertical lines and bands represent Quantum Chromodynamics predictions at next-to-next-to-leading order with soft-gluon re-summation at next-to-next-to-leading logarithmic accuracy [310, 311], with nuclear modification effects and their uncertainties, respectively, as parametrized by the nCTEQ15 bound-nucleon distribution functions [312]. The shown cross-section values are their nucleon–nucleon equivalent.

are potentially promising candidates despite their expected smaller quenching effects. Due to the potential for order-of-magnitudes higher effective integrated nucleon–nucleon luminosities, in this paragraph, we advocate the usage of an "optimal" nucleus–nucleus colliding system at the HL-LHC. Such an example for the inclusive top-quark pair production cross section is also shown in Fig. 14, considering the expected luminosity increase for the case of argon–argon collisions [314]. Substantially increased LHC partonic and photon–photon luminosities at the HL-LHC (or future higher-energy colliders) could be also achieved via isoscalar beams, even opening up opportunities for studies not accessible with high-pileup collisions [315]. The high-luminosity collisions of isoscalar nuclei could provide a new environment to study the QGP and complement the QGP studies in the low-luminosity collisions of heavy nuclei.

5. Ultra-peripheral collisions at hadronic colliders and exclusive reactions at the EIC

Main Contributors: M.A. Alcazar Peredo, J.G. Contreras, M. Hentschinski, S. Klein, D. Tapia Takaki

5.1. Existing measurements on diffractive vector meson photoproduction in UPCs

Photons are clean probes of the QCD structure of nuclear targets [316, 317]. At hadron colliders, such as RHIC and the LHC, photoproduction processes can be studied in ultra-peripheral collisions (UPCs), where the incoming particles pass each other at impact parameters larger than the sum of their radii, such that strong interactions are suppressed and photon-induced processes are dominant. For a recent review, see [318].

The most measured process in UPCs is the diffractive production of vector mesons. Photons fluctuate to virtual $q\bar{q}$ pairs which then scatter elastically from nuclear targets, emerging as real vector mesons. They are copiously produced. Their decays into few charged particles provide clean experimental signatures that can be used to trigger and select the corresponding events. On the theoretical side, the different vector meson masses allow us to study QCD at different scales: the production of a ρ^0 serves to investigate the approach to the black-disc limit of QCD, while that of a J/ψ sheds light onto aspects of perturbative QCD at high energies such as saturation [319] and shadowing [320]. Additionally, in the Good–Walker approach [321, 322], coherent and incoherent processes where the photon interacts with the full target or just with a piece of it, respectively, give access to the average behavior of the gluonic field (coherent) or to the variance of its quantum fluctuations (incoherent). Figure 15 shows the x and Q^2 ranges covered by UPCs at the LHC.

The coherent photoproduction of ρ^0 vector mesons off nuclear targets has been extensively studied in UPCs. The STAR Collaboration at RHIC has published measurements in Au–Au UPCs at different centre-of-mass energies per nucleon pair, $\sqrt{s_{NN}}$: 62.4 GeV [323], 130 GeV [324], and 200 GeV [325]. At the LHC, the ALICE Collaboration has carried out measurement at 2.76 TeV [326] and 5.02 TeV [327] in Pb–Pb UPCs and at 5.55 TeV in Xe–Xe UPCs [328]. The measured ρ cross-section is seen to scale nearly linearly with the atomic number, with ALICE finding a best fit $\sigma \propto A^{0.96\pm0.02}$. The cross section is smaller than is expected from a Glauber calculation (even including generalized vector meson dominance), but is consistent with a Glauber–Gribov calculation [329]. The latter approach includes high-mass intermediate state fluctuations. These topics can be further studied by examining excited meson states.

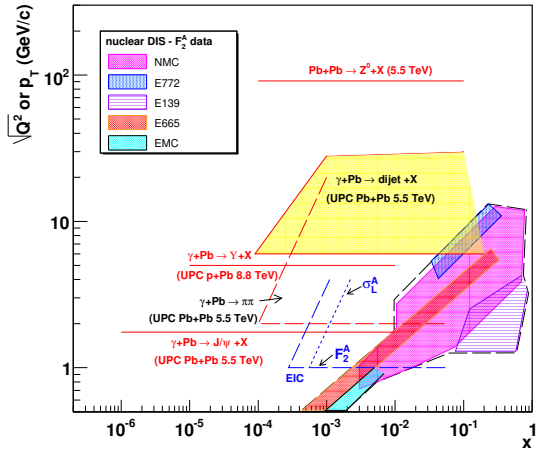

Fig. 15. The kinematic range in which UPCs at the LHC can probe gluons in protons and nuclei in quarkonium production, dijet, and di-hadron production. The Q value for typical gluon virtuality in exclusive quarkonium photoproduction is shown for J/Ψ and Υ. The transverse momentum of the jet or leading pion sets the scale for dijet and $\pi\pi$ production respectively. For comparison, the kinematic ranges for J/Ψ at RHIC, F_2^A and $\sigma_{\rm L}^A$ at eRHIC, and Z^0 hadroproduction at the LHC are also shown. Figure taken from [317].

The STAR Collaboration [330] also observed the coherent production of four charged pions [330] which could be related to an excited state of the ρ^0 vector meson but at a perturbative scale. Determining the cross section is not possible without making assumptions about the branching ratios, but the rate seems consistent with the expectations of generalized vector meson dominance [331]. Both collaborations also observed an intriguing signal of a state in coherent di-pion production at mass around 1.7 GeV/c^2 which could be related to another ρ^0 excited state [327, 332].

All these studies were performed at mid-rapidity in the corresponding laboratory frame. The availability of data for all these systems and energies provides an exacting challenge to theoretical descriptions of this process, whose cross section has been described more or less successfully using a variety of approaches; *e.g.* [333–335]. In addition, there are at least three specific measurements to highlight: (*i*) The observation of interference effects originated in the fact that each of the two incoming projectiles can act either as a source of the photon or as a target of the interaction [336, 337], (*ii*) the mapping of the impact-parameter dependence of the target structure for gold ions obtained as a Fourier transform of the Mandelstam-t dependence of the cross section [325], and (*iii*) the dependence on the atomic mass number of this process at centre-of-mass energy of the photon–nucleus system of

65 GeV per nucleon obtained from measurements off Pb [327], Xe [328], and protons [338], where a clear indication of strong shadowing was found along with the observation that the black-disc limit of QCD has not been yet reached.

Regarding the diffractive photoproduction of J/ψ, the main results from UPCs have been obtained at the LHC [339] after a first proof-of-principle measurement at RHIC [340]. Coherent production has been investigated by the ALICE Collaboration in two ranges of rapidity, central and forward, and two different energies $\sqrt{s_{NN}} = 2.76$ TeV and 5.02 TeV [341–345]. The CMS Collaboration published a cross section at semi-central rapidities [346] at $\sqrt{s_{NN}} = 2.76$ TeV, and recently the LHCb Collaboration presented results of $\sqrt{s_{NN}} = 5.02$ TeV covering forward rapidities [347]. Together, these measurements allow for the study of the rapidity dependence of J/ψ diffractive photoproduction in a large kinematic range which corresponds to three orders of magnitude in Bjorken x from 10^{-2} to 10^{-5}. These results provide new constraints on the evolution of the nuclear gluon distribution at large energies, see *e.g.* [348, 349]. In particular, the results from [345] provide a look at the transverse structure of Pb nuclei at the Bjorken-x range $(0.3\text{–}1.4)\times10^{-3}$ which are the first step toward the mapping of the gluon distribution in impact parameter at a perturbative scale. A proof-of-principle measurement for incoherent production has been performed by the ALICE Collaboration in Pb–Pb UPCs at $\sqrt{s_{NN}} = 2.76$ TeV [342].

The coherent production of ψ' has also been measured by the ALICE Collaboration [344, 350]; this state is interesting to understand the spin structure of the interaction, in particular, to constraint the modeling of the wave function of the vector meson (see *e.g.* [351]), which is a non-perturbative component of all theoretical predictions. Finally, the CMS Collaboration has made an initial measurement of Υ photoproduction in pA collisions [352]. Another interesting related result is the measurement of coherent J/ψ photoproduction in *peripheral* collisions, that is with a geometrical overlap of the colliding nuclei, that have been performed by the ALICE Collaboration in the Pb–Pb system [353] and by the STAR Collaboration in the Au–Au and U–U systems [354]. These measurements open up interesting questions about the meaning of coherence in these quantum processes and the possibility to study new effects, *e.g.* the interaction of the J/ψ with the quark–gluon plasma created in such collisions [355–357]. They also offer a tool to study the energy dependence of J/ψ production by offering a measurement in a different impact-parameter range than those in UPCs [358].

5.2. Future measurements on diffractive vector meson photoproduction in UPCs

In the near future, Runs 3 and 4 of the LHC will provide an enormous data set of UPCs; see *e.g.* Table 12 of [314]. In the middle term, the Electron Ion Collider will be the experimental facility to study the QCD structure of nuclei, including diffractive vector-meson production [117].

One of the key measurements to be performed with the new LHC data set is the Bjorken-x evolution of coherent diffractive vector-meson production for as many different mesons — that is mass scales — as possible. To achieve this, the two contributions to the nucleus–nucleus cross section, one with a high-, the other with a low-energy photon have to be disentangled. In principle, this requires performing a given measurement at a fixed rapidity, but different impact-parameter ranges. There are two proposals on how to do this: using UPCs in conjunction with the peripheral collisions mentioned above [358], and using events where in addition to the photon exchange producing the vector meson, there is an extra nuclear dissociation process that acts as a selector of a different impact-parameter range [359, 360]. Measurements of coherent ρ^0 production at mid-rapidity in Pb–Pb [327] and Xe–Xe [328] UPCs accompanied by neutrons at beam rapidities, the product of the nuclear dissociation, are correctly described by the NOON model [361] giving us confidence that the relevant physics is understood (at the current precision of the data) and paving the way to the application of this method.

Another eagerly awaited measurement is the dependence on Mandelstam-t of the incoherent production of vector mesons at a given rapidity. This process is sensitive to quantum fluctuations at the sub-nucleon scale [362]. Model predictions, *e.g.* [363, 364], expect one order of magnitude increase of the cross section at $|t| \sim 1$ GeV^2 when the sub-nuclear quantum fluctuations are taken into account with respect to the case where the relevant degrees of freedoms are the nucleons. Such a measurement will be feasible at the LHC in the near future.

Another interesting measurement to be performed at the LHC is the study of the angular correlations of the decay products of the vector meson. Both the quasi-real photons and the gluons participating in the interaction are linearly polarised. This and the presence of the interference effects mentioned above produce new angular correlations with a particular dependence on the transverse momentum of the vector meson. These observables are a complement to the traditional polarisation measurements and are also sensitive to the QCD structure of the target. See *e.g.* [365–367].

At least two other techniques can be used to measure gluon distributions using UPCs: dijets and open charm. These measurements are theoretically cleaner than vector mesons, since they involve only single-gluon exchange,

so the uncertainties involving color neutralization are much smaller. However, the final states are more complicated, and since there is a color string connecting the mid-rapidity state and the target nucleon remnants, the reaction cannot be fully exclusive. The ATLAS Collaboration has already made the first preliminary measurements of dijet photoproduction [368]. ATLAS explored the region where the leading jet had $p_\perp > 20$ GeV, and dijet mass above 35 GeV, giving them a reach down to $x \approx 3 \times 10^{-3}$. Charm photoproduction is an attractive alternative approach to reach down to lower-x values, since it should be possible to measure charm down to threshold, $M_{c\bar{c}} \approx 4$ GeV. The rates for charm are high [369–371], and, at the LHC, open $b\bar{b}$ and potentially, with pA collisions or lighter ions, $t\bar{t}$ [372].

5.3. The ratio of $\Psi(2s)$ and J/Ψ photoproduction cross-sections as a tool to quantify non-linear QCD evolution

Exclusive photoproduction of charmonium at the Large Hadron Collider (LHC) provides an excellent testing ground for the description of the low-x gluon distribution since it allows for a direct observation of the energy dependence of the photoproduction cross-section which directly translates into the x-dependence of the underlying gluon distribution. Photoproduction of bound states of charm quarks, *i.e.* J/Ψ and $\Psi(2s)$ vector mesons, is of particular interest, since the charm mass provides a hard scale at the border between soft and hard physics, and the observable is therefore expected to be particularly sensitive to the possible presence of a semi-hard scale associated with the transition to the saturation region, the so-called saturation scale. It is therefore ideal to search for potential deviations from linear QCD evolution.

Studies in the literature for this process, which take into account effects due to gluon saturation, exist both on the level of dipole models [364, 373–378] and complete solutions to the non-linear BK equation [379–381]. At the same time, also descriptions of colinear factorization [382–386] and linear NLO BFKL evolution [136, 381], provide an excellent description of data, see also the discussion in [138, 381]. It is therefore not entirely clear, which is the appropriate description of data. While, at first, one might conclude that center-of-mass energies are simply not yet high enough to see the onset of non-linear effects, there are also indications that at least some linear frameworks turn unstably at the highest center-of-mass energies available at LHC [381].

A similar conclusion has been drawn in [138], where it has been found that the energy dependence of the J/Ψ and $\Psi(2s)$ cross section is not able to distinguish between the non-linear (Kutak–Sapeta (KS) gluon [387], subject to non-linear Balitsky–Kovchegov (BK) evolution) and linear (Hentschinski–

Salas–Sabio Vera gluon (HSS) [126, 127], subject to linear NLO BFKL evolution) low-x evolution. On the other hand, the ratio of both cross sections was found to reveal a characteristically different energy dependence for linear and non-linear QCD evolution, see Fig. 16 (left). Leaving large

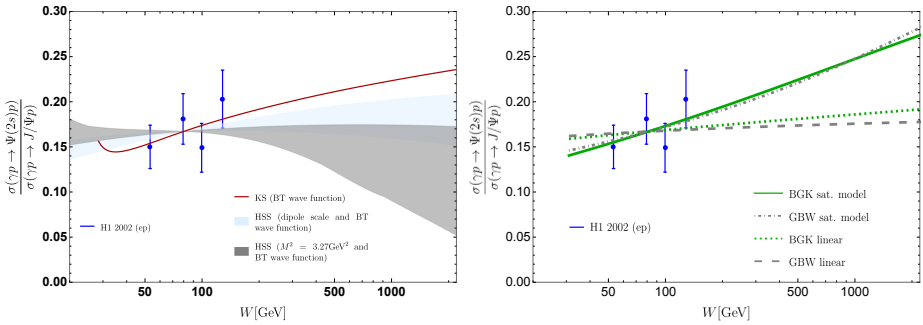

Fig. 16. Energy dependence of the ratio of $\Psi(2s)$ *versus* J/Ψ photoproduction cross section. We further display photoproduction data measured at HERA by the H1 Collaboration [388], which we further use to adjust the normalization. Left: Implementation of the KS and HSS gluon distributions for the Buchmüller–Tye (BT) vector meson wave functions, see [166] for details. The shaded regions correspond to a variation of the scale $\bar{M} \to \{\bar{M}/\sqrt{2}, \bar{M}\sqrt{2}\}$. Right: Implementation based on the BKG and GBW saturation model and their corresponding linearized versions, using numerical values found in [389] from a fit to HERA data.

uncertainties associated with fixed scale HSS evolution aside (see [138] for a detailed discussion), the stabilized "dipole scale" HSS gluon, subject to linear NLO BFKL evolution predicts a constant ratio of both photoproduction cross section. The KS gluon, subject to non-linear BK evolution, predicts on the other hand a rise in the ratio. To understand this behavior better, it is instructive to analyze the same observable within a simple saturation model. The latter yields a particular simple form which allows us to gain some intuitive understanding why linear and non-linear QCD dynamics yield a different prediction for the $\Psi(2s)$ over J/Ψ ratio. In the high-energy limit, the relevant quantity of interest is the imaginary part of the scattering amplitude,

$$\begin{aligned} &\Im\mathcal{A}_{\gamma p\to Vp}\left(W^2, t=0\right) \\ &= \int \mathrm{d}^2\boldsymbol{r} \left[\sigma_{q\bar{q}}\left(\frac{M_V^2}{W^2}, r\right)\bar{\Sigma}_\perp^{(1)}(r) + \frac{\mathrm{d}\sigma_{q\bar{q}}\left(\frac{M_V^2}{W^2}, r\right)}{\mathrm{d}r}\bar{\Sigma}_\perp^{(2)}(r)\right], \end{aligned} \tag{20}$$

which encodes the energy dependence related to the low-x evolution of inclusive low-x evolution. Here, $r = |\boldsymbol{r}|$ the transverse separation of the quark–

anti-quark pair, the z the photon momentum fraction, and $\bar{\Sigma}_{\perp}^{(1,2)}$ describes the transition of a transverse polarized photon into a vector meson V [390], see [166] for details. Within this approach, the entire energy dependence is contained in the dipole cross section $\sigma_{q\bar{q}}$, which for the Golec-Biernat–Wüsthoff saturation model takes the following simple form [391]:

$$\sigma_{q\bar{q}}(x,r) = \sigma_0 \left(1 - \mathrm{e}^{-r^2 Q_{\mathrm{s}}^2(x)/4}\right) , \qquad Q_{\mathrm{s}}^2(x) = Q_0^2 (x/x_0)^{\lambda} , \tag{21}$$

where $Q_{\mathrm{s}}(x)$ yields within this model the saturation scale, which carries the entire energy dependence; a linearized version of this model, which yields a power-like growth with energy is then obtained through an expansion of the above expression for small saturation scales

$$\sigma_{q\bar{q}}^{\mathrm{lin}}(x,r) = \sigma_0 r^2 Q_{\mathrm{s}}^2(x)/4 . \tag{22}$$

Inserting Eq. (22) into Eq. (20), it is immediately clear that the saturation scale — which carries the essential W dependence — cancels for the ratio of $\Psi(2s)$ and J/Ψ photoproduction cross sections, up to a small logarithmic correction, related to the energy dependence of the diffractive slope of J/Ψ and $\Psi(2s)$ cross sections [166, 390]. While the complete saturation model agrees with the linear approximation in the region of $r \to 0$, they start to disagree for large dipole sizes and it is this region where the wave-function overlap differs for the production of vector mesons $\Psi(2s)$ and J/Ψ due to the presence of the node in the $2s$ wave function. We further show results due to the DGLAP improved saturation model, the so-called Bartels–Golec-Biernat–Kowalski (BGK) model, which replaces $Q_{\mathrm{s}}^2(x) \to 4\pi\alpha_{\mathrm{s}}(\mu(r))xg(x,\mu(r))/3$, where $\alpha_{\mathrm{s}}(\mu)$ and $xg(x,\mu)$ denote the strong coupling constant and the colinear gluon distribution respectively, evaluated at an r-dependent scale μ in the perturbative region. Similar to the HSS gluon, such a dipole-size-dependent saturation scale prevents an exact cancellation of the energy dependence in the linear approximation. Nevertheless, this merely affects the perturbative region of small dipole sizes $r < 1$ GeV^{-1} and, therefore, maintains the observed rise of the ratio for the complete saturation *versus* an approximately constant ratio for the linear approximation. We therefore suggest to extract from existing data and future measurements $\Psi(2s)$ and J/Ψ ratio, since the energy behavior of this ratio allows to draw a conclusion on the presence of non-linear QCD dynamics. The feature is both present for unintegrated gluon distributions, which have been obtained from a numerical solution to linear and non-linear QCD evolution, fitted to DIS data, as well as for analytic dipole models, where the distinction of linear and non-linear realization is somehow easier. While there exist LHCb data for the energy dependence of the J/Ψ and $\Psi(2s)$ photoproduction cross section, extracted from pp collisions [392] (see also [344] for PbPb data), there exist only H1 data for

the energy dependence of the ratio of both cross sections, at relatively low values of W and with still considerable uncertainties. We believe that extraction of the ratio from both combined HERA and LHC data would be highly beneficial to pin down the size of non-linear low x QCD evolution at the LHC.

5.4. Planned measurements at the Electron Ion Collider

Looking further ahead, in the early 2030s, the U.S. Electron Ion Collider (EIC) should provide high-precision measurements of vector mesons over a wide range of Bjorken-x and Q^2; the Q^2 of the photon can be measured independently of the rest of the reaction, allowing us to probe the nucleus using $q\bar{q}$ dipoles of different lengths [117, 118]. The high center-of-mass energy (up to about 140 GeV) and high luminosity will allow the EIC to study large samples of light and heavy mesons (including the three Υ states) [393]. The expected event samples range from about 50 billion ρ^0 per year down to about 140,000 $\Upsilon(1S)$ per year. It will also be able to study exotic states (including the XYZ states) via Reggeon exchange reactions [394, 395]. The high luminosity will allow for precise multi-dimensional studies, including measurements of the Generalized Parton Distributions, measurements out to kinematic extremes (*i.e.* large $|t|$ *etc.*), and studies of rarely produced mesons and decays.

The EIC will take data with a variety of different ions, so will be able to study how low-x gluons evolve with nuclear size. Light ions will be of special interest. The EIC detectors forward spectrometers are expected to be able to detect scattered protons and light ions, allowing for a measurement of $|t|$ even if the scattered electron is not seen or poorly measured. Light-ion studies will allow for the study of neutron targets, and studies with deuterium and other very light ions will allow for measurements of the nuclear force in relatively simple systems.

The EIC detectors are being designed to be extremely hermetic, so will be able to record vector mesons over a wide range in Bjorken-x and to accurately separate coherent and incoherent production over a wide range of $|t|$ [118]; this is necessary to fully apply the Good–Walker paradigm. The large event samples and precision detectors will allow for precise studies of the variation in gluon density and transverse position within the target. The inclusion of relatively precise calorimetry that is sensitive down to low energies will allow us to study final states that include γ and π^0, allowing for the study of a wider range of mesons.

6. Odderon discovery and diffractive jets

Main contributor: Ch. Royon

In this section, we provide some details on the recent discovery of the Odderon as well as inclusive diffractive measurements and explorations of the soft Pomeron structure.

6.1. Soft diffraction and the Odderon discovery by the D0 and TOTEM experiments

Soft diffraction and elastic interactions have been studied for the last 50 years at different colliders. Elastic pp and $p\bar{p}$ scattering at high energies of the Tevatron and the LHC, for instance, corresponds to the $pp \to pp$ and $p\bar{p} \to p\bar{p}$ interactions, where the protons and anti-protons are intact after interaction and scattered at a very small angle, and nothing else is produced. In order to measure these events, it is necessary to detect the intact protons/anti-protons after interactions in dedicated detectors called Roman Pots and to veto any additional activity in the main detector.

Many experiments have been looking for evidence of the existence of the Odderon [396, 397] in the last 50 years, and one may wonder why the Odderon has been so elusive. At ISR energies, at about a center-of-mass energy of 52.8 GeV [398–402], there was already some indication of a possible difference between pp and $p\bar{p}$ interactions. Differences are about 3σ but this was not considered to be a clean proof of the Odderon. This is due to the fact that elastic scattering at low energies can be due to exchanges of additional particles to Pomeron and Odderon, namely ρ, ω, ϕ mesons, and Reggeons. It is not easy to distinguish between all these possible exchanges, and it becomes quickly model-dependent. This is why the observed difference at 52.8 GeV was estimated to be due to ω exchanges and not to the existence of the Odderon. The advantage of being at higher energies (1.96 TeV for the Tevatron and 2.76, 7, 8, and 13 TeV at the LHC [403–407]) is that meson and Reggeon exchanges can be neglected. It means that a possible observation of differences between pp and $p\bar{p}$ elastic interactions at high energies would be a clear signal of the Odderon. The D0 and TOTEM elastic $\mathrm{d}\sigma/\mathrm{d}t$ data are shown in Fig. 17. The difficulty to compare between pp and $p\bar{p}$ elastic scatterings is that one has to extrapolate the pp measurements from TOTEM to Tevatron center-of-mass energies [408].

The comparison between the $p\bar{p}$ elastic $\mathrm{d}\sigma/\mathrm{d}t$ measurement by the D0 Collaboration and the extrapolation of the TOTEM pp elastic $\mathrm{d}\sigma/\mathrm{d}t$ measurements is shown in Fig. 18, including the 1σ uncertainty band as a red dashed line [408]. The comparison is only made in the common t domain for both pp and $p\bar{p}$ measurements and shows some differences in the dip and

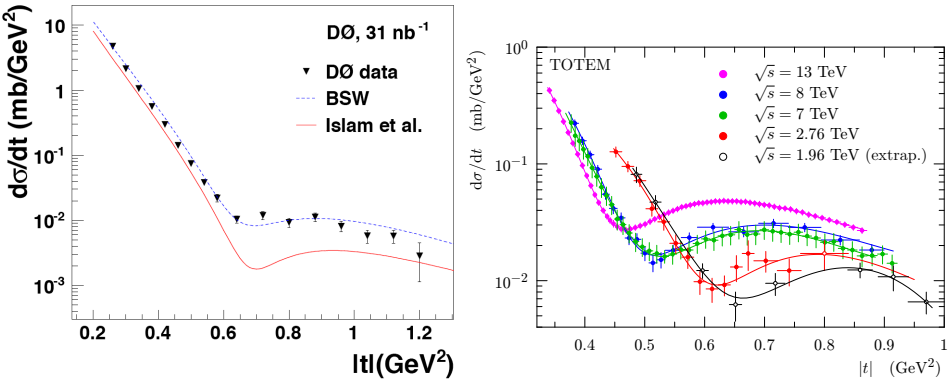

Fig. 17. Left: $p\bar{p}$ elastic cross section as a function of $|t|$ at 1.96 TeV from the D0 Collaboration at the Tevatron. Right: pp elastic cross sections as a function of $|t|$ at 2.76, 7, 8, and 13 TeV from the TOTEM Collaboration at the LHC (full circles), and extrapolation to the Tevatron center-of-mass energy at 1.96 TeV (empty circles).

bump region between $|t|$ of 0.55 and 0.85 GeV^2. Given the constraints on the optical point normalization and logarithmic slopes of the elastic cross sections, the χ^2 test leads to a significance of 3.4σ. Combining this result with previous measurements of TOTEM of ρ [409] and the total cross section, the significance ranges from 5.3 to 5.7σ (depending on the model). Models without colorless C-odd gluonic compound or the Odderon are excluded by more than 5σ.

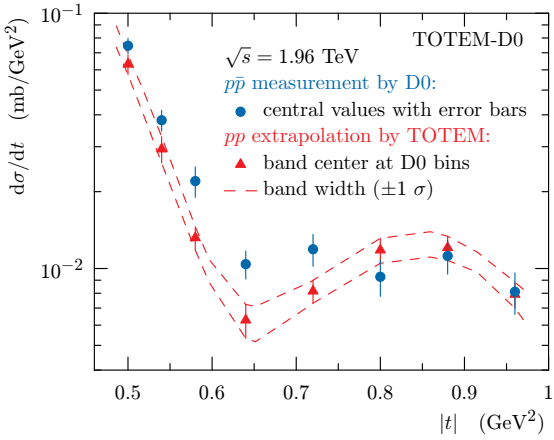

Fig. 18. Comparison between the D0 $p\bar{p}$ measurement at 1.96 TeV and the extrapolated TOTEM pp cross section, re-scaled to match the OP of the D0 measurement. The dashed lines show the 1σ uncertainty band on the extrapolated pp cross section.

Further measurements of elastic pp cross sections will happen at higher LHC energies (such as 13.6 and 14 TeV) and the Odderon production will be performed in additional channels, such as the production of ω mesons. It is also clear that the discovery of the Odderon is likely related to the existence of glueballs, and the search for their production will happen at the LHC, RHIC, and the EIC.

6.2. Inclusive diffraction measurements at the LHC and sensitivity to the Pomeron structure

Hard diffraction corresponds to events when at least one proton is intact after the interaction at the LHC and corresponds to the exchange of a colorless object called the Pomeron. Many measurements at the LHC can constrain the Pomeron structure in terms of quarks and gluons that has been derived from QCD fits at HERA and at the Tevatron. All the studies have been performed using the Forward Physics Monte Carlo (FPMC), a generator that has been designed to study forward physics, especially at the LHC [410, 411].

One can first probe if the Pomeron is universal between ep and pp colliders or, in other words, if we are sensitive to the same object at HERA and the LHC. Tagging both diffractive protons in ATLAS and CMS allows to probe the QCD evolution of the gluon and quark densities in the Pomeron and to compare with the HERA measurements. In addition, it is possible to assess the gluon and quark densities using the dijet and γ+jet productions [412–415]. The different diagrams of the processes that can be studied at the LHC are shown in Fig. 19, namely double Pomeron exchange (DPE) production of dijets (left), of γ+jet (middle), sensitive respectively to the gluon and quark contents of the Pomeron, and the jet–gap–jet events (right).

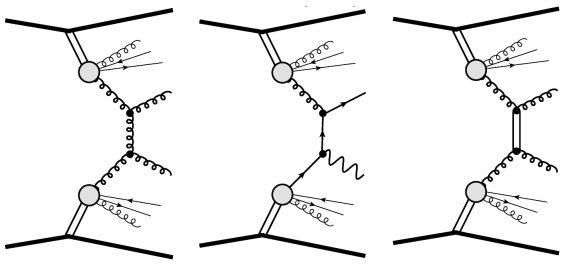

Fig. 19. Inclusive diffractive diagrams. From left to right: jet production and γ+jet production in inclusive double Pomeron exchange, as well as jet–gap–jet events involving double Pomeron exchange.

The measurement of the dijet cross section is directly sensitive to the gluon density in the Pomeron and the γ+jet and W asymmetry measurements [415] are sensitive to the quark densities in the Pomeron. However, diffractive measurements are also sensitive to the survival probability which needs to be disentangled from PDF effects, and many different measurements will be needed to distinguish between them.

It is clear that better understanding of diffraction and probing different models will be one of the key studies to be performed at the high luminosity LHC, the EIC, and any future hadron collider.

7. Electroweak and Beyond the Standard Model physics

Main Contributors: C. Baldenegro, A. Bellora, V.P. Gonçalves, S. Fichet, G. von Gersdorff, V. Khoze, M. Pitt, Ch. Royon, G. Gil da Silveira, M. Tasevsky

While the bulk of this white paper focuses on aspects related to strong interactions in the limit of high energies and densities, there exists also an increased interest in the study of electroweak processes, which rely on dedicated forward detectors for their analysis and which are capable to contribute to searches for new physics at the LHC.

7.1. Precision Proton Spectrometer (PPS) and ATLAS Forward Proton detector (AFP) at high luminosity

7.1.1. Introduction

The CERN's Large Hadron Collider (LHC) will be re-starting its operation this year at a record-breaking energy of $\sqrt{s} = 13.6$ TeV. The physics run is expected to last until the end of 2025, collecting integrated luminosity of about 300 fb^{-1}. The LHC will undergo a major upgrade following the four-year physics run, increasing its instantaneous luminosity by a factor of 5–10 larger than the nominal LHC value. The High Luminosity LHC (HL-LHC) is expected to collect data corresponding to an integrated luminosity of a few ab^{-1}, and measure the rarest processes of the Standard Model (SM).

Central Exclusive Production (CEP) is a unique process where an object X is produced via the t-channel exchange of colorless objects, photon (γ) for electromagnetic or Pomeron ($\mathbb{P}$) for strong interactions, $pp \to p \oplus X \oplus p$, where $\oplus$ stands for an absence of additional interaction between the final states. When final-state particles are produced with high invariant mass, the dominant production mechanism is via photon exchange [416], in which the LHC can be considered a photon collider. Figure 20 shows a comparison between Pomeron–Pomeron ($\mathbb{P}$–$\mathbb{P}$) and photon–photon (γ–γ) initiated

processes for production cross section of central exclusive $b\bar{b}$ and $\gamma\gamma$ events as a function of mass, which shows the enhancement of the photon–photon scattering at high masses.

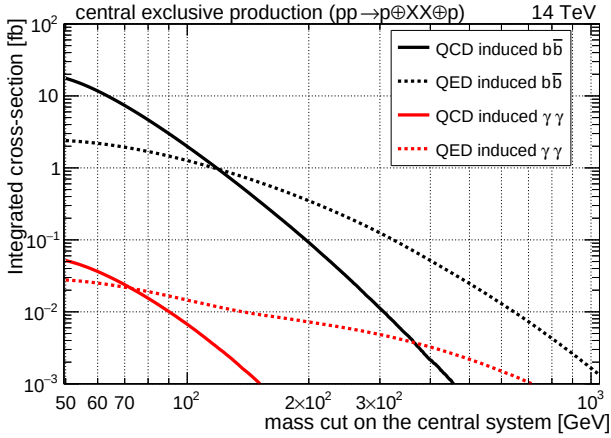

Fig. 20. Integrated cross sections of different exclusive processes with intact protons at $\sqrt{s} = 14$ TeV, plotted as a function of the required minimum central system mass. Taken from Ref. [417].

In CEP, interacting protons often emerge intact but lose a fraction of momentum and are scattered at small angles. The LHC accelerator magnets can be seen as longitudinal momentum spectrometers. The protons are deflected away from the proton bunch and can be measured by near-beam detectors installed downstream the LHC beamline, hundreds of meters from the interaction point. Such detectors, installed in movable vessels (Roman Pots) with tracking and timing capabilities, were brought online during Run 2 in 2016 by the ATLAS and CMS collaborations and were operated in standard runs.

7.1.2. Near-beam proton spectrometers in LHC Runs 2 and 3

The Precision Proton Spectrometer (PPS) [418] is a CMS sub-detector installed in 2016, $\sim$ 210 meters from the interaction point. Initially called CT-PPS (started as CMS and TOTEM project), the PPS apparatus is equipped with tracking and timing detectors. It collected more than 100 pb^{-1} of integrated luminosity during LHC Run 2 and will continue to be operational with some upgrades and optimizations during LHC Run 3. During Run 2, PPS tracking detectors measured protons that have lost approximately 2.5% to 15% of their initial momentum, resulting in mass acceptance between 350 GeV to 2 TeV [419]. The data collected with PPS during 2016, with an integrated luminosity of 10 fb^{-1}, led to the first measurement of

central exclusive di-lepton production [420], and the first search for the high mass exclusive production of photon pairs [421], both using tagged protons. Next, using 2017 data and integrated luminosity of ~ 30 fb^{-1} a search for the exclusive production of pair of top quarks and a search for new physics in the missing mass spectrum in $pp \to p \oplus Z/\gamma + X \oplus p$ events were performed [422, 423]. Finally, searches for the exclusive production of di-bosons using the full Run 2 dataset were published as well [424].

The ATLAS Forward Proton detector (AFP) [425], comprises two Roman Pot stations on each side from the interaction point with four planes of silicon pixel sensors to measure proton tracks. The far stations are additionally equipped with time-of-flight (ToF) detectors. During Run 2, ToF detectors demonstrated 20–40 ps resolution but suboptimal efficiency. AFP recorded ~ 30 fb^{-1} of integrated luminosity during Run 2, and this data was used to report on the exclusive di-lepton production [426].

7.1.3. Physics perspectives at HL-LHC

For the HL-LHC (LHC Run 4), the accelerator will be re-arranged, and the current forward detectors will be dismounted. While the new detector design of forward proton spectrometers is currently under development (for example [417]), the physics perspectives are presented in the following section. Two scenarios are under consideration:

— Station located in a "warm" region — comprise a few stations ~ 200 m from the interaction point, and which are suitable for the Roman Pot technology (ATLAS and CMS),

— Station located at 420 m in a "cold" region — which requires a bypass cryostat and a movable detector vessel approaching the beam from between the two beam pipes, for which new developments are needed (CMS).

While QCD-induced processes are typically dominant at low masses, the photon–photon scattering is enhanced at high masses (Fig. 20). Fiducial cross sections for different Standard Model processes at $\sqrt{s} = 14$ TeV for $\mathbb{P}$–$\mathbb{P}$ and γ–γ production modes are shown in Table 2 for different CMS PPS acceptance scenarios in HL-LHC [417].

Physics w/o 420-meter station:

Standard Model $\gamma\gamma \to \ell^+\ell^-$ production is an important channel for both calibration and validation of the proton reconstruction, and measuring ElectroWeak contribution to the Drell–Yan processes. In addition, the $\gamma\gamma \to \tau^+\tau^-$ channel is of particular interest as it is sensitive to the anomalous magnetic moment (or "$g-2$") of the τ lepton. For di-boson production,

Table 2. Fiducial cross sections of CEP of Standard Model processes in pp collisions at $\sqrt{s} = 14$ TeV. Two scenarios for proton tagging acceptance are shown: with and without the stations at ±420 m. (More details in [417].).

Process	Fiducial cross section [fb]			
	all stations		w/o 420	
	$\mathbb{P}$–$\mathbb{P}$	γ–γ	$\mathbb{P}$–$\mathbb{P}$	γ–γ
jj	$\mathcal{O}\left(10^6\right)$	60	$\mathcal{O}\left(10^4\right)$	2
W^+W^-	—	37	—	15
$\mu\mu$	—	46	—	1.3
$t\bar{t}$	—	0.15	—	0.1
H	0.6	0.07	0	0
$\gamma\gamma$	—	0.02	—	0.003

$\gamma\gamma \to W^+W^-$ (with $W^+W^- \to \mu^+e^-\nu_\mu\bar{\nu}_e$) is a particularly clean channel. The configuration of stations considered here would substantially increase the acceptance for 2-arm events, allowing a significant measurement of the SM cross section in the μ^+e^- final state, which will serve as a benchmark for di-boson searches in other channels and at higher masses, which provides a good means to test the interactions of photons and W bosons at high energies, and to search for Anomalous Quartic Gauge Couplings (AQGC) or other non-resonant signals of the BSM physics.

A wide variety of the BSM scenarios involving $\gamma\gamma$ production with forward protons have been explored in the theoretical literature (*e.g.* [427]). For exclusive production with intact protons, only spin-one resonances and any spin-odd states with negative parity are forbidden in $\gamma\gamma$ interactions [428, 429]. This type of search is particularly interesting for resonances with large couplings to photons but not to gluons, which may appear in the $\gamma\gamma \to X \to \gamma\gamma$ channel [430–434]. It was shown that the expected sensitivity for axion-like particles (ALP) in CEP is expected to be competitive and complementary to other collider searches for masses above 600 GeV [434]. Conversely, if a resonance is detected via decays to two photons, measuring the cross section with forward protons will help constrain its couplings to photons in a model-independent way [433]. The use of forward protons was recently been revisited as a possible means to improve searches for pair production of supersymmetric sleptons or charginos in compressed mass scenarios [435, 436].

Physics including the 420-meter station:

Central exclusive Higgs boson production has been extensively studied theoretically and in simulations (including the original detailed studies of the FP420 project [437]). In this case, unlike higher-mass and weakly coupled final states, gluon–gluon production is expected to dominate over $\gamma\gamma$ production. The cross section for CEP Higgs production in the SM has been evaluated by several groups, and the total cross section ranging between a few fb and a few tenths of fb, depending on details of the survival probabilities, parton distribution functions (PDFs), Sudakov factors, and other assumptions of the calculations. A measurement of CEP dijets at the same energy and mass range would therefore remove most of the remaining theoretical uncertainties in the Higgs cross-section predictions. For the 125.4 GeV Higgs boson production, protons could be detected in the 420 m stations on both arms, and in the combination of the 234 m and 420 m stations, while the associated production with W^+W^- vector-boson pair has the potential for probing the Higgs sector in CEP events in the absence of the $\pm$420 m stations. Although the exclusive production cross section is estimated to be $\sigma \approx 0.04\,\text{fb}$ at the tree-level, a high acceptance is expected because of the large invariant mass of the central system.

As discussed in [438, 439], the experiments with forward proton spectrometers at the HL-LHC would open a promising way to perform a search for the QCD instantons, which are a non-trivial consequence of the vacuum structure of the non-Abelian theories (for a recent review and references see *e.g.* [440]). Instantons describe quantum tunneling between different vacuum sectors of the QCD and are arguably the best motivated yet experimentally unobserved non-perturbative effects predicted by the Standard Model. It is shown in [439] that for an instanton mass $M_{\text{inst}} \geq 50$ GeV, the expected central production cross sections for the instanton-induced processes are of the order of picobarns in the pure exclusive case and increase up to hundreds of pb when the emission of spectator jets is allowed. These signal cross sections are encouragingly large, and under favorable background conditions there is a tantalizing chance that QCD instanton effects can either be seen or ruled out. The expected experimental signature for the instanton-induced process in the central detector is a large multiplicity and transverse energy ($\sum_i ET_i$) in a relatively small rapidity interval ($\delta y \simeq 2$–3) and large sphericity $S > 0.8$ of the event. Note that the mean number of gluon jets radiated by the instanton is $\sim 1/\alpha_s$, while the probability of the instanton creation is $\propto \exp(-4\pi/\alpha_s)$. Therefore to observe the clear signature of the instanton-induced signal, it is most feasible to consider the case of the moderately heavy instantons, $M_{\text{inst}} \geq 50$–100 GeV. This would require measurements with the 420 m stations.

7.2. Non-elastic contribution in photon–photon physics

The two-photon production of di-leptons has been largely studied at the LHC experiments in the past year [420, 426, 441–447], investigating elastic interactions at distinct colliding energies. This exclusive production presents a final state composed of the lepton pair produced at the central detector, where large rapidity gaps are present between the pair and the outgoing protons in the beam line direction. Such a signature differs from the usual QCD production by the absence of particle (gluon) radiation that populates the detector, largely reducing the possibility of observing this signature in the data [33]. The interest in di-leptons comes from the fact that they can be used as luminosity monitors [448, 449], however, the production of W boson pairs via their decay channel into leptons provides a way to investigate evidence of new physics with the use of effective theories including anomalous gauge couplings. The signal yields include both the elastic production — with two intact outgoing protons in the forward direction — as well as the non-elastic production, with one or both protons dissociating into a hadronic final state, classified as semi-elastic and inelastic production, respectively (see *e.g.* Ref. [450] for more details).

Figure 21 illustrates the production cases. While the former is easily computed analytically with the use of photon fluxes [451], the latter is based on parton distribution functions (PDFs) with QED contribution. The typical production cross section can be expressed in terms of effective photon luminosities: $\sigma^i \propto \mathcal{L}^i_{\text{eff}} \times \hat{\sigma}(\gamma\gamma \to \ell^+\ell^-)$, where $\hat{\sigma}(\gamma\gamma \to \ell^+\ell^-)$ is the tree-level cross section and $\mathcal{L}^i_{\text{eff}}$ is the photon luminosity for each processes

$$\text{Fig. 21 (a)} \;:\; \mathcal{L}^{\text{el}}_{\text{eff}} \propto x_1 f^{\text{el}}_{\gamma,1}\left(x_1;Q^2\right) x_2 f^{\text{el}}_{\gamma,2}\left(x_2;Q^2\right) , \tag{23}$$

$$\begin{aligned}\text{Fig. 21 (b)} \;:\; \mathcal{L}^{\text{semi}}_{\text{eff}} \propto\; & x_1 f^{\text{inel}}_{\gamma,1}\left(x_1;Q^2\right) x_2 f^{\text{el}}_{\gamma,2}\left(x_2;Q^2\right) \\ & + x_1 f^{\text{el}}_{\gamma,1}\left(x_1;Q^2\right) x_2 f^{\text{inel}}_{\gamma,2}\left(x_2;Q^2\right) ,\end{aligned} \tag{24}$$

$$\text{Fig. 21 (c)} \;:\; \mathcal{L}^{\text{inel}}_{\text{eff}} \propto x_1 f^{\text{inel}}_{\gamma,1}\left(x_1;Q^2\right) x_2 f^{\text{inel}}_{\gamma,2}\left(x_2;Q^2\right) , \tag{25}$$

with x_i being the momentum fraction of the proton carried by the photon and Q^2 the photon virtuality. The non-elastic cases made use of photon PDFs based on the DGLAP evolution equations modified to include the QED parton splitting functions. Considering the different approaches used in the literature for the elastic and non-elastic contributions, we present an estimate for the uncertainties associated with these choices in Fig. 22, which shows the differential cross section as a function of the invariant mass of muon pairs [452]

$$\frac{\mathrm{d}\sigma^i}{\mathrm{d}M_{\gamma\gamma}} = 2M_{\gamma\gamma}\int \mathrm{d}Y \, \frac{\partial^2 \mathcal{L}^i_{\text{eff}}}{\partial M^2_{\gamma\gamma}\partial Y}\, \hat{\sigma}_{\gamma\gamma\to\mu^+\mu^-}\left(M^2_{\gamma\gamma} = x_1 x_2 s\right) . \tag{26}$$

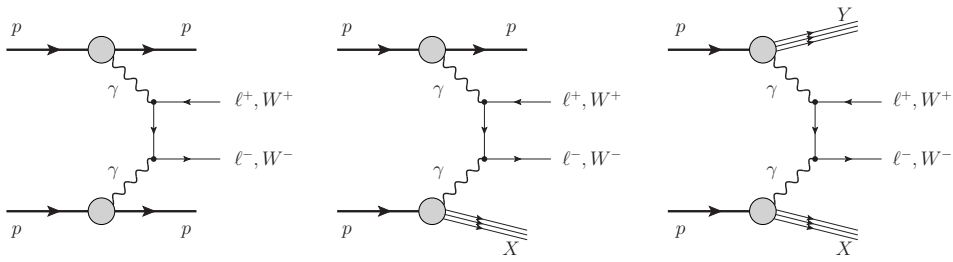

Fig. 21. Processes of particle production in two-photon interactions in hadronic collisions: (a) elastic, (b) semi-elastic, and (c) inelastic case [452].

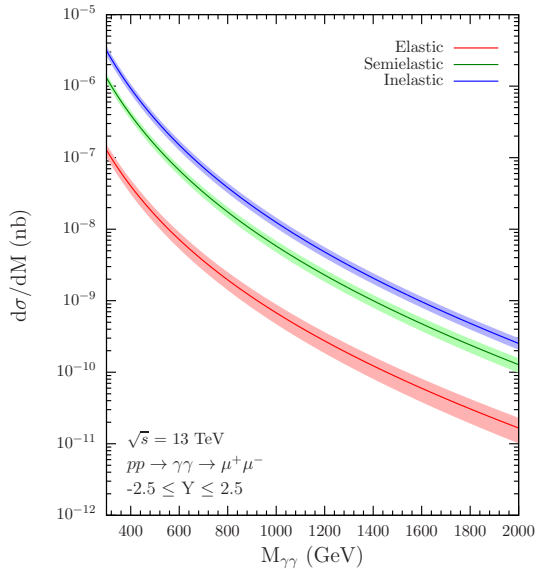

Fig. 22. Invariant mass distributions for the di-muon production by $\gamma\gamma$ interactions in pp collisions at $\sqrt{s} = 13$ TeV considering two distinct ranges of $M_{\gamma\gamma}$. The solid lines are the average values for the predictions and the band represent the one standard deviation uncertainty based on the different predictions [452].

The curves correspond to the predictions averaged at $Q = 300$ GeV among the recent parametrizations for the photon PDF: LUXqed17 [453], MMHT2015qed [454], and NNPDF31luxQED [455]. All these parametrizations are based on the approach proposed in Ref. [456] (see also Ref. [457]). The bands are evaluated as one standard deviation around the averages.

There are Monte Carlo event generators providing predictions for the elastic contribution in the two-photon di-lepton and WW productions, however, the non-elastic contribution is not a common feature. Given that the

curves show similar shapes, it favors the possibility of obtaining a multiplicative factor that can be used to re-weight generated event samples to account for the non-elastic contributions [452]. This prediction can be experimentally tested with forward detectors capable of observing the intact protons emerging from elastic and semi-elastic collisions, such as CMS Precision Proton Spectrometer (PPS) [418] and ATLAS Atlas Forward Proton (AFP) [425]. A multiplicative factor has been already evaluated in previous CMS analyses [445, 446] in the high-mass region

$$F = \left. \frac{N_{\mu\mu(\text{data})} - N_{\text{DY}}}{N_{\text{elastic}}} \right|_{M(\mu^+\mu^-)>160\ \text{GeV}}, \tag{27}$$

where $N_{\mu\mu(\text{data})}$ is the total number of events passing the selection criteria, N_{DY} the total number of events identified as coming from the Drell–Yan production process related to events with one or more extra tracks, and N_{elastic} is the estimated number of elastic events from theory. In a similar fashion, theoretical predictions are used to provide an estimate of this ratio

$$F_1 = \frac{\frac{\mathrm{d}\sigma^{\text{el}}}{\mathrm{d}M_{\gamma\gamma}} + \frac{\mathrm{d}\sigma^{\text{semi}}}{\mathrm{d}M_{\gamma\gamma}} + \frac{\mathrm{d}\sigma^{\text{inel}}}{\mathrm{d}M_{\gamma\gamma}}}{\frac{\mathrm{d}\sigma^{\text{el}}}{\mathrm{d}M_{\gamma\gamma}}} \quad \text{and} \quad F_2 = \frac{\frac{\mathrm{d}\sigma^{\text{el}}}{\mathrm{d}M_{\gamma\gamma}} + \frac{\mathrm{d}\sigma^{\text{semi}}}{\mathrm{d}M_{\gamma\gamma}}}{\frac{\mathrm{d}\sigma^{\text{el}}}{\mathrm{d}M_{\gamma\gamma}}}. \tag{28}$$

Using the set of parametrizations for the photon PDF, one is able to evaluate these ratios in the phase-space region accessible by the LHC forward detectors. Figure 23 presents the predictions in the mass range from 300 GeV to 2 TeV including different approaches for the elastic photon flux, see also [458] for a recent study on these effects for WW production. It shows an uncertainty of 20–40% considering the available parametrizations. An experimental measurement of this observable would provide new insight

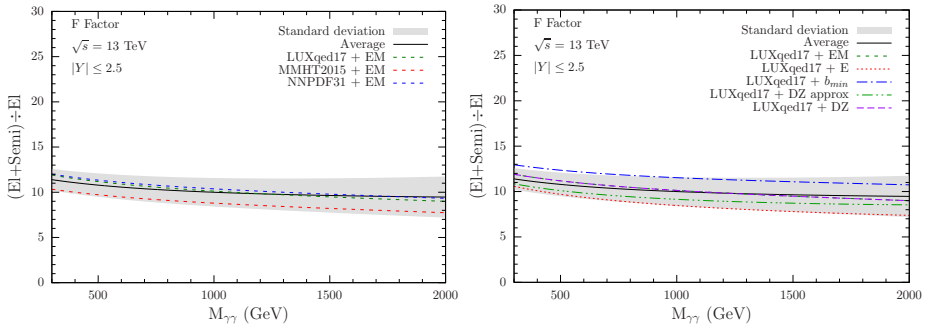

Fig. 23. Dependence on the invariant di-muon mass of the fraction F_2 for different models of the elastic (left panel) and inelastic (right panel) photon distributions [452].

into the parametrizations and account for a data-driven result that could be used in event generators and extend the stringency of limits for anomalous couplings. The upcoming Run 3 of the LHC may provide a unique opportunity to collect enough luminosity for such measurement, opening new fronts for the investigation of photon interactions and improvement of the computational tools available in the literature (see *e.g.* dark matter searches [436] or $t\bar{t}$ production [459, 460], both in the exclusive mode).

7.3. Exclusive production of Higgs boson

Central Exclusive Production (CEP) is especially attractive for three reasons: firstly, if the outgoing protons remain intact and scatter through small angles then, to a very good approximation, the primary di-gluon system obeys a $J_z = 0$, $\mathcal{C}$-even, $\mathcal{P}$-even selection rule [461, 462]. Here, J_z is the projection of the total angular momentum along the proton beam axis. This therefore allows for a clean determination of the quantum numbers of any observed resonance. Thus, in principle, only a few such events are necessary to determine the quantum numbers, since the mere observation of the process establishes that the exchanged object is in the 0^{++} state. Secondly, from precise measurements of the proton momentum losses, ξ_1 and ξ_2, and from the fact that the process is exclusive, the mass of the central system can be measured much more precisely than from the central detector, by the so-called missing mass method [463], $M^2 = \xi_1\xi_2 s$ which is independent of the decay mode. Thirdly, in CEP, the signal-to-background (S/B) ratios turn out to be close to unity, if the contribution from pile-up is not considered. This advantageous S/B ratio is due to the combination of the $J_z = 0$ selection rule, the potentially excellent mass resolution, and the simplicity of the event signature in the central detector.

For pp collisions, the dominant contribution is expected to be from exclusive gluon-fusion production $gg \to h$ for which the cross-section predictions are still known with limited accuracy. A similar statement applies to photon-fusion production, which is strongly enhanced in PbPb collisions with respect to the pp case, see for instance [464]. While the $gg \to h$ is in principle calculable in perturbative QCD, a non-negligible (but conservative) spread in cross section predictions of 0.5–3.0 fb is seen due to such basic ingredients as the parton distribution function (PDF) used and limited control over the non-perturbative theory of soft survival factors, S^2, for gluon-initiated processes in this mass range [465] (although these uncertainties cancel in the S/B ratio for many backgrounds). Existing experimental data from CDF exclusive di-photon [466] or LHCb J/Ψ pair [467] or quarkonia [468] analyses rather prefer values toward the higher end of the spread (see discussions in Refs. [469, 470]), nevertheless, direct measurements of the

exclusive Higgs production would undoubtedly allow its production rate to be directly constrained (or for example by monitoring rates of CEP dijets or di-photons, since the same PDFs and S^2 enter the respective production cross sections at the same central system mass).

The exclusive production of Higgs boson was a flagship topic of the project FP420 (see *e.g.* [437]) whose main goal was to install forward proton detectors (FPDs) at 420 m from the interaction point of ATLAS and CMS experiments to detect forward protons coming from diffractive proton-induced or photon-induced interactions.

Another important feature of forward proton tagging in the case of the Higgs boson is the fact that it enables the dominant decay modes, namely $b\bar{b}$, $WW^{(*)}$, $ZZ^{(*)}$, and $\tau\tau$ to be observed in one process. In this way, it may be possible to access the Higgs boson coupling to bottom quarks. This is challenging in conventional search channels at the LHC due to large QCD backgrounds, even though $h \to b\bar{b}$ is the dominant decay mode for a light SM Higgs boson. The $b\bar{b}$, $WW^{(*)}$, and $\tau\tau$ decay modes were studied in detail and are documented in the literature ($b\bar{b}$ in Refs. [471–478], $WW^{(*)}$ in Refs. [471, 473, 477–480], and $\tau\tau$ in Refs. [473, 474] and in an unpublished diploma thesis [481]). It was the $b\bar{b}$ mode that was studied in greatest detail — thanks to the advantages enumerated above and also thanks to the most favorable prospects for this decay mode in enhancing the production cross section in Minimal SuperSymmetric SM (MSSM), the most popular model of BSM of those days. Prospects for other extensions were outlined in Ref. [482] for NMSSM (Next-to-Minimal SuperSymmetric SM) and in Ref. [483] for a possible triplet Higgs sector. Results of the above studies, including SM and BSM Higgs bosons, were reviewed in 2014 in Ref. [484] and can be summarized in the following way, noting especially the fact that all were performed prior to the Higgs boson discovery.

Although studies of properties of the Higgs boson with mass close to 125.5 GeV discovered by the ATLAS [485] and CMS [486] (see, for example, a global analysis in Ref. [487]) suggest that the Higgs boson is compatible with the Standard Model, there is still room for models of new physics, *e.g.* at lower or higher masses than 125.5 GeV, and the central exclusive production of the Higgs boson still represents a powerful tool to complement the standard strategies at the LHC. A striking feature of the CEP Higgs-boson is that this channel provides valuable additional information on the spin and the coupling structure of Higgs candidates at the LHC. We emphasize that the $J_z = 0$, $\mathcal{C}$-even, $\mathcal{P}$-even selection rule of the CEP process enables us to estimate very precisely (and event-by-event) the quantum numbers of any resonance produced via CEP.

Signal selection and background rejection cuts are based on requiring a match between measurements in the central detector and FPD within assumed subdetector resolutions. In addition, pile-up backgrounds are suppressed by using Time-of-Flight (ToF) detectors, a natural part of FPD whose utilization necessitates protons to be tagged on both sides from the interaction point (see a recent ToF performance study in Ref. [488]). The significances for the CEP Higgs boson decaying into $b\bar{b}$, WW or $\tau\tau$ pairs in SM are moderate but $3\,\sigma$ can surely be reached if the analysis tools, ToF measurement resolution or L1 trigger strategies are improved, among others by knowing the Higgs boson mass precisely, as discussed in Ref. [484]. For example, we can surely expect improvements in the gluon–jet/b-jet misidentification probability $P_{g/b}$. In the original analyses in Refs. [472–475, 478] a conservative approach has been followed by taking the maximum of two values available at that time in ATLAS and CMS. Meanwhile, new developments were reported in reducing the light-quark-b misidentification probabilities in ATLAS [489] and CMS [490]. Other possibilities to improve the significance in searching for the SM Higgs in CEP are a possible sub-10 ps resolution or finer granularity of timing detectors, the use of multivariate techniques or further fine-tuning or optimization of the signal selection and background rejection cuts, thanks to the fact that the mass of the SM-like Higgs boson is already known with relatively high precision. The known Higgs boson mass can also greatly facilitate proposals for a dedicated L1 trigger to efficiently save events with the CEP $H \to b\bar{b}$ candidates. Proposals made in Ref. [491], well before the SM-like Higgs boson discovery, can thus be further optimized.

Studying the properties of Higgs bosons born exclusively with a mass around 125 GeV would require building FPDs in the region of 420 m from the interaction point. Such a possibility, as a possible upgrade of FPDs at HL-LHC, is considered by the CMS Collaboration (see *e.g.* Ref. [417]). Equipping that region of the LHC beam pipe (so-called "cold region") by Roman Pots or Hamburg Beampipe devices was thoroughly discussed in the framework of the FP420 Collaboration and all the know-how has been then put in the R&D document [437]. The constraints coming from experimental data exclude the heavy Higgs boson mass region below 400 GeV, although in special MSSM scenarios, for example, Mh125 alignment scenario [492], masses lower than 400 GeV would still be possible, but for "fine-tuned" points rather than larger areas. Other extreme scenarios that are still possible are represented by the M_H^{125} scenario [492], in which the light CP-even Higgs is lighter than 125 GeV, and the discovered Higgs boson corresponds to the heavy CP-even MSSM Higgs boson. The development of the M_H^{125} scenario was triggered by the observation of a local excess of 3σ at about 96 GeV in the di-photon final state, based on the CMS Run 2 data [493]. First Run 2

results from ATLAS with 80 fb^{-1} in the $\gamma\gamma$ final state (see *e.g.* Ref [494]) or full Run 2 ATLAS results in the $\tau^+\tau^-$ final state [495] turned out to be weaker, but a full Run 2 analysis of the CMS data is still awaited.

7.4. Anomalous quartic couplings with proton tagging

High-energy photon–photon fusion processes can be studied at the CERN LHC in proton–proton collisions. In comparison to the ultra-peripheral heavy-ion collisions, the impact parameter range is much smaller in *pp* collisions for photon exchange. The quasi-real photon energy spectrum can easily reach the TeV scale for 14 TeV *pp* collisions, although with a much smaller photon flux since one does not have the same Z^4 enhancement factor as in heavy-ion collisions. One of the main interests in studying photon-fusion processes in proton–proton collisions is its potential for discovering the BSM physics. Such prospects for discovering new physics are complementary to the standard searches at the LHC, which rely on quark- and gluon-initiated processes.

In a fraction of the quasi-real photon exchange processes, the colliding protons may remain intact. In these central exclusive production processes, the photon exchange can be modeled within the equivalent photon approximation, which is based on the parametrization of the electromagnetic form factors of the proton from elastic photon–proton precision data. Non-perturbative corrections related to the underlying event activity or QCD initial-state radiation effects are absent in this case. The survival probability, which quantifies the probability that the protons remain intact after the photon exchange, has been calculated and measured to be of the order of 70–90% (depending on the invariant mass of the central system).

The intact protons retain most of the original beam momentum and are thus deflected at small angles with respect to the beam line. The magnetic lattice of the LHC can be used to separate these intact protons from the beam protons that did not collide. Then, these intact protons can be detected with the Roman Pot detectors located at about 200 m with respect to the interaction point. If these two protons are detected together with a hard, central system at central pseudo-rapidities, then all the decay products of the collision have been successfully measured. The PPS and AFP detectors of CMS and ATLAS have such setups for the detection of protons at the nominal instantaneous luminosities.

The mass m_X and rapidity y_X of the central system are directly related to the fractional momentum loss of the scattered protons $\xi_{1,2} = \Delta p_{1,2}/p_{1,2}^{\text{beam}}$ via

$$m_X = \sqrt{\xi_1 \xi_2 s}\,, \qquad y_X = \frac{1}{2}\ln(\xi_1/\xi_2)\,. \tag{29}$$

This kinematical correlation is used to suppress the contributions from pileup interactions, which is the largest source of background for these measurements. The pileup contributions are such that a hard scale process (*e.g.*, QCD production of a photon pair, jets) is paired with uncorrelated forward protons from diffractive pileup interactions. The signature would be similar to that of central exclusive production: two protons and a hard scale system at central rapidities. The cross section for soft diffractive interactions is large (of the order of 20 mb at 13 TeV). Together with the high pileup multiplicities at the LHC and at the future HL-LHC, it becomes more important to control this background. The aforementioned kinematical correlation between the forward and central system mitigates pileup. Pileup is further mitigated with time-of-flight measurements.

We now discuss a number of examples of new physics searches using proton tagging at the LHC. The scattering of light-by-light ($\gamma\gamma \to \gamma\gamma$) is induced via box diagrams in the SM at the lowest order in perturbation theory. The experimental signature would be two photons back-to-back, with no hadronic activity, and two scattered protons. Exotic particles can contribute to light-by-light scattering via virtual exchanges at high mass [496, 497]. Generic manifestations of the BSM physics can be modeled within the effective field theory (EFT) formalism, under the assumption that the invariant mass of the di-photon system is much smaller than the energy scale where new physics manifests. Among these operators, the pure photon dimension-eight operators $\mathcal{L}_{4\gamma} = \zeta_1^{4\gamma} F_{\mu\nu}F^{\mu\nu}F_{\rho\sigma}F^{\rho\sigma} + \zeta_2^{4\gamma} F_{\mu\nu}F^{\nu\rho}F_{\rho\lambda}F^{\lambda\mu}$ induce the $\gamma\gamma\gamma\gamma$ interaction. The quartic photon couplings have been constrained at the CERN LHC by the CMS Collaboration with values of $|\zeta_1^{4\gamma}|(|\zeta_2^{4\gamma}|) < 2.88(6.02) \times 10^{-13}$ GeV^{-4} at 95% C.L. [421]. At the HL-LHC, these bounds can in principle be improved down to $|\zeta_1| \approx 4(8) \times 10^{-14}$ GeV^{-4} [498]. Time-of-flight measurements will be very important to suppress the larger amount of pileup interactions. Projections for the HL-LHC conditions are shown in Fig. 24.

The $\gamma\gamma \to \gamma Z$ scattering process can be probed with proton tagging as well [499]. This process is induced at the lowest order in perturbation theory via box diagrams of particles charged under hypercharge, analogous to the SM light-by-light scattering box diagram. In the leptonic decay channel, the background can be controlled to a similar degree as the one in light-by-light scattering. New physics manifestations can be modeled using dimension-eight effective operators $\mathcal{L}_{\gamma\gamma\gamma Z} = \zeta_1^{3\gamma Z} F^{\mu\nu}F_{\mu\nu}F^{\rho\sigma}Z_{\rho\sigma} + \zeta_2^{3\gamma Z} F^{\mu\nu}\tilde{F}_{\mu\nu}F^{\rho\sigma}\tilde{Z}_{\rho\sigma}$. The quartic ζ_1, ζ_2 couplings can be constrained down to $\approx 2 \times 10^{-13}$ GeV^{-4} in Run 3 conditions [499]. This constrain surpasses projections based on measurements of the branching fraction of the rare $Z \to \gamma\gamma\gamma$ decay at the HL-LHC by about two orders of magnitude. The channel is experimentally very clean (an isolated photon recoiling back-to-back against a reconstructed

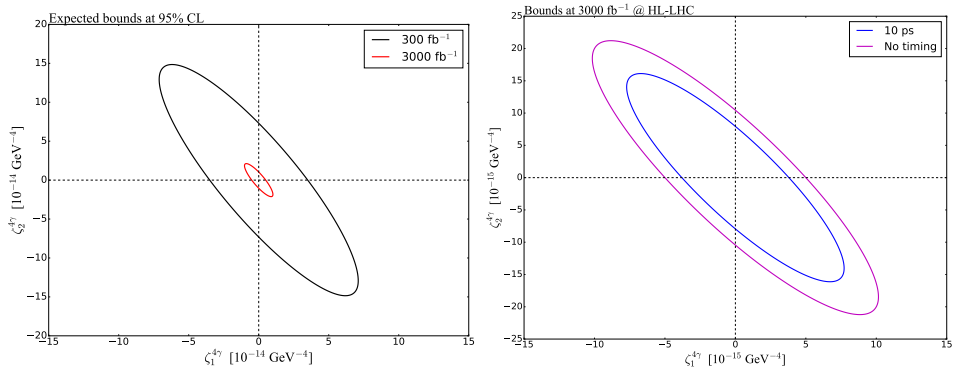

Fig. 24. Left: Expected bounds at 95% C.L. on the anomalous quartic coupling for 300 fb^{-1} and at the HL-LHC with 3000 fb^{-1} (no time-of-flight measurement). Right: Expected bounds at 95% C.L. on the anomalous couplings at the HL-LHC with time-of-flight measurement with precision of 10 ps and without time-of-flight measurement. Figure extracted from Ref. [498].

Z boson with no soft hadronic activity associated with the primary vertex). Competitive limits can already be extracted with existing data collected by ATLAS and CMS. At the future HL-LHC, the search can be expanded by considering boosted topologies of the Z boson. This could help populate the region of phase-space at large γZ invariant masses, complementing the reach with the (cleaner) fully leptonic decay channel. Projections for the HL-LHC conditions are shown in Fig. 25.

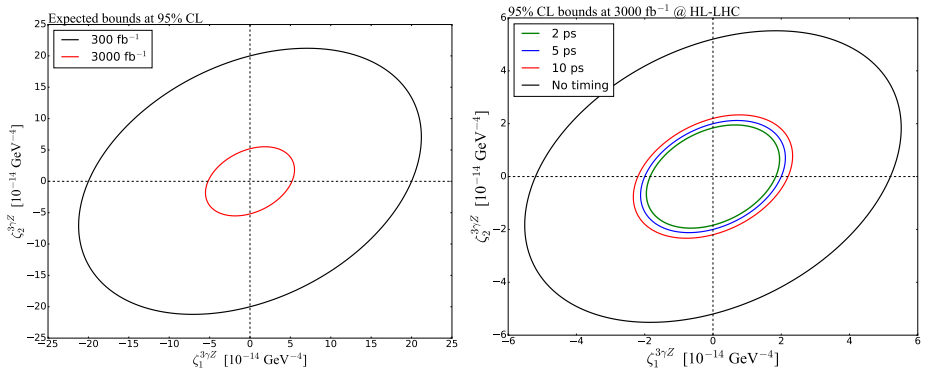

Fig. 25. Left: Expected bounds on the anomalous couplings at 95% C.L. with 300 fb^{-1} and 3000 fb^{-1} at the HL-LHC (no time-of-flight measurement). Right: Expected bounds at 95% C.L. for timing precision of δt = 2, 5, 10 ps at the HL-LHC. Figure extracted from Ref. [498].

Another process of interest is the electroweak gauge boson scattering $\gamma\gamma \to W^+W^-$. Unlike the two previous instances, the $\gamma\gamma \to W^+W^-$ process is induced at tree-level in the SM via the triple γWW and quartic couplings $\gamma\gamma WW$ in the electroweak sector [500]. The process has been observed already by the ATLAS Collaboration without the use of proton tagging by focusing on the purely leptonic decay channel [501]. However, in order to probe a region of phase-space that is sensitive to modifications of the SM interactions (high-mass modifications specifically), the proton tagging technique is necessary [502]. At high di-boson invariant masses and high boson $p_\perp$, boosted topologies are kinematically favorable. The fully hadronic channel, where each of the hadronically decaying W bosons is reconstructed as large-radius jets, provides the best sensitivity to new physics manifestations [502]. Modifications to the SM can be modeled with a dimension-six interaction Lagrangian density, $\mathcal{L}_6^{\text{eff}} = -\frac{e^2}{8} a_0^W F_{\mu\nu} F^{\mu\nu} W^{+\alpha} W_\alpha^- - \frac{e^2}{16} a_{\text{C}}^W F_{\mu\alpha} F^{\mu\beta} (W^{+\alpha} W_\beta^- + W^{-\alpha} W_\beta^+)$. These are the only operators allowed after imposing $\text{U}(1)_{\text{em}}$ and global custodial $\text{SU}(2)_{\text{C}}$ symmetries. The expected limit on the anomalous a_0^W and a_{C}^W couplings would be at least one order of magnitude larger in the hadronic channel than in the semi-leptonic or leptonic channel combined. The projections for 14 TeV Run 3 combining all channels is shown in Fig. 26. However, the use of jet substructure variables that are sen-

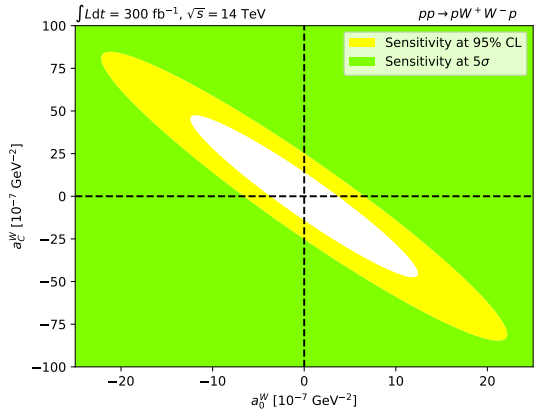

Fig. 26. Projected sensitivities on the anomalous coupling parameters a_0^W and a_{C}^W without form factors. The projections are shown for $pp \to pW^+W^-p$ at 14 TeV assuming an integrated luminosity of 300 fb^{-1}. The yellow and green areas represent, respectively, the projected sensitivities at 95% C.L. and 5σ combining the hadronic, semi-leptonic, and leptonic decay channels of the W^+W^- system. The blank area in the center represents the region where we do not expect sensitivity to the anomalous coupling parameter. Time-of-flight measurements with 20 ps precision are assumed. Figure extracted from Ref. [502].

sitive to the number of hard prongs in the jet is necessary (for example, N-subjettiness ratios) in order to tame the large QCD jet background. The sensitivity can be further expanded by considering ungroomed jet substructure variables; the ungroomed jet mass and jet shapes for central exclusive W boson jets should render similar resemblance to the jet substructure of a groomed W boson jet from a typical QCD interaction. The SM $\gamma\gamma \to WW$ scattering can be probed in the semi-leptonic channel at high WW invariant masses, in a way such that it complements the phase-space covered by the fully leptonic channel.

In addition to pure gauge boson scattering, one can probe electromagnetic interactions in other processes such as in $\gamma\gamma \to t\bar{t}$ scattering, which is induced at the tree-level in the SM with the elementary QED vertices of the top quark and the photon. The SM process has not yet been observed. The CMS Collaboration has set an upper limit on the cross section of 0.59 pb at 95% C.L. [422]. Although the process is induced at the tree-level, the cross section is of the order of 10^{-1} fb before branching fraction corrections and for a typical RP acceptance in ξ. It is likely that evidence could be established considering the full HL-LHC luminosity. For the BSM physics, we considered six different operators (four dimension-six and two dimension-eight) with $\gamma\gamma t\bar{t}$ quartic couplings. We embedded the corresponding amplitudes for six different operators, each representative of different underlying symmetries of the BSM scenarios at high masses. The constraints we expect for a typical Run 3 scenario is about $\zeta_i^{\gamma\gamma t\bar{t}} \approx 10^{-12}$ GeV^{-4}, for $i = 1, \ldots, 6$, where ζ_i represent the anomalous quartic couplings. Focusing on high-mass back-to-back top-quark pairs with proton tagging, one expects a residual QCD $t\bar{t}$ background of the order of 100 counts for 300 fb^{-1} at 14 TeV. The mass

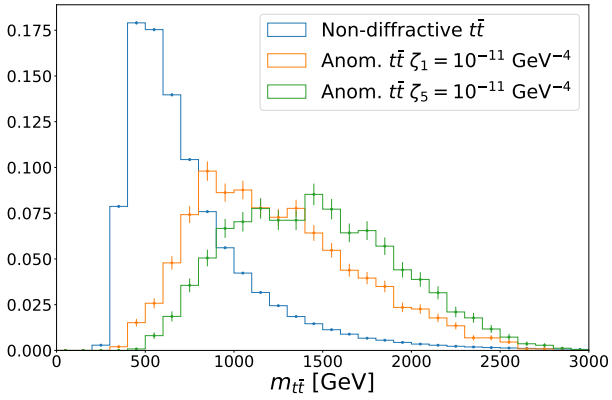

Fig. 27. Mass spectrum of the $t\bar{t}$ system as reconstructed from its decay products. Only events passing the pre-selection are shown. Histograms are normalized to unity. The corresponding publication is in preparation.

distributions at the particle-level for QCD $t\bar{t}$ production and predictions for anomalous couplings are shown in Fig. 27. The search could be expanded to include the fully-hadronic case at the HL-LHC, where the larger statistical sample allows the coverage of the region of phase-space of highly boosted top quarks.

To summarize this section, there are good prospects for expanding the search for new physics at the LHC in photon-fusion processes such that they are complementary to the existing program of the CERN LHC. Other prospects for the HL-LHC era can be read in Ref. [417].

8. Conclusions

Forward physics allows to address fundamental research questions related to the growth of gluon distributions in the perturbative high-energy limit and their potential saturation due to the onset of unitarity corrections. It allows searching for imprints of such effects in both parton distribution functions of colliding hadrons and directly in the final state of events. Carrying out this physics program is essential for two reasons: preparation for the future Electron Ion Collider (EIC) and the potential to answer central research questions already at the LHC runs. In comparison to the LHC forward physics program, the future EIC will allow to probe the dense nuclear matter with an electron beam, ideal for the investigation and characterization of hadronic structure.

Identifying suitable probes at the LHC is on the other hand far more cumbersome. Nevertheless, this is a worthwhile effort: due to its high center-of-mass energy, the LHC allows to probe hadronic matter at unprecedented values of x, which are several orders of magnitude below the values to be reached at the Electron Ion Collider. This is particularly true when using dedicated events in the forward region. It therefore covers regions of phase space which are completely inaccessible at the EIC and allows for a direct comparison between high parton densities generated through low-x evolution and those present in large nuclei.

A related topic addresses the direct analysis of emission patterns, related to low x — in that case BFKL — evolution, which can be studied using multi-jet events. While challenging at the LHC, a study of such evolution effects is clearly limited at the Electron Ion Collider to the limitations in available phase space. Within the foreseeable future, such questions will be either studied at the LHC within the Forward Physics program, or they will not be studied at all.

While somewhat orthogonal from the point of view of the physics program, it is natural to employ forward detectors not only for the exploration of strong interactions but also for new physics searches and the study of

electroweak dynamics. In particular, photon–photon reactions and related Pomeron–Pomeron fusion processes allow for the observation of very clean events at the LHC, due to the detection of intact scattered protons and/or large rapidity gaps between the centrally produced object and the scattered proton. While their exploration is of high interest by itself, such events have further the potential to improve existing bounds on new degrees of freedom and to contribute to searches for new physics at the LHC.

Forward Physics allows therefore to address central physics questions of both nuclear and particle physics. Its physics program is strongly related to the physics at the future EIC as well as searches for new physics at the LHC. The region of phase space explored by the LHC forward physics is unique and therefore allows us to address research questions which are not accessible anywhere else.

This project has received funding from the European Union's Horizon 2020 research and innovation programme under grant agreement STRONG-2020 No. 824093 in order to contribute to the EU Virtual Access NLOAccess (VA1-WG10) and to the Joint Research activity "Fixed Target Experiments at the LHC" (JRA2), from the Agence Nationale de la Recherche (ANR) via the grant ANR-20-CE31-0015 ("PrecisOnium") and via the IDEX Paris-Saclay "Investissements d'Avenir" (ANR-11-IDEX-0003-01) through the GLUODYNAMICS project funded by the "P2IO LabEx (ANR-10-LABX-0038)". This work was also partly supported by the French CNRS via the GDR QCD, via the IN2P3 project GLUE@NLO, via the Franco–Polish EIA (Gluegraph). F.G. Celiberto acknowledges support from the INFN/NINPHA project and thanks the Università degli Studi di Pavia for the warm hospitality. G. Chachamis acknowledges support by the Fundação para a Ciência e a Tecnologia (Portugal) under project CERN/FIS-PAR/0024/2019 and contract 'Investigador auxiliar FCT — Individual Call/03216/2017', and from the European Union's Horizon 2020 research and innovation programme under grant agreement No. 824093. M. Fucilla, M.M.A. Mohammed, and A. Papa acknowledge support from the INFN/QFT@COLLIDERS project. K. Kutak acknowledges the support by the National Science Centre, Poland (NCN) grant No. DEC-2017/27/B/ST2/01985. A. van Hameren acknowledges the support by the National Science Centre, Poland (NCN) grant No. 2019/35/B/ST2/03531. M.A. Ozcelik's work was partly supported by the ERC grant 637019 "MathAm". The work of S.R. Klein is supported in part by the U.S. Department of Energy, Office of Science, Office of Nuclear Physics, under contract number DE-AC02-05CH11231. M. Hentschinski acknowledges support by Consejo Nacional de Ciencia y Tecnología grant number A1 S-43940 (CONACYT-SEP Ciencias Básicas). The work of L. Szy-

manowski is supported by the grant 2017/26/M/ST2/01074 of the National Science Centre, Poland (NCN). J. Jalilian-Marian acknowledges support by the U.S. Department of Energy, Office of Nuclear Physics through grant No. DE-SC0002307. The research of M. Strikman was supported by the U.S. Department of Energy, Office of Science, Office of Nuclear Physics, under Award No. DE-FG02-93ER40771. M. Taševský supported by MEYS of Czech Republic within the project LTT17018.

REFERENCES

[1] E.A. Kuraev, L.N. Lipatov, V.S. Fadin, «The Pomeranchuk Singularity in Nonabelian Gauge Theories», *Sov. Phys. JETP* **45**, 199 (1977).

[2] E.A. Kuraev, L.N. Lipatov, V.S. Fadin, «Multi-Reggeon Processes in the Yang–Mills Theory», *Sov. Phys. JETP* **44**, 443 (1976).

[3] V.S. Fadin, E.A. Kuraev, L.N. Lipatov, «On the Pomeranchuk Singularity in Asymptotically Free Theories», *Phys. Lett. B* **60**, 50 (1975).

[4] L.N. Lipatov, «Reggeization of the Vector Meson and the Vacuum Singularity in Nonabelian Gauge Theories», *Sov. J. Nucl. Phys.* **23**, 338 (1976).

[5] I.I. Balitsky, L.N. Lipatov, «The Pomeranchuk Singularity in Quantum Chromodynamics», *Sov. J. Nucl. Phys.* **28**, 822 (1978).

[6] L.N. Lipatov, «The Bare Pomeron in Quantum Chromodynamics», *Sov. Phys. JETP* **63**, 904 (1986).

[7] V.S. Fadin, L.N. Lipatov, «BFKL pomeron in the next-to-leading approximation», *Phys. Lett. B* **429**, 127 (1998).

[8] M. Ciafaloni, G. Camici, «Energy scale(s) and next-to-leading BFKL equation», *Phys. Lett. B* **430**, 349 (1998).

[9] V. Gribov, L. Lipatov, «Deep inelastic *ep* scattering in perturbation theory», *Sov. J. Nucl. Phys.* **15**, 438 (1972).

[10] V.N. Gribov, L.N. Lipatov, «e^+e^- pair annihilation and deep inelastic *ep* scattering in perturbation theory», *Sov. J. Nucl. Phys.* **15**, 675 (1972).

[11] L.N. Lipatov, «The parton model and perturbation theory», *Yad. Fiz.* **20**, 181 (1974).

[12] G. Altarelli, G. Parisi, «Asymptotic freedom in parton language», *Nucl. Phys. B* **126**, 298 (1977).

[13] Y.L. Dokshitzer, «Calculation of the Structure Functions for Deep Inelastic Scattering and e^+e^- Annihilation by Perturbation Theory in Quantum Chromodynamics», *Sov. Phys. JETP* **46**, 641 (1977).

[14] A.H. Mueller, H. Navelet, «An inclusive mini-jet cross-section and the bare Pomeron in QCD», *Nucl. Phys. B* **282**, 727 (1987).

[15] V. Del Duca, C.R. Schmidt, «Dijet production at large rapidity intervals», *Phys. Rev. D* **49**, 4510 (1994).

[16] W.J. Stirling, «Production of jet pairs at large relative rapidity in hadron–hadron collisions as a probe of the perturbative Pomeron», *Nucl. Phys. B* **423**, 56 (1994).

[17] V. Del Duca, C.R. Schmidt, «Balitsky–Fadin–Kuraev–Lipatov approximation *versus* $O(\alpha_s^3)$ corrections to large-rapidity dijet production», *Phys. Rev. D* **51**, 2150 (1995).

[18] L.H. Orr, W.J. Stirling, «Dijet production at hadron–hadron colliders in the Balitskii–Fadin–Kuraev–Lipatov approach», *Phys. Rev. D* **56**, 5875 (1997).

[19] J. Kwieciński, A.D. Martin, L. Motyka, J. Outhwaite, «Azimuthal decorrelation of forward and backward jets at the Tevatron», *Phys. Lett. B* **514**, 355 (2001).

[20] J.R. Andersen *et al.*, «Mueller–Navelet jets at hadron colliders», *J. High Energy Phys.* **2001**, 007 (2001).

[21] A. Sabio Vera, «The Effect of NLO conformal spins in azimuthal angle decorrelation of jet pairs», *Nucl. Phys. B* **746**, 1 (2006).

[22] A. Sabio Vera, F. Schwennsen, «The Azimuthal decorrelation of jets widely separated in rapidity as a test of the BFKL kernel», *Nucl. Phys. B* **776**, 170 (2007).

[23] C. Marquet, C. Royon, «Azimuthal decorrelation of Mueller–Navelet jets at the Tevatron and the LHC», *Phys. Rev. D* **79**, 034028 (2009).

[24] J. Bartels, D. Colferai, G.P. Vacca, «The NLO jet vertex for Mueller–Navelet and forward jets: The quark part», *Eur. Phys. J. C* **24**, 83 (2002).

[25] J. Bartels, D. Colferai, G.P. Vacca, «The NLO jet vertex for Mueller–Navelet and forward jets: The gluon part», *Eur. Phys. J. C* **29**, 235 (2003).

[26] D. Colferai, F. Schwennsen, L. Szymanowski, S. Wallon, «Mueller–Navelet jets at LHC — complete NLL BFKL calculation», *J. High Energy Phys.* **2010**, 026 (2010).

[27] F. Caporale *et al.*, «The next-to-leading order jet vertex for Mueller–Navelet and forward jets revisited», *J. High Energy Phys.* **2012**, 101 (2012).

[28] B. Ducloué, L. Szymanowski, S. Wallon, «Confronting Mueller–Navelet jets in NLL BFKL with LHC experiments at 7 TeV», *J. High Energy Phys.* **2013**, 096 (2013).

[29] B. Ducloué, L. Szymanowski, S. Wallon, «Evidence for high-energy resummation effects in Mueller–Navelet jets at the LHC», *Phys. Rev. Lett.* **112**, 082003 (2014).

[30] F. Caporale, D.Yu. Ivanov, B. Murdaca, A. Papa, «Mueller–Navelet jets in next-to-leading order BFKL: theory *versus* experiment», *Eur. Phys. J. C* **74**, 3084 (2014); *Erratum ibid.* **75**, 535 (2015).

[31] F.G. Celiberto, D.Yu. Ivanov, B. Murdaca, A. Papa, «Mueller–Navelet jets at LHC: BFKL *versus* high-energy DGLAP», *Eur. Phys. J. C* **75**, 292 (2015).

[32] A. Mueller *et al.*, «Sudakov Resummations in Mueller–Navelet Dijet Production», *J. High Energy Phys.* **2016**, 096 (2016).

[33] LHC Forward Physics Working Group (K. Akiba *et al.*), «LHC Forward Physics», *J. Phys. G: Nucl. Part. Phys.* **43**, 110201 (2016).

[34] D. Colferai, F. Deganutti, A. Niccoli, «Improved theoretical description of Mueller–Navelet jets at LHC», in: «Proceedings of 25$^{\text{th}}$ Low-x Meeting», Bisceglie (Puglia), Italy, 12–18 June, 2017.

[35] ATLAS Collaboration (G. Aad *et al.*), «Measurement of dijet production with a veto on additional central jet activity in pp collisions at $\sqrt{s} = 7$ TeV using the ATLAS detector», *J. High Energy Phys.* **2011**, 053 (2011).

[36] CMS Collaboration (S. Chatrchyan *et al.*), «Ratios of dijet production cross sections as a function of the absolute difference in rapidity between jets in proton–proton collisions at $\sqrt{s} = 7$ TeV», *Eur. Phys. J. C* **72**, 2216 (2012).

[37] ATLAS Collaboration (G. Aad *et al.*), «Measurements of jet vetoes and azimuthal decorrelations in dijet events produced in pp collisions at $\sqrt{s} = 7$ TeV using the ATLAS detector», *Eur. Phys. J. C* **74**, 3117 (2014).

[38] CMS Collaboration (V. Khachatryan *et al.*), «Azimuthal decorrelation of jets widely separated in rapidity in pp collisions at $\sqrt{s} = 7$ TeV», *J. High Energy Phys.* **2016**, 139 (2016).

[39] G. Chachamis, A. Sabio Vera, «The high-energy radiation pattern from BFKLex with double-log colinear contributions», *J. High Energy Phys.* **2016**, 064 (2016).

[40] N.B. de León, G. Chachamis, A. Sabio Vera, «Average mini-jet rapidity ratios in Mueller–Navelet jets», *Eur. Phys. J. C* **81**, 1019 (2021).

[41] J.R. Forshaw, D.A. Ross, A. Sabio Vera, «Solving the BFKL equation with running coupling», *Phys. Lett. B* **498**, 149 (2001).

[42] G. Chachamis, M. Lublinsky, A. Sabio Vera, «Higher order effects in non-linear evolution from a veto in rapidities», *Nucl. Phys. A* **748**, 649 (2005).

[43] J.R. Forshaw, D.A. Ross, A. Sabio Vera, «Rapidity veto effects in the NLO BFKL equation», *Phys. Lett. B* **455**, 273 (1999).

[44] C.R. Schmidt, «Rapidity separation dependence and the large next-to-leading corrections to the BFKL equation», *Phys. Rev. D* **60**, 074003 (1999).

[45] C.R. Schmidt, «A Monte Carlo solution to the BFKL equation», *Phys. Rev. Lett.* **78**, 4531 (1997).

[46] J.R. Andersen, A. Sabio Vera, «Solving the BFKL equation in the next-to-leading approximation», *Phys. Lett. B* **567**, 116 (2003).

[47] J.R. Andersen, A. Sabio Vera, «The gluon Green's function in the BFKL approach at next-to-leading logarithmic accuracy», *Nucl. Phys. B* **679**, 345 (2004).

[48] G. Chachamis, M. Deak, A. Sabio Vera, P. Stephens, «A comparative study of small x Monte Carlos with and without QCD coherence effects», *Nucl. Phys. B* **849**, 28 (2011).

[49] G. Chachamis, A. Sabio Vera, «The colour octet representation of the non-forward BFKL Green function», *Phys. Lett. B* **709**, 301 (2012).

[50] G. Chachamis, A. Sabio Vera, «The NLO $N = 4$ SUSY BFKL Green function in the adjoint representation», *Phys. Lett. B* **717**, 458 (2012).

[51] G. Chachamis, A. Sabio Vera, C. Salas, «Bootstrap and momentum transfer dependence in small x evolution equations», *Phys. Rev. D* **87**, 016007 (2013).

[52] F. Caporale *et al.*, «A study of the diffusion pattern in $N = 4$ SYM at high energies», *Phys. Lett. B* **724**, 127 (2013).

[53] G. Chachamis, A. Sabio Vera, «Monte Carlo study of double logarithms in the small x region», *Phys. Rev. D* **93**, 074004 (2016).

[54] P. Nason, «A new method for combining NLO QCD with shower Monte Carlo algorithms», *J. High Energy Phys.* **2004**, 040 (2004).

[55] S. Frixione, P. Nason, C. Oleari, «Matching NLO QCD computations with Parton Shower simulations: the POWHEG method», *J. High Energy Phys.* **2007**, 070 (2007).

[56] S. Alioli, P. Nason, C. Oleari, E. Re, «A general framework for implementing NLO calculations in shower Monte Carlo programs: the POWHEG BOX», *J. High Energy Phys.* **2010**, 043 (2010).

[57] T. Sjöstrand *et al.*, «An introduction to PYTHIA 8.2», *Comput. Phys. Commun.* **191**, 159 (2015).

[58] M. Cacciari, G.P. Salam, G. Soyez, «FastJet User Manual», *Eur. Phys. J. C* **72**, 1896 (2012).

[59] M. Cacciari, G.P. Salam, «Dispelling the N^3 myth for the k_t jet-finder», *Phys. Lett. B* **641**, 57 (2006).

[60] NNPDF Collaboration (R.D. Ball *et al.*), «Parton distributions from high-precision collider data», *Eur. Phys. J. C* **77**, 663 (2017).

[61] F.G. Celiberto, D.Yu. Ivanov, B. Murdaca, A. Papa, «Mueller–Navelet Jets at the LHC: Discriminating BFKL from DGLAP by Asymmetric Cuts», *Acta Phys. Pol. B Proc. Suppl.* **8**, 935 (2015).

[62] F. Caporale, D.Yu. Ivanov, B. Murdaca, A. Papa, «Mueller–Navelet small-cone jets at LHC in next-to-leading BFKL», *Nucl. Phys. B* **877**, 73 (2013).

[63] F. Caporale, B. Murdaca, A. Sabio Vera, C. Salas, «Scale choice and colinear contributions to Mueller–Navelet jets at LHC energies», *Nucl. Phys. B* **875**, 134 (2013).

[64] F. Caporale, D.Yu. Ivanov, B. Murdaca, A. Papa, «Brodsky–Lepage–Mackenzie optimal renormalization scale setting for semihard processes», *Phys. Rev. D* **91**, 114009 (2015).

[65] F.G. Celiberto, D.Yu. Ivanov, B. Murdaca, A. Papa, «Mueller–Navelet jets at 13 TeV LHC: dependence on dynamic constraints in the central rapidity region», *Eur. Phys. J. C* **76**, 224 (2016).

[66] F.G. Celiberto, D.Yu. Ivanov, B. Murdaca, A. Papa, «BFKL effects and central rapidity dependence in Mueller–Navelet jet production at 13 TeV LHC», *PoS* **(DIS2016)**, 176 (2016).

[67] F. Caporale *et al.*, «Inclusive dijet hadroproduction with a rapidity veto constraint», *Nucl. Phys. B* **935**, 412 (2018).

[68] CMS Collaboration (V. Khachatryan *et al.*), «Azimuthal decorrelation of jets widely separated in rapidity in pp collisions at $\sqrt{s} = 7$ TeV», *J. High Energy Phys.* **2016**, 139 (2016).

[69] F.G. Celiberto, «Hunting BFKL in semi-hard reactions at the LHC», *Eur. Phys. J. C* **81**, 691 (2021).

[70] F.G. Celiberto, «High-energy resummation in semi-hard processes at the LHC», Ph.D. Thesis, Calabria University, 2017.

[71] F.G. Celiberto, D.Yu. Ivanov, B. Murdaca, A. Papa, «Inclusive charged light di-hadron production at 7 and 13 TeV LHC in the full NLA BFKL approach», arXiv:1709.01128 [hep-ph].

[72] F.G. Celiberto, D.Yu. Ivanov, B. Murdaca, A. Papa, «Inclusive dihadron production at the LHC in NLA BFKL», in: «Proceedings of 17$^{\text{th}}$ Conference on Elastic and Diffractive Scattering (EDS Blois 2017)», Prague, Czechia, 26–30 June 2017, arXiv:1709.04758 [hep-ph].

[73] A.D. Bolognino *et al.*, «Hadron-jet correlations in high-energy hadronic collisions at the LHC», *Eur. Phys. J. C* **78**, 772 (2018).

[74] A.D. Bolognino *et al.*, «Inclusive Hadron-jet Production at the LHC», *Acta Phys. Pol. B Proc. Suppl.* **12**, 773 (2019).

[75] A.D. Bolognino *et al.*, «High-energy effects in forward inclusive dijet and hadron-jet production», *PoS* **(DIS2019)**, 049 (2019).

[76] F.G. Celiberto, D.Yu. Ivanov, A. Papa, «Diffractive production of Λ hyperons in the high-energy limit of strong interactions», *Phys. Rev. D* **102**, 094019 (2020).

[77] F.G. Celiberto *et al.*, «BFKL phenomenology: resummation of high-energy logs in inclusive processes», *SciPost Phys. Proc.* **10**, 002 (2022), arXiv:2110.12649 [hep-ph].

[78] F.G. Celiberto, D.Yu. Ivanov, B. Murdaca, A. Papa, «High energy resummation in dihadron production at the LHC», *Phys. Rev. D* **94**, 034013 (2016).

[79] F.G. Celiberto, D.Yu. Ivanov, B. Murdaca, A. Papa, «Dihadron production at LHC: BFKL predictions for cross sections and azimuthal correlations», *AIP Conf. Proc.* **1819**, 060005 (2017).

[80] F.G. Celiberto, D.Yu. Ivanov, B. Murdaca, A. Papa, «Dihadron production at the LHC: full next-to-leading BFKL calculation», *Eur. Phys. J. C* **77**, 382 (2017).

[81] F. Caporale, G. Chachamis, B. Murdaca, A. Sabio Vera, «Balitsky–Fadin–Kuraev–Lipatov Predictions for Inclusive Three Jet Production at the LHC», *Phys. Rev. Lett.* **116**, 012001 (2016).

[82] F. Caporale, F.G. Celiberto, G. Chachamis, A. Sabio Vera, «Multi-Regge kinematics and azimuthal angle observables for inclusive four-jet production», *Eur. Phys. J. C* **76**, 165 (2016).

[83] F. Caporale *et al.*, «BFKL azimuthal imprints in inclusive three-jet production at 7 and 13 TeV», *Nucl. Phys. B* **910**, 374 (2016).

[84] G. Chachamis *et al.*, «Inclusive three jet production at the LHC for 7 and 13 TeV collision energies», *PoS* **(DIS2016)**, 178 (2016).

[85] F. Caporale, F.G. Celiberto, G. Chachamis, A. Sabio Vera, «Inclusive four-jet production: a study of Multi-Regge kinematics and BFKL observables», *PoS* **(DIS2016)**, 177 (2016).

[86] G. Chachamis *et al.*, «Inclusive three jet production at the LHC at 7 and 13 TeV collision energies», arXiv:1610.01342 [hep-ph].

[87] F. Caporale *et al.*, «High energy effects in multi-jet production at LHC», arXiv:1610.04765 [hep-ph].

[88] F. Caporale *et al.*, «Inclusive four-jet production at 7 and 13 TeV: azimuthal profile in multi-Regge kinematics», *Eur. Phys. J. C* **77**, 5 (2017).

[89] F.G. Celiberto, «BFKL phenomenology: resummation of high-energy logs in semi-hard processes at LHC», *Frascati Phys. Ser.* **63**, 43 (2016).

[90] F. Caporale *et al.*, «Inclusive three- and four-jet production in multi-Regge kinematics at the LHC», *AIP Conf. Proc.* **1819**, 060009 (2017).

[91] F. Caporale *et al.*, «Probing the BFKL dynamics in inclusive three jet production at the LHC», *EPJ Web Conf.* **164**, 07027 (2017).

[92] F. Caporale *et al.*, «Stability of azimuthal-angle observables under higher order corrections in inclusive three-jet production», *Phys. Rev. D* **95**, 074007 (2017).

[93] G. Chachamis *et al.*, «Azimuthal-angle Observables in Inclusive Three-jet Production», *PoS* **(DIS2017)**, 067 (2018).

[94] F. Caporale *et al.*, «Multi-jet production in the high energy limit at LHC», arXiv:1801.00014 [hep-ph].

[95] R. Boussarie, B. Ducloué, L. Szymanowski, S. Wallon, «Forward J/ψ and very backward jet inclusive production at the LHC», *Phys. Rev. D* **97**, 014008 (2018).

[96] F.G. Celiberto, M. Fucilla, «Inclusive production of a J/ψ or a Υ from single-parton fragmentation plus a jet in hybrid factorization», *Eur. Phys. J. C* **82**, 929 (2022), arXiv:2202.12227 [hep-ph].

[97] F.G. Celiberto, D.Yu. Ivanov, B. Murdaca, A. Papa, «High-energy resummation in heavy-quark pair photoproduction», *Phys. Lett. B* **777**, 141 (2018).

[98] A.D. Bolognino *et al.*, «High-energy resummation in heavy-quark pair hadroproduction», *Eur. Phys. J. C* **79**, 939 (2019).

[99] A.D. Bolognino *et al.*, «Inclusive production of two rapidity-separated heavy quarks as a probe of BFKL dynamics», *PoS* **(DIS2019)**, 067 (2019).

[100] K. Golec-Biernat, L. Motyka, T. Stebel, «Forward Drell–Yan and backward jet production as a probe of the BFKL dynamics», *J. High Energy Phys.* **2018**, 091 (2018).

[101] S.J. Brodsky, F. Hautmann, D.E. Soper, «Probing the QCD Pomeron in e^+e^- Collisions», *Phys. Rev. Lett.* **78**, 803 (1997); *Erratum ibid.* **79**, 3544 (1997).

[102] S.J. Brodsky, F. Hautmann, D.E. Soper, «Virtual photon scattering at high-energies as a probe of the short distance Pomeron», *Phys. Rev. D* **56**, 6957 (1997).

[103] S.J. Brodsky *et al.*, «The QCD Pomeron with optimal renormalization», *JETP Lett.* **70**, 155 (1999).

[104] S.J. Brodsky *et al.*, «High-energy QCD asymptotics of photon–photon collisions», *JETP Lett.* **76**, 249 (2002).

[105] F.G. Celiberto, D.Yu. Ivanov, M.M.A. Mohammed, A. Papa, «High-energy resummed distributions for the inclusive Higgs-plus-jet production at the LHC», *Eur. Phys. J. C* **81**, 293 (2021).

[106] F.G. Celiberto, D.Yu. Ivanov, M.M.A. Mohammed, A. Papa, «High-energy resummation in inclusive hadroproduction of Higgs plus jet», *SciPost Phys. Proc.* **8**, 039 (2022), arXiv:2107.13037 [hep-ph].

[107] F.G. Celiberto *et al.*, «Higgs-plus-jet inclusive production as stabilizer of the high-energy resummation», *PoS* **(EPS-HEP2021)**, 589 (2022).

[108] M. Fucilla *et al.*, «Higgs production in the high-energy limit of pQCD», *PoS* **(PANIC2021)**, 352 (2022).

[109] A.D. Bolognino *et al.*, «Inclusive production of a heavy-light dijet system in hybrid high-energy and colinear factorization», *Phys. Rev. D* **103**, 094004 (2021).

[110] A.D. Bolognino *et al.*, «Hybrid high-energy/colinear factorization in a heavy-light dijets system reaction», *SciPost Phys. Proc.* **8**, 068 (2022).

[111] A.D. Bolognino *et al.*, «Heavy-flavored emissions in hybrid colinear/high-energy factorization», *PoS* **(EPS-HEP2021)**, 389 (2022), arXiv:2110.12772 [hep-ph].

[112] F.G. Celiberto, M. Fucilla, D.Yu. Ivanov, A. Papa, «High-energy resummation in Λ_c baryon production», *Eur. Phys. J. C* **81**, 780 (2021).

[113] F.G. Celiberto *et al.*, «Bottom-flavored inclusive emissions in the variable-flavor number scheme: A high-energy analysis», *Phys. Rev. D* **104**, 114007 (2021).

[114] B.A. Kniehl, G. Kramer, I. Schienbein, H. Spiesberger, «$\Lambda_c^\pm$ production in pp collisions with a new fragmentation function», *Phys. Rev. D* **101**, 114021 (2020).

[115] B.A. Kniehl, G. Kramer, I. Schienbein, H. Spiesberger, «Finite-mass effects on inclusive B meson hadroproduction», *Phys. Rev. D* **77**, 014011 (2008).

[116] G. Kramer, H. Spiesberger, «b-hadron production in the general-mass variable-flavour-number scheme and LHC data», *Phys. Rev. D* **98**, 114010 (2018).

[117] A. Accardi *et al.*, «Electron Ion Collider: The next QCD frontier: Understanding the glue that binds us all», *Eur. Phys. J. A* **52**, 268 (2016).

[118] R. Abdul Khalek *et al.*, «Science Requirements and Detector Concepts for the Electron–Ion Collider: EIC Yellow Report», arXiv:2103.05419 [physics.ins-det].

[119] R.A. Khalek *et al.*, «Snowmass 2021 White Paper: Electron Ion Collider for High Energy Physics», arXiv:2203.13199 [hep-ph].

[120] E. Chapon *et al.*, «Prospects for quarkonium studies at the high-luminosity LHC», *Prog. Part. Nucl. Phys.* **122**, 103906 (2022).

[121] ILC International Development Team and ILC Community (I. Adachi *et al.*), «The International Linear Collider: Report to Snowmass 2021», arXiv:2203.07622 [physics.acc-ph].

[122] L.A. Anchordoqui *et al.*, «The Forward Physics Facility: Sites, experiments, and physics potential», *Phys. Rep.* **968**, 1 (2022), arXiv:2109.10905 [hep-ph].

[123] J.L. Feng *et al.*, «The Forward Physics Facility at the High-Luminosity LHC», *J. Phys. G: Nucl. Part. Phys.* **50**, 030501 (2023).

[124] A. Arbuzov *et al.*, «On the physics potential to study the gluon content of proton and deuteron at NICA SPD», *Prog. Part. Nucl. Phys.* **119**, 103858 (2021).

[125] SPD proto Collaboration (V.M. Abazov *et al.*), «Conceptual design of the Spin Physics Detector», arXiv:2102.00442 [hep-ex].

[126] M. Hentschinski, A. Sabio Vera, C. Salas, «Hard to Soft Pomeron Transition in Small-x Deep Inelastic Scattering Data Using Optimal Renormalization», *Phys. Rev. Lett.* **110**, 041601 (2013).

[127] M. Hentschinski, A. Sabio Vera, C. Salas, «F_2 and F_L at small x using a colinearly improved BFKL resummation», *Phys. Rev. D* **87**, 076005 (2013).

[128] I.V. Anikin *et al.*, «QCD factorization of exclusive processes beyond leading twist: $\gamma^*_\mathrm{T} \to \rho_\mathrm{T}$ impact factor with twist three accuracy», *Nucl. Phys. B* **828**, 1 (2010).

[129] I. Anikin *et al.*, «A phenomenological study of helicity amplitudes of high energy exclusive leptoproduction of the ρ meson», *Phys. Rev. D* **84**, 054004 (2011).

[130] A. Besse, L. Szymanowski, S. Wallon, «Saturation effects in exclusive $\rho_{\mathrm{T,L}}$ meson electroproduction», *J. High Energy Phys.* **2013**, 062 (2013).

[131] A.D. Bolognino, F.G. Celiberto, D.Yu. Ivanov, A. Papa, «Unintegrated gluon distribution from forward polarized ρ-electroproduction», *Eur. Phys. J. C* **78**, 1023 (2018).

[132] A.D. Bolognino, F.G. Celiberto, D.Yu. Ivanov, A. Papa, «ρ-meson leptoproduction as testfield for the unintegrated gluon distribution in the proton», *Frascati Phys. Ser.* **67**, 76 (2018).

[133] A.D. Bolognino, F.G. Celiberto, D.Yu. Ivanov, A. Papa, «Leptoproduction of ρ-mesons as Discriminator for the Unintegrated Gluon Distribution in the Proton», *Acta Phys. Pol. B Proc. Suppl.* **12**, 891 (2019).

[134] A.D. Bolognino, A. Szczurek, W. Schaefer, «Exclusive production of ϕ meson in the $\gamma^* p \to \phi p$ reaction at large photon virtualities within $k_\perp$-factorization approach», *Phys. Rev. D* **101**, 054041 (2020).

[135] F.G. Celiberto, «Unraveling the Unintegrated Gluon Distribution in the Proton via ρ-Meson Leptoproduction», *Nuovo Cim. C* **42**, 220 (2019).

[136] I. Bautista, A. Fernandez Tellez, M. Hentschinski, «BFKL evolution and the growth with energy of exclusive J/ψ and Υ photoproduction cross sections», *Phys. Rev. D* **94**, 054002 (2016).

[137] A. Arroyo Garcia, M. Hentschinski, K. Kutak, «QCD evolution based evidence for the onset of gluon saturation in exclusive photo-production of vector mesons», *Phys. Lett. B* **795**, 569 (2019).

[138] M. Hentschinski, E. Padrón Molina, «Exclusive J/Ψ and $\Psi(2s)$ photo-production as a probe of QCD low x evolution equations», *Phys. Rev. D* **103**, 074008 (2021).

[139] A.D. Bolognino *et al.*, «Exclusive production of ρ-mesons in high-energy factorization at HERA and EIC», *Eur. Phys. J. C* **81**, 846 (2021).

[140] A.D. Bolognino, F.G. Celiberto, D.Yu. Ivanov, A. Papa, «Exclusive emissions of rho-mesons and the unintegrated gluon distribution», *SciPost Phys. Proc.* **8**, 089 (2022).

[141] A.D. Bolognino *et al.*, «Hadron structure at small-x via unintegrated gluon densities», *Rev. Mex. Fis. Suppl.* **3**, 0308109 (2022), arXiv:2202.02513 [hep-ph].

[142] G. Chachamis *et al.*, «Single bottom quark production in $k_\perp$-factorization», *J. High Energy Phys.* **2015**, 123 (2015).

[143] L. Motyka, M. Sadzikowski, T. Stebel, «Twist expansion of Drell–Yan structure functions in color dipole approach», *J. High Energy Phys.* **2015**, 087 (2015).

[144] D. Brzemiński, L. Motyka, M. Sadzikowski, T. Stebel, «Twist decomposition of Drell–Yan structure functions: phenomenological implications», *J. High Energy Phys.* **2017**, 005 (2017).

[145] L. Motyka, M. Sadzikowski, T. Stebel, «Lam–Tung relation breaking in Z^0 hadroproduction as a probe of parton transverse momentum», *Phys. Rev. D* **95**, 114025 (2017).

[146] F.G. Celiberto, D. Gordo Gomez, A. Sabio Vera, «Forward Drell–Yan production at the LHC in the BFKL formalism with colinear corrections», *Phys. Lett. B* **786**, 201 (2018).

[147] S. Catani, M. Ciafaloni, F. Hautmann, «Gluon contributions to small x heavy flavor production», *Phys. Lett. B* **242**, 97 (1990).

[148] S. Catani, M. Ciafaloni, F. Hautmann, «High-energy factorization and small x heavy flavor production», *Nucl. Phys. B* **366**, 135 (1991).

[149] J.C. Collins, R. Ellis, «Heavy quark production in very high-energy hadron collisions», *Nucl. Phys. B* **360**, 3 (1991).

[150] M. Ciafaloni, «Coherence effects in initial jets at small Q^2/s», *Nucl. Phys. B* **296**, 49 (1988).

[151] S. Catani, F. Fiorani, G. Marchesini, «Small-x behavior of initial state radiation in perturbative QCD», *Nucl. Phys. B* **336**, 18 (1990).

[152] S. Catani, F. Fiorani, G. Marchesini, «QCD coherence in initial state radiation», *Phys. Lett. B* **234**, 339 (1990).

[153] G. Marchesini, «QCD coherence in the structure function and associated distributions at small x», *Nucl. Phys. B* **445**, 49 (1995).

[154] J. Kwieciński, «Unintegrated Gluon Distributions from the Transverse Coordinate Representation of the CCFM Equation in the Single Loop Approximation», *Acta Phys. Pol. B* **33**, 1809 (2002).

[155] R.D. Ball, S. Forte, «Summation of leading logarithms at small x», *Phys. Lett. B* **351**, 313 (1995).

[156] R.D. Ball, S. Forte, «Asymptotically free partons at high-energy», *Phys. Lett. B* **405**, 317 (1997).

[157] G. Altarelli, R.D. Ball, S. Forte, «Factorization and resummation of small x scaling violations with running coupling», *Nucl. Phys. B* **621**, 359 (2002).

[158] G. Altarelli, R.D. Ball, S. Forte, «An anomalous dimension for small x evolution», *Nucl. Phys. B* **674**, 459 (2003).

[159] G. Altarelli, R.D. Ball, S. Forte, «Perturbatively stable resummed small x evolution kernels», *Nucl. Phys. B* **742**, 1 (2006).

[160] G. Altarelli, R.D. Ball, S. Forte, «Small x resummation with quarks: Deep-inelastic scattering», *Nucl. Phys. B* **799**, 199 (2008).

[161] C. White, R. Thorne, «A global fit to scattering data with next-to-leading logarithmic BFKL resummations», *Phys. Rev. D* **75**, 034005 (2007).

[162] R.D. Ball *et al.*, «Parton distributions with small-x resummation: evidence for BFKL dynamics in HERA data», *Eur. Phys. J. C* **78**, 321 (2018).

[163] xFitter Developers' Team Collaboration (H. Abdolmaleki *et al.*), «Impact of low-x resummation on QCD analysis of HERA data», *Eur. Phys. J. C* **78**, 621 (2018).

[164] M. Bonvini, F. Giuli, «A new simple PDF parametrization: improved description of the HERA data», *Eur. Phys. J. Plus* **134**, 531 (2019).

[165] F. Dominguez, C. Marquet, B.-W. Xiao, F. Yuan, «Universality of Unintegrated Gluon Distributions at small x», *Phys. Rev. D* **83**, 105005 (2011).

[166] M. Hentschinski, «Transverse momentum dependent gluon distribution within high energy factorization at next-to-leading order», *Phys. Rev. D* **104**, 054014 (2021).

[167] M. Nefedov, «Sudakov resummation from the BFKL evolution», *Phys. Rev. D* **104**, 054039 (2021).

[168] T. Altinoluk, R. Boussarie, P. Kotko, «Interplay of the CGC and TMD frameworks to all orders in kinematic twist», *J. High Energy Phys.* **2019**, 156 (2019).

[169] H. Fujii, C. Marquet, K. Watanabe, «Comparison of improved TMD and CGC frameworks in forward quark dijet production», *J. High Energy Phys.* **2020**, 181 (2020).

[170] R. Boussarie, H. Mäntysaari, F. Salazar, B. Schenke, «The importance of kinematic twists and genuine saturation effects in dijet production at the Electron–Ion Collider», *J. High Energy Phys.* **2021**, 178 (2021).

[171] P. Kotko *et al.*, «Improved TMD factorization for forward dijet production in dilute-dense hadronic collisions», *J. High Energy Phys.* **2015**, 106 (2015).

[172] A. van Hameren *et al.*, «Forward di-jet production in p+Pb collisions in the small-x improved TMD factorization framework», *J. High Energy Phys.* **2016**, 034 (2016); *Erratum ibid.* **2019**, 158 (2019).

[173] N. Brambilla *et al.*, «Heavy quarkonium: progress, puzzles, and opportunities», *Eur. Phys. J. C* **71**, 1534 (2011).

[174] N. Brambilla *et al.*, «QCD and strongly coupled gauge theories: challenges and perspectives», *Eur. Phys. J. C* **74**, 2981 (2014).

[175] J.-P. Lansberg, «New observables in inclusive production of quarkonia», *Phys. Rep.* **889**, 1 (2020).

[176] C. Hadjidakis *et al.*, «A fixed-target programme at the LHC: Physics case and projected performances for heavy-ion, hadron, spin and astroparticle studies», *Phys. Rep.* **911**, 1 (2021).

[177] S.J. Brodsky, F. Fleuret, C. Hadjidakis, J.P. Lansberg, «Physics Opportunities of a Fixed-Target Experiment using the LHC Beams», *Phys. Rep.* **522**, 239 (2013).

[178] R. Gastmans, W. Troost, T.T. Wu, «Cross sections for gluon+gluon $\to$ heavy quarkonium+gluon», *Phys. Lett. B* **184**, 257 (1987).

[179] G.T. Bodwin, E. Braaten, G. Lepage, «Rigorous QCD analysis of inclusive annihilation and production of heavy quarkonium», *Phys. Rev. D* **51**, 1125 (1995); *Erratum ibid.* **55**, 5853 (1997).

[180] N. Brambilla, H.S. Chung, A. Vairo, «Inclusive production of heavy quarkonia in pNRQCD», *J. High Energy Phys.* **2021**, 032 (2021).

[181] Y.-Q. Ma, K.-T. Chao, «New factorization theory for heavy quarkonium production and decay», *Phys. Rev. D* **100**, 094007 (2019).

[182] R. Li, Y. Feng, Y.-Q. Ma, «Exclusive quarkonium production or decay in soft gluon factorization», *J. High Energy Phys.* **2020**, 009 (2020).

[183] J.-P. Lansberg, M.A. Ozcelik, «Curing the unphysical behaviour of NLO quarkonium production at the LHC and its relevance to constrain the gluon PDF at low scales», *Eur. Phys. J. C* **81**, 497 (2021).

[184] A. Colpani Serri *et al.*, «Revisiting NLO QCD corrections to total inclusive J/ψ and Υ photoproduction cross sections in lepton–proton collisions», *Phys. Lett. B* **835**, 137556 (2022), arXiv:2112.05060 [hep-ph].

[185] S. Catani, F. Hautmann, «High-energy factorization and small x deep inelastic scattering beyond leading order», *Nucl. Phys. B* **427**, 475 (1994).

[186] J.-P. Lansberg, M. Nefedov, M.A. Ozcelik, «Matching next-to-leading-order and high-energy-resummed calculations of heavy-quarkonium-hadro-production cross sections», *J. High Energy Phys.* **2022**, 083 (2022), arXiv:2112.06789 [hep-ph].

[187] M.G. Echevarria *et al.*, «Matching factorization theorems with an inverse-error weighting», *Phys. Lett. B* **781**, 161 (2018).

[188] C. Barschel *et al.*, «LHC fixed target experiments: Report from the LHC Fixed Target Working Group of the CERN Physics Beyond Colliders Forum», *CERN Yellow Rep. Monogr.* **4**, 1 (2020).

[189] A.H. Mueller, W.-K. Tang, «High-energy parton–parton elastic scattering in QCD», *Phys. Lett. B* **284**, 123 (1992).

[190] D0 Collaboration (S. Abachi *et al.*), «Rapidity Gaps Between Jets in $p\bar{p}$ Collisions at $\sqrt{s} = 1.8$ TeV», *Phys. Rev. Lett.* **72**, 2332 (1994).

[191] CDF Collaboration (F. Abe *et al.*), «Events with a Rapidity Gap Between Jets in $\bar{p}p$ Collisions at $\sqrt{s} = 630$ GeV», *Phys. Rev. Lett.* **81**, 5278 (1998).

[192] CMS Collaboration (A.M. Sirunyan *et al.*), «Study of dijet events with a large rapidity gap between the two leading jets in pp collisions at $\sqrt{s} = 7$ TeV», *Eur. Phys. J. C* **78**, 242 (2018), *Erratum ibid.* **80**, 441 (2020).

[193] CMS and TOTEM collaborations, «Hard color-singlet exchange in dijet events in proton–proton collisions at $\sqrt{s} = 13$ TeV», *Phys. Rev. D* **104**, 032009 (2021), arXiv:2102.06945 [hep-ex].

[194] B. Cox, J.R. Forshaw, L. Lönnblad, «Hard color-singlet exchange at the Tevatron», *J. High Energy Phys.* **1999**, 023 (1999).

[195] L. Motyka, A.D. Martin, M.G. Ryskin, «The Nonforward BFKL amplitude and rapidity gap physics», *Phys. Lett. B* **524**, 107 (2002).

[196] R. Enberg, G. Ingelman, L. Motyka, «Hard color-singlet exchange and gaps between jets at the Tevatron», *Phys. Lett. B* **524**, 273 (2002).

[197] O. Kepka, C. Marquet, C. Royon, «Gaps between jets in hadronic collisions», *Phys. Rev. D* **83**, 034036 (2011).

[198] A. Ekstedt, R. Enberg, G. Ingelman, «Hard color-singlet BFKL exchange and gaps between jets at the LHC», arXiv:1703.10919 [hep-ph].

[199] CMS Collaboration (A.M. Sirunyan *et al.*), «Extraction and validation of a new set of CMS PYTHIA 8 tunes from underlying-event measurements», *Eur. Phys. J. C* **80**, 4 (2020).

[200] CMS Collaboration (A.M. Sirunyan *et al.*), «Measurement of exclusive $\rho(770)^0$ photoproduction in ultraperipheral pPb collisions at $\sqrt{s_{NN}} = 5.02$ TeV», *Eur. Phys. J. C* **79**, 702 (2019).

[201] M. Hentschinski, J.D. Madrigal Martínez, B. Murdaca, A. Sabio Vera, «The next-to-leading order vertex for a forward jet plus a rapidity gap at high energies», *Phys. Lett. B* **735**, 168 (2014).

[202] M. Hentschinski, J.D. Madrigal Martínez, B. Murdaca, A. Sabio Vera, «The gluon-induced Mueller–Tang jet impact factor at next-to-leading order», *Nucl. Phys. B* **889**, 549 (2014).

[203] A. Banfi, G. Marchesini, G. Smye, «Away from jet energy flow», *J. High Energy Phys.* **2002**, 006 (2002).

[204] Y. Hatta, T. Ueda, «Jet energy flow at the LHC», *Phys. Rev. D* **80**, 074018 (2009).

[205] J. Jalilian-Marian, A. Kovner, L.D. McLerran, H. Weigert, «The intrinsic glue distribution at very small x», *Phys. Rev. D* **55**, 5414 (1997).

[206] J. Jalilian-Marian, A. Kovner, A. Leonidov, H. Weigert, «The BFKL equation from the Wilson renormalization group», *Nucl. Phys. B* **504**, 415 (1997).

[207] J. Jalilian-Marian, A. Kovner, A. Leonidov, H. Weigert, «The Wilson renormalization group for low x physics: Towards the high density regime», *Phys. Rev. D* **59**, 014014 (1998).

[208] J. Jalilian-Marian, A. Kovner, H. Weigert, «The Wilson renormalization group for low x physics: Gluon evolution at finite parton density», *Phys. Rev. D* **59**, 014015 (1998).

[209] J. Jalilian-Marian, A. Kovner, A. Leonidov, H. Weigert, «Unitarization of gluon distribution in the doubly logarithmic regime at high density», *Phys. Rev. D* **59**, 034007 (1999); *Erratum ibid.* **59**, 099903 (1999).

[210] A. Kovner, J.G. Milhano, H. Weigert, «Relating different approaches to nonlinear QCD evolution at finite gluon density», *Phys. Rev. D* **62**, 114005 (2000).

[211] H. Weigert, «Unitarity at small Bjorken x», *Nucl. Phys. A* **703**, 823 (2002).

[212] A. Kovner, J.G. Milhano, «Vector potential *versus* color charge density in low x evolution», *Phys. Rev. D* **61**, 014012 (2000).

[213] E. Iancu, A. Leonidov, L.D. McLerran, «Nonlinear gluon evolution in the color glass condensate. 1.», *Nucl. Phys. A* **692**, 583 (2001).

[214] E. Iancu, A. Leonidov, L.D. McLerran, «The Renormalization group equation for the color glass condensate», *Phys. Lett. B* **510**, 133 (2001).

[215] E. Ferreiro, E. Iancu, A. Leonidov, L. McLerran, «Nonlinear gluon evolution in the color glass condensate. 2.», *Nucl. Phys. A* **703**, 489 (2002).

[216] I. Balitsky, «Operator expansion for high-energy scattering», *Nucl. Phys. B* **463**, 99 (1996).

[217] Y.V. Kovchegov, «Small-x F_2 structure function of a nucleus including multiple Pomeron exchanges», *Phys. Rev. D* **60**, 034008 (1999).

[218] J. Collins, «Foundations of perturbative QCD», *Camb. Monogr. Part. Phys. Nucl. Phys. Cosmol.* **32**, 1 (2011).

[219] J.C. Collins, D.E. Soper, «Back-to-back jets in QCD», *Nucl. Phys. B* **193**, 381 (1981); *Erratum ibid.* **213**, 545 (1983).

[220] P.J. Mulders, J. Rodrigues, «Transverse momentum dependence in gluon distribution and fragmentation functions», *Phys. Rev. D* **63**, 094021 (2001).

[221] S. Meissner, A. Metz, K. Goeke, «Relations between generalized and transverse momentum dependent parton distributions», *Phys. Rev. D* **76**, 034002 (2007).

[222] C. Lorcé, B. Pasquini, «Structure analysis of the generalized correlator of quark and gluon for a spin-1/2 target», *J. High Energy Phys.* **2013**, 138 (2013).

[223] G. Bozzi, S. Catani, D. de Florian, M. Grazzini, «The q_{T} spectrum of the Higgs boson at the LHC in QCD perturbation theory», *Phys. Lett. B* **564**, 65 (2003).

[224] S. Catani, M. Grazzini, «QCD transverse-momentum resummation in gluon fusion processes», *Nucl. Phys. B* **845**, 297 (2011).

[225] M.G. Echevarria, T. Kasemets, P.J. Mulders, C. Pisano, «QCD evolution of (un)polarized gluon TMDPDFs and the Higgs q_{T}-distribution», *J. High Energy Phys.* **2015**, 158 (2015); *Erratum ibid.* **2017**, 073 (2017).

[226] D. Boer, S.J. Brodsky, P.J. Mulders, C. Pisano, «Direct Probes of Linearly Polarized Gluons Inside Unpolarized Hadrons», *Phys. Rev. Lett.* **106**, 132001 (2011).

[227] P. Sun, B.-W. Xiao, F. Yuan, «Gluon distribution functions and higgs boson production at moderate transverse momentum», *Phys. Rev. D* **84**, 094005 (2011).

[228] D. Boer *et al.*, «Linearly Polarized Gluons and the Higgs Transverse Momentum Distribution», *Phys. Rev. Lett.* **108**, 032002 (2012).

[229] C. Pisano *et al.*, «Linear polarization of gluons and photons in unpolarized collider experiments», *J. High Energy Phys.* **2013**, 024 (2013).

[230] W.J. den Dunnen, J.-P. Lansberg, C. Pisano, M. Schlegel, «Accessing the Transverse Dynamics and Polarization of Gluons Inside the Proton at the LHC», *Phys. Rev. Lett.* **112**, 212001 (2014).

[231] J.-P. Lansberg, C. Pisano, M. Schlegel, «Associated production of a dilepton and a $\Upsilon(J/\psi)$ at the LHC as a probe of gluon transverse momentum dependent distributions», *Nucl. Phys. B* **920**, 192 (2017).

[232] R. Boussarie, Y. Hatta, L. Szymanowski, S. Wallon, «Probing the Gluon Sivers Function with an Unpolarized Target: GTMD Distributions and the Odderons», *Phys. Rev. Lett.* **124**, 172501 (2020).

[233] J.-P. Lansberg, C. Pisano, F. Scarpa, M. Schlegel, «Pinning down the linearly-polarised gluons inside unpolarised protons using quarkonium-pair production at the LHC», *Phys. Lett. B* **784**, 217 (2018); *Corrigendum ibid.* **791**, 420 (2019).

[234] D. Gutierrez-Reyes, S. Leal-Gomez, I. Scimemi, A. Vladimirov, «Linearly polarized gluons at next-to-next-to leading order and the Higgs transverse momentum distribution», *J. High Energy Phys.* **2019**, 121 (2019).

[235] F. Scarpa *et al.*, «Studies of gluon TMDs and their evolution using quarkonium-pair production at the LHC», *Eur. Phys. J. C* **80**, 87 (2020).

[236] COMPASS Collaboration (C. Adolph *et al.*), «First measurement of the Sivers asymmetry for gluons using SIDIS data», *Phys. Lett. B* **772**, 854 (2017).

[237] U. D'Alesio, F. Murgia, C. Pisano, P. Taels, «Probing the gluon Sivers function in $p^\uparrow p \to J/\psi\, X$ and $p^\uparrow p \to D\, X$», *Phys. Rev. D* **96**, 036011 (2017).

[238] U. D'Alesio *et al.*, «Unraveling the gluon Sivers function in hadronic collisions at RHIC», *Phys. Rev. D* **99**, 036013 (2019).

[239] U. D'Alesio, F. Murgia, C. Pisano, P. Taels, «Azimuthal asymmetries in semi-inclusive J/ψ + jet production at an EIC», *Phys. Rev. D* **100**, 094016 (2019).

[240] Z. Lu, B.-Q. Ma, «Gluon Sivers function in a light-cone spectator model», *Phys. Rev. D* **94**, 094022 (2016).

[241] J. M. Pereira-Resina-Rodrigues, «Modelling quark and gluon correlation functions», Ph.D. Thesis, Vrije University, Amsterdam, 2001.

[242] A. Bacchetta, F. Conti, M. Radici, «Transverse-momentum distributions in a diquark spectator model», *Phys. Rev. D* **78**, 074010 (2008).

[243] A. Bacchetta, M. Radici, F. Conti, M. Guagnelli, «Weighted azimuthal asymmetries in a diquark spectator model», *Eur. Phys. J. A* **45**, 373 (2010).

[244] L.P. Gamberg, G.R. Goldstein, «"T-odd" effects in unpolarized Drell–Yan scattering», *Phys. Lett. B* **650**, 362 (2007).

[245] L.P. Gamberg, G.R. Goldstein, M. Schlegel, «Transverse Quark Spin Effects and the Flavor Dependence of the Boer–Mulders Function», *Phys. Rev. D* **77**, 094016 (2008).

[246] R. Jakob, P.J. Mulders, J. Rodrigues, «Modeling quark distribution and fragmentation functions», *Nucl. Phys. A* **626**, 937 (1997).

[247] A. Bacchetta, F.G. Celiberto, M. Radici, P. Taels, «Transverse-momentum-dependent gluon distribution functions in a spectator model», *Eur. Phys. J. C* **80**, 733 (2020).

[248] F.G. Celiberto, «3D tomography of the nucleon: transverse-momentum-dependent gluon distributions», *Nuovo Cim. C* **44**, 36 (2021).

[249] A. Bacchetta, F.G. Celiberto, M. Radici, P. Taels, «A spectator-model way to transverse-momentum-dependent gluon distribution functions», *SciPost Phys. Proc.* **8**, 040 (2022).

[250] F.G. Celiberto, «Phenomenology of the hadronic structure at small-x», arXiv:2202.04207 [hep-ph].

[251] A. Bacchetta, F.G. Celiberto, M. Radici, «Toward twist-2 T-odd transverse-momentum-dependent gluon distributions: the f-type Sivers function», *PoS* **(EPS-HEP2021)**, 376 (2022), arXiv:2111.01686 [hep-ph].

[252] A. Bacchetta, F.G. Celiberto, M. Radici, «Toward twist-2 T-odd transverse-momentum-dependent gluon distributions: the f-type linearity function», *PoS* **(PANIC2021)**, 378 (2022), arXiv:2111.03567 [hep-ph].

[253] A. Bacchetta, F.G. Celiberto, M. Radici, «Towards leading-twist T-odd TMD gluon distributions», *JPS Conf. Proc.* **37**, 020124 (2022), arXiv:2201.10508 [hep-ph].

[254] F. Dominguez, J.-W. Qiu, B.-W. Xiao, F. Yuan, «On the linearly polarized gluon distributions in the color dipole model», *Phys. Rev. D* **85**, 045003 (2012).

[255] C. Marquet, E. Petreska, C. Roiesnel, «Transverse-momentum-dependent gluon distributions from JIMWLK evolution», *J. High Energy Phys.* **2016**, 065 (2016).

[256] P. Taels, «Quantum Chromodynamics at small Bjorken-x», Ph.D. Thesis, Antwerp University, 2017.

[257] C. Marquet, C. Roiesnel, P. Taels, «Linearly polarized small-x gluons in forward heavy-quark pair production», *Phys. Rev. D* **97**, 014004 (2018).

[258] E. Petreska, «TMD gluon distributions at small x in the CGC theory», *Int. J. Mod. Phys. E* **27**, 1830003 (2018).

[259] Y. Hatta, B.-W. Xiao, F. Yuan, «Probing the Small-x Gluon Tomography in Correlated Hard Diffractive Dijet Production in Deep Inelastic Scattering», *Phys. Rev. Lett.* **116**, 202301 (2016).

[260] R. Boussarie *et al.*, «Next-to-Leading Order Computation of Exclusive Diffractive Light Vector Meson Production in a Saturation Framework», *Phys. Rev. Lett.* **119**, 072002 (2017).

[261] P. Caucal, F. Salazar, R. Venugopalan, «Dijet impact factor in DIS at next-to-leading order in the Color Glass Condensate», *J. High Energy Phys.* **2021**, 222 (2021).

[262] R. Boussarie, A.V. Grabovsky, L. Szymanowski, S. Wallon, «Impact factor for high-energy two and three jets diffractive production», *J. High Energy Phys.* **2014**, 026 (2014).

[263] R. Boussarie, A.V. Grabovsky, L. Szymanowski, S. Wallon, «On the one loop $\gamma^{(*)} \to q\bar{q}$ impact factor and the exclusive diffractive cross sections for the production of two or three jets», *J. High Energy Phys.* **2016**, 149 (2016).

[264] Y. Hagiwara *et al.*, «Accessing the gluon Wigner distribution in ultraperipheral pA collisions», *Phys. Rev. D* **96**, 034009 (2017).

[265] R. Boussarie, A.V. Grabovsky, L. Szymanowski, S. Wallon, «Towards a complete next-to-logarithmic description of forward exclusive diffractive dijet electroproduction at HERA: real corrections», *Phys. Rev. D* **100**, 074020 (2019).

[266] R. Boussarie, B. Pire, L. Szymanowski, S. Wallon, «Exclusive photoproduction of a $\gamma\,\rho$ pair with a large invariant mass», *J. High Energy Phys.* **2017**, 054 (2017); *Erratum ibid.* **2018**, 029 (2018).

[267] G. Duplančić *et al.*, «Probing axial quark generalized parton distributions through exclusive photoproduction of a $\gamma\,\pi^{\pm}$ pair with a large invariant mass», *J. High Energy Phys.* **2018**, 179 (2018).

[268] M. Bury, P. Kotko, K. Kutak, «TMD gluon distributions for multiparton processes», *Eur. Phys. J. C* **79**, 152 (2019).

[269] M. Bury, A. van Hameren, P. Kotko, K. Kutak, «Forward trijet production in p–p and p–Pb collisions at LHC», *J. High Energy Phys.* **2020**, 175 (2020).

[270] R. Boussarie, Y. Mehtar-Tani, «Gauge invariance of transverse momentum dependent distributions at small x», *Phys. Rev. D* **103**, 094012 (2021).

[271] T. Altinoluk, C. Marquet, P. Taels, «Low-x improved TMD approach to the lepto- and hadroproduction of a heavy-quark pair», *J. High Energy Phys.* **2021**, 085 (2021).

[272] M. Deak, F. Hautmann, H. Jung, K. Kutak, «Forward Jet Production at the Large Hadron Collider», *J. High Energy Phys.* **2009**, 121 (2009).

[273] A. van Hameren, P. Kotko, K. Kutak, S. Sapeta, «Small-x dynamics in forward-central dijet decorrelations at the LHC», *Phys. Lett. B* **737**, 335 (2014).

[274] A. van Hameren, P. Kotko, K. Kutak, «Resummation effects in the forward production of Z_0+jet at the LHC», *Phys. Rev. D* **92**, 054007 (2015).

[275] A. Mueller, B.-W. Xiao, F. Yuan, «Sudakov double logarithms resummation in hard processes in the small-x saturation formalism», *Phys. Rev. D* **88**, 114010 (2013).

[276] A. Mueller, B.-W. Xiao, F. Yuan, «Sudakov Resummation in Small-x Saturation Formalism», *Phys. Rev. Lett.* **110**, 082301 (2013).

[277] K. Kutak, «Hard scale dependent gluon density, saturation and forward–forward dijet production at the LHC», *Phys. Rev. D* **91**, 034021 (2015).

[278] A. van Hameren, P. Kotko, K. Kutak, S. Sapeta, «Broadening and saturation effects in dijet azimuthal correlations in p–p and p–Pb collisions at $\sqrt{s} = 5.02$ TeV», *Phys. Lett. B* **795**, 511 (2019).

[279] A. van Hameren *et al.*, «Probing gluon number density with electron-dijet correlations at EIC», *Eur. Phys. J. C* **81**, 741 (2021).

[280] ATLAS Collaboration (M. Aaboud *et al.*), «Dijet azimuthal correlations and conditional yields in pp and p+Pb collisions at $\sqrt{s_{NN}} = 5.02$ TeV with the ATLAS detector», *Phys. Rev. C* **100**, 034903 (2019).

[281] V. Guzey, M. Strikman, W. Vogelsang, «Observations on dA scattering at forward rapidities», *Phys. Lett. B* **603**, 173 (2004).

[282] A. Dumitru, A. Hayashigaki, J. Jalilian-Marian, «The color glass condensate and hadron production in the forward region», *Nucl. Phys. A* **765**, 464 (2006).

[283] J. Jalilian-Marian, «Rapidity loss, spin, and angular asymmetries in the scattering of a quark from the color field of a proton or nucleus», *Phys. Rev. D* **102**, 014008 (2020).

[284] J. Jalilian-Marian, «Quark jets scattering from a gluon field: from saturation to high p_t», *Phys. Rev. D* **99**, 014043 (2019).

[285] J. Jalilian-Marian, «Elastic scattering of a quark from a color field: longitudinal momentum exchange», *Phys. Rev. D* **96**, 074020 (2017).

[286] M. Hentschinski, A. Kusina, K. Kutak, M. Serino, «TMD splitting functions in $k_\perp$ factorization: the real contribution to the gluon-to-gluon splitting», *Eur. Phys. J. C* **78**, 174 (2018).

[287] O. Gituliar, M. Hentschinski, K. Kutak, «Transverse-momentum-dependent quark splitting functions in $k_\perp$-factorization: real contributions», *J. High Energy Phys.* **2016**, 181 (2016).

[288] L. Frankfurt, M. Strikman, «Energy losses in the black disc regime and correlation effects in the STAR forward pion production in dAu collisions», *Phys. Lett. B* **645**, 412 (2007).

[289] A. Dumitru, L. Gerland, M. Strikman, «Proton Breakup in High-energy pA Collisions from Perturbative QCD», *Phys. Rev. Lett.* **90**, 092301 (2003); *Erratum ibid.* **91**, 259901 (2003).

[290] BRAHMS Collaboration (I. Arsene *et al.*), «On the Evolution of the Nuclear Modification Factors with Rapidity and Centrality in d+Au Collisions at $\sqrt{s_{NN}} = 200$ GeV», *Phys. Rev. Lett.* **93**, 242303 (2004).

[291] STAR Collaboration (J. Adams *et al.*), «Forward Neutral Pion Production in $p+p$ and d+Au Collisions at $\sqrt{s_{NN}} = 200$ GeV», *Phys. Rev. Lett.* **97**, 152302 (2006).

[292] ALICE Collaboration (J. Adam *et al.*), «Centrality dependence of particle production in p–Pb collisions at $\sqrt{s_{NN}} = 5.02$ TeV», *Phys. Rev. C* **91**, 064905 (2015).

[293] T.C. Rogers, A.M. Staśto, M.I. Strikman, «Unitarity Constraints on Semi-hard Jet Production in Impact Parameter Space», *Phys. Rev. D* **77**, 114009 (2008).

[294] M. Azarkin, P. Kotko, A. Siodmok, M. Strikman, «Studying mini-jets and MPI with rapidity correlations», *Eur. Phys. J. C* **79**, 180 (2019).

[295] M. Alvioli, M. Azarkin, B. Blok, M. Strikman, «Revealing mini-jet dynamics via centrality dependence of double parton interactions in proton–nucleus collisions», *Eur. Phys. J. C* **79**, 482 (2019).

[296] D. d'Enterria, J. Rojo, «Quantitative constraints on the gluon distribution function in the proton from collider isolated-photon data», *Nucl. Phys. B* **860**, 311 (2012).

[297] LHCb Collaboration (J. Alves *et al.*), «The LHCb Detector at the LHC», *J. Instrum.* **3**, S08005 (2008).

[298] LHCb Collaboration (R. Aaij *et al.*), «LHCb detector performance», *Int. J. Mod. Phys. A* **30**, 1530022 (2015).

[299] ALICE Collaboration, «Letter of Intent: A Forward Calorimeter (FoCal) in the ALICE experiment», CERN-LHCC-2020-009, LHCC-I-036, 2020, http://cds.cern.ch/record/2719928

[300] G.P. Salam, «An Introduction to Leading and Next-to-leading BFKL», *Acta Phys. Pol. B* **30**, 3679 (1999).

[301] A.H. Mueller, «A Simple derivation of the JIMWLK equation», *Phys. Lett. B* **523**, 243 (2001).

[302] T. Lappi, H. Mäntysaari, «Next-to-leading order Balitsky–Kovchegov equation with resummation», *Phys. Rev. D* **93**, 094004 (2016).

[303] NNPDF Collaboration (R. Abdul Khalek, J.J. Ethier, J. Rojo), «Nuclear parton distributions from lepton–nucleus scattering and the impact of an electron–ion collider», *Eur. Phys. J. C* **79**, 471 (2019).

[304] R. Abdul Khalek, J.J. Ethier, J. Rojo, G. van Weelden, «nNNPDF2.0: quark flavor separation in nuclei from LHC data», *J. High Energy Phys.* **2020**, 183 (2020).

[305] E.C. Aschenauer *et al.*, «Nuclear structure functions at a Future Electron–Ion Collider», *Phys. Rev. D* **96**, 114005 (2017).

[306] LHCb Collaboration (R. Aaij *et al.*), «Study of prompt D^0 meson production in pPb collisions at $\sqrt{s_{NN}} = 5$ TeV», *J. High Energy Phys.* **2017**, 090 (2017).

[307] R.A. Khalek *et al.*, «nNNPDF3.0: Evidence for a modified partonic structure in heavy nuclei», *Eur. Phys. J. C* **82**, 507 (2022), arXiv:2201.12363 [hep-ph].

[308] CMS Collaboration (A.M. Sirunyan *et al.*), «Evidence for Top Quark Production in Nucleus–Nucleus Collisions», *Phys. Rev. Lett.* **125**, 222001 (2020).

[309] D. d'Enterria, K. Krajczár, H. Paukkunen, «Top-quark production in proton–nucleus and nucleus–nucleus collisions at LHC energies and beyond», *Phys. Lett. B* **746**, 64 (2015).

[310] M. Czakon, A. Mitov, «Top++: A Program for the Calculation of the Top-Pair Cross-Section at Hadron Colliders», *Comput. Phys. Commun.* **185**, 2930 (2014).

[311] M. Czakon, P. Fiedler, A. Mitov, «Total Top-Quark Pair-Production Cross Section at Hadron Colliders Through $O(\alpha_S^4)$», *Phys. Rev. Lett.* **110**, 252004 (2013).

[312] K. Kovarik *et al.*, «nCTEQ15 — Global analysis of nuclear parton distributions with uncertainties in the CTEQ framework», *Phys. Rev. D* **93**, 085037 (2016).

[313] L. Apolinário, J.G. Milhano, G.P. Salam, C.A. Salgado, «Probing the Time Structure of the Quark–Gluon Plasma with Top Quarks», *Phys. Rev. Lett.* **120**, 232301 (2018).

[314] Z. Citron *et al.*, «Report from Working Group 5: Future physics opportunities for high-density QCD at the LHC with heavy-ion and proton beams», *CERN Yellow Rep. Monogr.* **7**, 1159 (2019).

[315] M.W. Krasny, A. Petrenko, W. Płaczek, «High-luminosity Large Hadron Collider with laser-cooled isoscalar ion beams», *Prog. Part. Nucl. Phys.* **114**, 103792 (2020).

[316] S.R. Klein *et al.*, «New opportunities at the photon energy frontier», arXiv:2009.03838 [hep-ph].

[317] A.J. Baltz, «The Physics of Ultraperipheral Collisions at the LHC», *Phys. Rep.* **458**, 1 (2008).

[318] S.R. Klein, H. Mäntysaari, «Imaging the nucleus with high-energy photons», *Nature Rev. Phys.* **1**, 662 (2019).

[319] A. Morreale, F. Salazar, «Mining for Gluon Saturation at Colliders», *Universe* **7**, 312 (2021).

[320] N. Armesto, «Nuclear shadowing», *J. Phys. G: Nucl. Part. Phys.* **32**, R367 (2006).

[321] M.L. Good, W.D. Walker, «Diffraction disssociation of beam particles», *Phys. Rev.* **120**, 1857 (1960).

[322] H.I. Miettinen, J. Pumplin, «Diffraction scattering and the parton structure of hadrons», *Phys. Rev. D* **18**, 1696 (1978).

[323] STAR Collaboration (G. Agakishiev *et al.*), «ρ^0 Photoproduction in AuAu Collisions at $\sqrt{s_{NN}} = 62.4$ GeV with STAR», *Phys. Rev. C* **85**, 014910 (2012).

[324] STAR Collaboration (C. Adler *et al.*), «Coherent ρ^0 Production in Ultraperipheral Heavy-Ion Collisions», *Phys. Rev. Lett.* **89**, 272302 (2002).

[325] STAR Collaboration (L. Adamczyk *et al.*), «Coherent diffractive photoproduction of ρ^0 mesons on gold nuclei at 200 GeV/nucleon-pair at the Relativistic Heavy Ion Collider», *Phys. Rev. C* **96**, 054904 (2017).

[326] ALICE Collaboration (J. Adam *et al.*), «Coherent ρ^0 photoproduction in ultra-peripheral Pb–Pb collisions at $\sqrt{s_{NN}} = 2.76$ TeV», *J. High Energy Phys.* **2015**, 095 (2015).

[327] ALICE Collaboration (S. Acharya *et al.*), «Coherent photoproduction of ρ^0 vector mesons in ultra-peripheral Pb–Pb collisions at $\sqrt{s_{NN}} = 5.02$ TeV», *J. High Energy Phys.* **2020**, 035 (2020).

[328] ALICE Collaboration (S. Acharya *et al.*), «First measurement of coherent ρ^0 photoproduction in ultra-peripheral Xe–Xe collisions at $\sqrt{s_{NN}} = 5.44$ TeV», *Phys. Lett. B* **820**, 136481 (2021).

[329] L. Frankfurt, V. Guzey, M. Strikman, M. Zhalov, «Nuclear shadowing in photoproduction of ρ mesons in ultraperipheral nucleus collisions at RHIC and the LHC», *Phys. Lett. B* **752**, 51 (2016).

[330] STAR Collaboration (B.I. Abelev *et al.*), «Observation of $\pi^+\pi^-\pi^+\pi^-$ Photoproduction in Ultra-Peripheral Heavy Ion Collisions at STAR», *Phys. Rev. C* **81**, 044901 (2010).

[331] L. Frankfurt, M. Strikman, M. Zhalov, «Predictions of the generalized Glauber model for the coherent ρ production at RHIC and the STAR data», *Phys. Rev. C* **67**, 034901 (2003).

[332] STAR Collaboration (S.R. Klein), «Ultra-Peripheral Collisions with gold ions in STAR», *PoS* **(DIS2016)**, 188 (2016).

[333] S.R. Klein, J. Nystrand, «Exclusive vector meson production in relativistic heavy ion collisions», *Phys. Rev. C* **60**, 014903 (1999).

[334] V. Guzey, E. Kryshen, M. Zhalov, «Coherent photoproduction of vector mesons in ultraperipheral heavy ion collisions: Update for Run 2 at the CERN Large Hadron Collider», *Phys. Rev. C* **93**, 055206 (2016).

[335] J. Cepila, J.G. Contreras, M. Krelina, J.D. Tapia Takaki, «Mass dependence of vector meson photoproduction off protons and nuclei within the energy-dependent hot-spot model», *Nucl. Phys. B* **934**, 330 (2018).

[336] S.R. Klein, J. Nystrand, «Interference in Exclusive Vector Meson Production in Heavy Ion Collisions», *Phys. Rev. Lett.* **84**, 2330 (2000).

[337] STAR Collaboration (B.I. Abelev *et al.*), «Observation of Two-source Interference in the Photoproduction Reaction AuAu $\to$ AuAuρ^0», *Phys. Rev. Lett.* **102**, 112301 (2009).

[338] H1 Collaboration (V. Andreev *et al.*), «Measurement of exclusive $\pi^+\pi^-$ and ρ^0 meson photoproduction at HERA», *Eur. Phys. J. C* **80**, 1189 (2020), arXiv:2005.14471 [hep-ex].

[339] J.G. Contreras, J.D. Tapia Takaki, «Ultra-peripheral heavy-ion collisions at the LHC», *Int. J. Mod. Phys. A* **30**, 1542012 (2015).

[340] PHENIX Collaboration (S. Afanasiev *et al.*), «Photoproduction of J/ψ and of high mass e^+e^- in ultra-peripheral Au+Au collisions at $\sqrt{s_{NN}} = 200$ GeV», *Phys. Lett. B* **679**, 321 (2009).

[341] ALICE Collaboration (B. Abelev *et al.*), «Coherent J/ψ photoproduction in ultra-peripheral Pb–Pb collisions at $\sqrt{s_{NN}} = 2.76$ TeV», *Phys. Lett. B* **718**, 1273 (2013).

[342] ALICE Collaboration (E. Abbas *et al.*), «Charmonium and e^+e^- pair photoproduction at mid-rapidity in ultra-peripheral Pb–Pb collisions at $\sqrt{s_{NN}} = 2.76$ TeV», *Eur. Phys. J. C* **73**, 2617 (2013).

[343] ALICE Collaboration (S. Acharya *et al.*), «Coherent J/ψ photoproduction at forward rapidity in ultra-peripheral Pb–Pb collisions at $\sqrt{s_{NN}} = 5.02$ TeV», *Phys. Lett. B* **798**, 134926 (2019).

[344] ALICE Collaboration (S. Acharya *et al.*), «Coherent J/ψ and ψ' photoproduction at midrapidity in ultra-peripheral Pb–Pb collisions at $\sqrt{s_{NN}} = 5.02$ TeV», *Eur. Phys. J. C* **81**, 712 (2021).

[345] ALICE Collaboration (S. Acharya *et al.*), «First measurement of the $|t|$-dependence of coherent J/ψ photonuclear production», *Phys. Lett. B* **817**, 136280 (2021).

[346] CMS Collaboration (V. Khachatryan *et al.*), «Coherent J/ψ photoproduction in ultra-peripheral PbPb collisions at $\sqrt{s_{NN}} = 2.76$ TeV with the CMS experiment», *Phys. Lett. B* **772**, 489 (2017).

[347] LHCb Collaboration (R. Aaij *et al.*), «Study of coherent J/ψ production in lead–lead collisions at $\sqrt{s_{NN}} = 5$ TeV», *J. High Energy Phys.* **2022**, 117 (2022), arXiv:2107.03223 [hep-ex].

[348] V. Guzey, E. Kryshen, M. Strikman, M. Zhalov, «Nuclear suppression from coherent J/ψ photoproduction at the Large Hadron Collider», *Phys. Lett. B* **816**, 136202 (2021).

[349] D. Bendova, J. Cepila, J.G. Contreras, M. Matas, «Solution to the Balitsky–Kovchegov equation with the colinearly improved kernel including impact-parameter dependence», *Phys. Rev. D* **100**, 054015 (2019).

[350] ALICE Collaboration (J. Adam *et al.*), «Coherent $\psi(2S)$ photo-production in ultra-peripheral Pb–Pb collisions at $\sqrt{s_{NN}} = 2.76$ TeV», *Phys. Lett. B* **751**, 358 (2015).

[351] M. Krelina, J. Nemchik, R. Pasechnik, J. Cepila, «Spin rotation effects in diffractive electroproduction of heavy quarkonia», *Eur. Phys. J. C* **79**, 154 (2019).

[352] CMS Collaboration (R. Chudasama, D. Dutta), «Exclusive Photoproduction of Upsilon in pPb collisions with the CMS», *PoS* **(ICPAQGP2015)**, 042 (2017).

[353] ALICE Collaboration (J. Adam *et al.*), «Measurement of an Excess in the Yield of J/ψ at Very Low $p_\perp$ in Pb–Pb Collisions at $\sqrt{s_{NN}} = 2.76$ TeV», *Phys. Rev. Lett.* **116**, 222301 (2016).

[354] STAR Collaboration (J. Adam *et al.*), «Observation of Excess J/ψ Yield at Very Low Transverse Momenta in Au+Au Collisions at $\sqrt{s_{NN}} = 200$ GeV and U+U Collisions at $\sqrt{s_{NN}} = 193$ GeV», *Phys. Rev. Lett.* **123**, 132302 (2019).

[355] M. Kłusek-Gawenda, A. Szczurek, «Photoproduction of J/ψ mesons in peripheral and semicentral heavy ion collisions», *Phys. Rev. C* **93**, 044912 (2016).

[356] W. Shi, W. Zha, B. Chen, «Charmonium coherent photoproduction and hadroproduction with effects of quark gluon plasma», *Phys. Lett. B* **777**, 399 (2018).

[357] W. Zha *et al.*, «Coherent J/ψ photoproduction in hadronic heavy-ion collisions», *Phys. Rev. C* **97**, 044910 (2018).

[358] J.G. Contreras, «Gluon shadowing at small x from coherent J/ψ photoproduction data at energies available at the CERN Large Hadron Collider», *Phys. Rev. C* **96**, 015203 (2017).

[359] A.J. Baltz, S.R. Klein, J. Nystrand, «Coherent Vector-Meson Photoproduction with Nuclear Breakup in Relativistic Heavy-Ion Collisions», *Phys. Rev. Lett.* **89**, 012301 (2002).

[360] V. Guzey, M. Strikman, M. Zhalov, «Disentangling coherent and incoherent quasielastic J/ψ photoproduction on nuclei by neutron tagging in ultraperipheral ion collisions at the LHC», *Eur. Phys. J. C* **74**, 2942 (2014).

[361] M. Broz, J.G. Contreras, J.D. Tapia Takaki, «A generator of forward neutrons for ultra-peripheral collisions: nOOn», *Comput. Phys. Commun.* **253**, 107181 (2020), arXiv:1908.08263 [nucl-th].

[362] H. Mäntysaari, «Review of proton and nuclear shape fluctuations at high energy», *Rep. Prog. Phys.* **83**, 082201 (2020).

[363] H. Mäntysaari, B. Schenke, «Probing subnucleon scale fluctuations in ultraperipheral heavy ion collisions», *Phys. Lett. B* **772**, 832 (2017).

[364] J. Cepila, J.G. Contreras, M. Krelina, «Coherent and incoherent J/ψ photonuclear production in an energy-dependent hot-spot model», *Phys. Rev. C* **97**, 024901 (2018).

[365] W. Zha *et al.*, «Double-slit experiment at Fermi scale: Coherent photoproduction in heavy-ion collisions», *Phys. Rev. C* **99**, 061901 (2019).

[366] H. Xing, C. Zhang, J. Zhou, Y.-J. Zhou, «The cos 2ϕ azimuthal asymmetry in ρ^0 meson production in ultraperipheral heavy ion collisions», *J. High Energy Phys.* **2020**, 064 (2020).

[367] W. Zha *et al.*, «Exploring the double-slit interference with linearly polarized photons», *Phys. Rev. D* **103**, 033007 (2021).

[368] ATLAS Collaboration (A. Angerami), «Measurements of photo-nuclear jet production in Pb+Pb collisions with ATLAS», *Nucl. Phys. A* **967**, 277 (2017).

[369] S.R. Klein, J. Nystrand, R. Vogt, «Heavy quark photoproduction in ultraperipheral heavy ion collisions», *Phys. Rev. C* **66**, 044906 (2002).

[370] A. Adeluyi, C. Bertulani, «Gluon distributions in nuclei probed at the CERN Large Hadron Collider», *Phys. Rev. C* **84**, 024916 (2011).

[371] V.P. Gonçalves, G. Sampaio dos Santos, C.R. Sena, «Inclusive heavy quark photoproduction in pp, pPb and PbPb collisions at Run 2 LHC energies», *Nucl. Phys. A* **976**, 33 (2018).

[372] S.R. Klein, J. Nystrand, R. Vogt, «Photoproduction of top quarks in peripheral heavy ion collisions», *Eur. Phys. J. C* **21**, 563 (2001).

[373] T. Lappi, H. Mantysaari, «J/ψ production in ultraperipheral Pb+Pb and p+Pb collisions at energies available at the CERN Large Hadron Collider», *Phys. Rev. C* **87**, 032201 (2013).

[374] N. Armesto, A.H. Rezaeian, «Exclusive vector meson production at high energies and gluon saturation», *Phys. Rev. D* **90**, 054003 (2014).

[375] V.P. Goncalves, B.D. Moreira, F.S. Navarra, «Investigation of diffractive photoproduction of J/Ψ in hadronic collisions», *Phys. Rev. C* **90**, 015203 (2014).

[376] V.P. Gonçalves, B.D. Moreira, F.S. Navarra, «Exclusive Υ photoproduction in hadronic collisions at CERN LHC energies», *Phys. Lett. B* **742**, 172 (2015).

[377] H. Kowalski, L. Motyka, G. Watt, «Exclusive diffractive processes at HERA within the dipole picture», *Phys. Rev. D* **74**, 074016 (2006).

[378] B.E. Cox, J.R. Forshaw, R. Sandapen, «Diffractive Υ production at the LHC», *J. High Energy Phys.* **2009**, 034 (2009).

[379] B. Ducloué, T. Lappi, H. Mäntysaari, «Forward J/ψ production at high energy: centrality dependence and mean transverse momentum», *Phys. Rev. D* **94**, 074031 (2016).

[380] J. Cepila, J.G. Contreras, M. Matas, «Collinearly improved kernel suppresses Coulomb tails in the impact-parameter dependent Balitsky–Kovchegov evolution», *Phys. Rev. D* **99**, 051502 (2019).

[381] A. Arroyo Garcia, M. Hentschinski, K. Kutak, «QCD evolution based evidence for the onset of gluon saturation in exclusive photo-production of vector mesons», *Phys. Lett. B* **795**, 569 (2019).

[382] S.P. Jones, A.D. Martin, M.G. Ryskin, T. Teubner, «Predictions of exclusive $\psi(2S)$ production at the LHC», *J. Phys. G: Nucl. Part. Phys.* **41**, 055009 (2014).

[383] S.P. Jones, A.D. Martin, M.G. Ryskin, T. Teubner, «Probes of the small x gluon via exclusive J/ψ and Υ production at HERA and the LHC», *J. High Energy Phys.* **2013**, 085 (2013).

[384] S.P. Jones, A.D. Martin, M.G. Ryskin, T. Teubner, «Exclusive J/ψ production at the LHC in the $k_\perp$ factorization approach», *J. Phys. G: Nucl. Part. Phys.* **44**, 03LT01 (2017).

[385] A. Szczurek, A. Cisek, W. Schafer, «Some New Aspects of Quarkonia Production at the LHC», *Acta Phys. Pol. B* **48**, 1207 (2017).

[386] C.A. Flett, A.D. Martin, M.G. Ryskin, T. Teubner, «Very low x gluon density determined by LHCb exclusive J/ψ data», *Phys. Rev. D* **102**, 114021 (2020).

[387] K. Kutak, S. Sapeta, «Gluon saturation in dijet production in p–Pb collisions at Large Hadron Collider», *Phys. Rev. D* **86**, 094043 (2012).

[388] H1 Collaboration (C. Adloff *et al.*), «Diffractive photoproduction of $\psi(2S)$ mesons at HERA», *Phys. Lett. B* **541**, 251 (2002).

[389] K. Golec-Biernat, S. Sapeta, «Saturation model of DIS: an update», *J. High Energy Phys.* **2018**, 102 (2018).

[390] J. Cepila, J. Nemchik, M. Krelina, R. Pasechnik, «Theoretical uncertainties in exclusive electroproduction of S-wave heavy quarkonia», *Eur. Phys. J. C* **79**, 495 (2019).

[391] K.J. Golec-Biernat, M. Wüsthoff, «Saturation effects in deep inelastic scattering at low Q^2 and its implications on diffraction», *Phys. Rev. D* **59**, 014017 (1998).

[392] LHCb Collaboration (R. Aaij *et al.*), «Central exclusive production of J/ψ and $\psi(2S)$ mesons in pp collisions at $\sqrt{s} = 13$ TeV», *J. High Energy Phys.* **2018**, 167 (2018).

[393] M. Lomnitz, S. Klein, «Exclusive vector meson production at an electron-ion collider», *Phys. Rev. C* **99**, 015203 (2019).

[394] S.R. Klein, Y.-P. Xie, «Photoproduction of charged final states in ultraperipheral collisions and electroproduction at an electron-ion collider», *Phys. Rev. C* **100**, 024620 (2019).

[395] Joint Physics Analysis Center (M. Albaladejo *et al.*), «XYZ spectroscopy at electron–hadron facilities: Exclusive processes», *Phys. Rev. D* **102**, 114010 (2020).

[396] L. Lukaszuk, B. Nicolescu, «A Possible interpretation of pp rising total cross-sections», *Lett. Nuovo Cim.* **8**, 405 (1973).

[397] E. Martynov, B. Nicolescu, «Odderon effects in the differential cross-sections at Tevatron and LHC energies», *Eur. Phys. J. C* **79**, 461 (2019).

[398] A. Breakstone *et al.*, «A measurement of $\bar{p}p$ and pp Elastic Scattering in the Dip Region at $\sqrt{s} = 53$ GeV», *Phys. Rev. Lett.* **54**, 2180 (1985).

[399] S. Erhan *et al.*, «Comparison of $\bar{p}p$ and pp elastic scattering with $0.6 < t < 2.1$ GeV^2 at the CERN-ISR», *Phys. Lett. B* **152**, 131 (1985).

[400] UA4 Collaboration (D. Bernard *et al.*), «Large-t Elastic Scattering at the CERN SPS Collider at $\sqrt{s} = 630$ GeV», *Phys. Lett. B* **171**, 142 (1986).

[401] UA4 Collaboration (M. Bozzo *et al.*), «Elastic Scattering at the CERN SPS Collider Up to a Four Momentum Transfer of 1.55 GeV^2», *Phys. Lett. B* **155**, 197 (1985).

[402] E. Nagy *et al.*, «Measurements of Elastic Proton–Proton Scattering at Large Momentum Transfer at the CERN Intersecting Storage Rings», *Nucl. Phys. B* **150**, 221 (1979).

[403] D0 Collaboration (V.M. Abazov *et al.*), «Measurement of the differential cross section $\mathrm{d}\sigma/\mathrm{d}t$ in elastic $p\bar{p}$ scattering at $\sqrt{s} = 1.96$ TeV», *Phys. Rev. D* **86**, 012009 (2012).

[404] TOTEM Collaboration (G. Antchev *et al.*), «Elastic differential cross-section $\mathrm{d}\sigma/\mathrm{d}t$ at $\sqrt{s} = 2.76$ TeV and implications on the existence of a colourless C-odd three-gluon compound state», *Eur. Phys. J. C* **80**, 91 (2020).

[405] TOTEM Collaboration (G. Antchev *et al.*), «Proton–proton elastic scattering at the LHC energy of $\sqrt{s} = 7$ TeV», *Europhys. Lett.* **95**, 41001 (2011).

[406] TOTEM Collaboration (G. Antchev *et al.*), «Evidence for non-exponential elastic proton–proton differential cross-section at low $|t|$ and $\sqrt{s} = 8$ TeV by TOTEM», *Nucl. Phys. B* **899**, 527 (2015).

[407] TOTEM Collaboration (G. Antchev *et al.*), «Elastic differential cross-section measurement at $\sqrt{s} = 13$ TeV by TOTEM», *Eur. Phys. J. C* **79**, 861 (2019).

[408] TOTEM, D0 collaborations (V.M. Abazov *et al.*), «Odderon Exchange from Elastic Scattering Differences between pp and $p\bar{p}$ Data at 1.96 TeV and from pp Forward Scattering Measurements», *Phys. Rev. Lett.* **127**, 062003 (2021).

[409] TOTEM Collaboration (G. Antchev *et al.*), «First determination of the ρ parameter at $\sqrt{s} = 13$ TeV: probing the existence of a colourless C-odd three-gluon compound state», *Eur. Phys. J. C* **79**, 785 (2019).

[410] M. Boonekamp *et al.*, «FPMC: A Generator for forward physics», arXiv:1102.2531 [hep-ph].

[411] H. Jung, A. de Roeck (Eds.) «Proceedings of HERA and the LHC Workshop Series on the implications of HERA for LHC physics: 2006–2008», *DESY*, Hamburg, Germany 2009, arXiv:0903.3861 [hep-ph].

[412] C. Marquet, C. Royon, M. Saimpert, D. Werder, «Probing the Pomeron structure using dijets and γ+jet events at the LHC», *Phys. Rev. D* **88**, 074029 (2013).

[413] O. Kepka, C. Royon, «Search for exclusive events using the dijet mass fraction at the Tevatron», *Phys. Rev. D* **76**, 034012 (2007).

[414] C. Marquet *et al.*, «Diffractive di-jet production at the LHC with a Reggeon contribution», *Phys. Lett. B* **766**, 23 (2017).

[415] A. Chuinard, C. Royon, R. Staszewski, «Testing Pomeron flavour symmetry with diffractive W charge asymmetry», *J. High Energy Phys.* **2016**, 092 (2016).

[416] V.A. Khoze, A.D. Martin, M.G. Ryskin, «Prospects for new physics observations in diffractive processes at the LHC and Tevatron», *Eur. Phys. J. C* **23**, 311 (2002).

[417] CMS Collaboration (M. Albrow *et al.*), «The CMS Precision Proton Spectrometer at the HL-LHC — Expression of Interest», arXiv:2103.02752 [physics.ins-det].

[418] CMS and TOTEM collaborations, «CMS-TOTEM Precision Proton Spectrometer», CERN-LHCC-2014-021, TOTEM-TDR-003, CMS-TDR-13, 2014, https://cds.cern.ch/record/1753795

[419] CMS and TOTEM collaborations, «Proton reconstruction with the Precision Proton Spectrometer in Run 2», CMS Physics Analysis Summary, CMS-PAS-PRO-21-001, 2022.

[420] CMS and TOTEM collaborations, «Observation of proton-tagged, central (semi)exclusive production of high-mass lepton pairs in pp collisions at 13 TeV with the CMS-TOTEM precision proton spectrometer», *J. High Energy Phys.* **2018**, 153 (2018).

[421] CMS and TOTEM collaborations, «First search for exclusive diphoton production at high mass with tagged protons in proton–proton collisions at $\sqrt{s} = 13$ TeV», arXiv:2110.05916 [hep-ex].

[422] CMS and TOTEM collaborations, «Search for central exclusive production of top quark pairs in proton–proton collisions at $\sqrt{s} = 13$ TeV with tagged protons», CMS Physics Analysis Summary, 2022.

[423] CMS and TOTEM collaborations, «A search for new physics in central exclusive production using the missing mass technique with the CMS-TOTEM precision proton spectrometer», CMS Physics Analysis Summary, CERN-TOTEM-NOTE-2022-003, CMS-PAS-EXO-19-009, 2022.

[424] CMS and TOTEM collaborations, «Search for exclusive $\gamma\gamma \to WW$ and $\gamma\gamma \to ZZ$ production in final states with jets and forward protons», CMS Physics Analysis Summary, CERN-TOTEM-NOTE-2022-004, CMS-PAS-SMP-21-014, 2022.

[425] L. Adamczyk *et al.*, «Technical Design Report for the ATLAS Forward Proton Detector», CERN-LHCC-2015-009, ATLAS-TDR-024, 2015.

[426] ATLAS Collaboration (G. Aad *et al.*), «Observation and Measurement of Forward Proton Scattering in Association with Lepton Pairs Produced via the Photon Fusion Mechanism at ATLAS», *Phys. Rev. Lett.* **125**, 261801 (2020).

[427] J. de Favereau de Jeneret *et al.*, «High energy photon interactions at the LHC», arXiv:0908.2020 [hep-ph].

[428] L.D. Landau, «On the angular momentum of a system of two photons», *Dokl. Akad. Nauk SSSR* **60**, 207 (1948).

[429] C.-N. Yang, «Selection Rules for the Dematerialization of a Particle Into Two Photons», *Phys. Rev.* **77**, 242 (1950).

[430] D. d'Enterria, G.G. da Silveira, «Observing Light-by-Light Scattering at the Large Hadron Collider», *Phys. Rev. Lett.* **111**, 080405 (2013); *Erratum ibid.* **116**, 129901 (2016).

[431] C. Csáki, J. Hubisz, J. Terning, «Minimal model of a diphoton resonance: Production without gluon couplings», *Phys. Rev. D* **93**, 035002 (2016).

[432] L.A. Harland-Lang, V.A. Khoze, M.G. Ryskin, «The production of a diphoton resonance via photon–photon fusion», *J. High Energy Phys.* **2016**, 182 (2016).

[433] S. Fichet, G. von Gersdorff, C. Royon, «Measuring the Diphoton Coupling of a 750 GeV Resonance», *Phys. Rev. Lett.* **116**, 231801 (2016).

[434] C. Baldenegro, S. Fichet, G. von Gersdorff, C. Royon, «Searching for axion-like particles with proton tagging at the LHC», *J. High Energy Phys.* **2018**, 131 (2018).

[435] L. Beresford, J. Liu, «Search Strategy for Sleptons and Dark Matter Using the LHC as a Photon Collider», *Phys. Rev. Lett.* **123**, 141801 (2019).

[436] L.A. Harland-Lang, V.A. Khoze, M.G. Ryskin, M. Tasevsky, «LHC searches for Dark Matter in compressed mass scenarios: challenges in the forward proton mode», *J. High Energy Phys.* **2019**, 010 (2019).

[437] M.G. Albrow *et al.*, «The FP420 R&D Project: Higgs and New Physics with forward protons at the LHC», *J. Instrum.* **4**, T10001 (2009).

[438] V.A. Khoze, V.V. Khoze, D.L. Milne, M. G. Ryskin, «Hunting for QCD instantons at the LHC in events with large rapidity gaps», *Phys. Rev. D* **104**, 054013 (2021).

[439] V.A. Khoze, V.V. Khoze, D.L. Milne, M.G. Ryskin, «Central instanton production», *Phys. Rev. D* **105**, 036008 (2022).

[440] E. Shuryak, I. Zahed, «How to observe the QCD instanton/sphaleron processes at hadron colliders?», arXiv:2102.00256 [hep-ph].

[441] CMS Collaboration (S. Chatrchyan *et al.*), «Exclusive photon–photon production of muon pairs in proton–proton collisions at $\sqrt{s} = 7$ TeV», *J. High Energy Phys.* **2012**, 052 (2012).

[442] CMS Collaboration (S. Chatrchyan *et al.*), «Search for exclusive or semi-exclusive $\gamma\gamma$ production and observation of exclusive and semi-exclusive e^+e^- production in pp collisions at $\sqrt{s} = 7$ TeV», *J. High Energy Phys.* **2012**, 080 (2012).

[443] ATLAS Collaboration (G. Aad *et al.*), «Measurement of exclusive $\gamma\gamma \to \ell^+\ell^-$ production in proton–proton collisions at $\sqrt{s} = 7$ TeV with the ATLAS detector», *Phys. Lett. B* **749**, 242 (2015).

[444] ATLAS Collaboration (M. Aaboud *et al.*), «Measurement of the exclusive $\gamma\gamma \to \mu^+\mu^-$ process in proton–proton collisions at $\sqrt{s} = 13$ TeV with the ATLAS detector», *Phys. Lett. B* **777**, 303 (2018).

[445] CMS Collaboration (S. Chatrchyan *et al.*), «Study of exclusive two-photon production of W^+W^- in pp collisions at $\sqrt{s} = 7$ TeV and constraints on anomalous quartic gauge couplings», *J. High Energy Phys.* **2013**, 116 (2013).

[446] CMS Collaboration (V. Khachatryan *et al.*), «Evidence for exclusive $\gamma\gamma \to W^+W^-$ production and constraints on anomalous quartic gauge couplings in pp collisions at $\sqrt{s} = 7$ and 8 TeV», *J. High Energy Phys.* **2016**, 119 (2016).

[447] ATLAS Collaboration (M. Aaboud *et al.*), «Measurement of exclusive $\gamma\gamma \to W^+W^-$ production and search for exclusive Higgs boson production in pp collisions at $\sqrt{s} = 8$ TeV using the ATLAS detector», *Phys. Rev. D* **94**, 032011 (2016).

[448] V.A. Khoze, A.D. Martin, R. Orava, M.G. Ryskin, «Luminosity monitors at the LHC», *Eur. Phys. J. C* **19**, 313 (2001).

[449] A.G. Shamov, V.I. Telnov, «Precision luminosity measurement at LHC using two photon production of $\mu^+\mu^-$ pairs», *Nucl. Instrum. Methods Phys. Res. A* **494**, 51 (2002).

[450] L.A. Harland-Lang, M. Tasevsky, V.A. Khoze, M.G. Ryskin, «A new approach to modelling elastic and inelastic photon-initiated production at the LHC: SuperChic 4», *Eur. Phys. J. C* **80**, 925 (2020).

[451] V.M. Budnev, I.F. Ginzburg, G.V. Meledin, V.G. Serbo, «The two-photon particle production mechanism. Physical problems. Applications. Equivalent photon approximation», *Phys. Rep.* **15**, 181 (1975).

[452] G.G. da Silveira, V.P. Gonçalves, G.G. Vargas Veronez, «Nonexclusive particle production by $\gamma\gamma$ interactions in pp collisions at the LHC», *Phys. Rev. D* **103**, 074021 (2021).

[453] A.V. Manohar, P. Nason, G.P. Salam, G. Zanderighi, «The Photon Content of the Proton», *J. High Energy Phys.* **2017**, 046 (2017).

[454] L.A. Harland-Lang, A.D. Martin, R. Nathvani, R.S. Thorne, «Ad Lucem: QED Parton Distribution Functions in the MMHT Framework», *Eur. Phys. J. C* **79**, 811 (2019).

[455] NNPDF Collaboration (V. Bertone, S. Carrazza, N.P. Hartland, J. Rojo), «Illuminating the photon content of the proton within a global PDF analysis», *SciPost Phys.* **5**, 008 (2018).

[456] A. Manohar, P. Nason, G.P. Salam, G. Zanderighi, «How Bright is the Proton? A Precise Determination of the Photon Parton Distribution Function», *Phys. Rev. Lett.* **117**, 242002 (2016).

[457] M. Łuszczak, W. Schäfer, A. Szczurek, «Two-photon dilepton production in proton–proton collisions: two alternative approaches», *Phys. Rev. D* **93**, 074018 (2016).

[458] S. Bailey, L.A. Harland-Lang, «Modelling W^+W^- production with rapidity gaps at the LHC», *Phys. Rev. D* **105**, 093010 (2022), arXiv:2201.08403 [hep-ph].

[459] V.P. Gonçalves, D.E. Martins, M.S. Rangel, M. Tasevsky, «Top quark pair production in the exclusive processes at the LHC», *Phys. Rev. D* **102**, 074014 (2020).

[460] D.E. Martins, M. Tasevsky, V.P. Goncalves, «Challenging exclusive top quark pair production at low and high luminosity LHC», *Phys. Rev. D* **105**, 114002 (2022), arXiv:2202.01257 [hep-ph].

[461] V.A. Khoze, A.D. Martin, M. Ryskin, «Double diffractive processes in high resolution missing mass experiments at the Tevatron», *Eur. Phys. J. C* **19**, 477 (2001); *Erratum ibid.* **20**, 599 (2001).

[462] A. Kaidalov, V. Khoze, A. Martin, M. Ryskin, «Central exclusive diffractive production as a spin-parity analyser: from hadrons to Higgs», *Eur. Phys. J. C* **31**, 387 (2003).

[463] M. Albrow, A. Rostovtsev, «Searching for the Higgs at hadron colliders using the missing mass method», arXiv:hep-ph/0009336.

[464] D. d'Enterria, D.E. Martins, P. Rebello Teles, «Higgs boson production in photon–photon interactions with proton, light-ion, and heavy-ion beams at current and future colliders», *Phys. Rev. D* **101**, 033009 (2020).

[465] L.A. Harland-Lang, V.A. Khoze, M.G. Ryskin, W.J. Stirling, «Central exclusive production within the Durham model: a review», *Int. J. Mod. Phys. A* **29**, 1430031 (2014).

[466] CDF Collaboration (T. Aaltonen *et al.*), «Observation of Exclusive Gamma Gamma Production in $p\bar{p}$ Collisions at $\sqrt{s} = 1.96$ TeV», *Phys. Rev. Lett.* **108**, 081801 (2012).

[467] LHCb Collaboration (R. Aaij *et al.*), «Observation of charmonium pairs produced exclusively in pp collisions», *J. Phys. G: Nucl. Part. Phys.* **41**, 115002 (2014).

[468] LHCb Collaboration, «Central Exclusive Dimuon Production at $\sqrt{s} = 7$ TeV», LHCb-CONF-2011-022, CERN-LHCb-CONF-2011-022, 2011.

[469] L.A. Harland-Lang, V.A. Khoze, M.G. Ryskin, «Exclusive production of double J/ψ mesons in hadronic collisions», *J. Phys. G: Nucl. Part. Phys.* **42**, 055001 (2015).

[470] L.A. Harland-Lang, V.A. Khoze, M.G. Ryskin, «Exclusive physics at the LHC with SuperChic 2», *Eur. Phys. J. C* **76**, 9 (2016).

[471] CMS, TOTEM diffractive, forward physics working Group Collaboration (M. Albrow *et al.*), «Prospects for Diffractive and Forward Physics at the LHC», CERN-LHCC-2006-039, CMS-Note-2007-002, TOTEM-Note-2006-005.

[472] B.E. Cox, F.K. Loebinger, A. D. Pilkington, «Detecting Higgs bosons in the $b\bar{b}$ decay channel using forward proton tagging at the LHC», *J. High Energy Phys.* **2007**, 090 (2007).

[473] S. Heinemeyer *et al.*, «Studying the MSSM Higgs sector by forward proton tagging at the LHC», *Eur. Phys. J. C* **53**, 231 (2008).

[474] S. Heinemeyer *et al.*, «BSM Higgs Physics in the Exclusive Forward Proton Mode at the LHC», *Eur. Phys. J. C* **71**, 1649 (2011).

[475] M. Tasevsky, «Exclusive MSSM Higgs production at the LHC after Run I», *Eur. Phys. J. C* **73**, 2672 (2013).

[476] M. Boonekamp *et al.*, «Diffractive SUSY particle production at the LHC», *Phys. Rev. D* **73**, 115011 (2006).

[477] M. Tasevsky, «Diffractive Higgs boson production at LHC», *AIP Conf. Proc.* **828**, 401 (2006).

[478] A. Brandt, V. Juranek, A. Pal, M. Tasevsky, ATL-COM-PHYS-2010-337, 2010.

[479] B. Cox *et al.*, «Detecting the standard model Higgs boson in the WW decay channel using forward proton tagging at the LHC», *Eur. Phys. J. C* **45**, 401 (2006).

[480] V. Khoze, M. Ryskin, W. Stirling, «Diffractive $W + 2$ jet production: a background to exclusive $H \to WW$ production at hadron colliders», *Eur. Phys. J. C* **44**, 227 (2005).

[481] V. Kůs, private communication, Diploma thesis, private communication, 2015.

[482] J.R. Forshaw *et al.*, «Reinstating the 'no-lose' theorem for NMSSM Higgs discovery at the LHC», *J. High Energy Phys.* **2008**, 090 (2008).

[483] M. Chaichian *et al.*, «Searching for the triplet Higgs sector via central exclusive production at the LHC», *J. High Energy Phys.* **2009**, 011 (2009).

[484] M. Tasevsky, «Review of Central Exclusive Production of the Higgs Boson Beyond the Standard Model», *Int. J. Mod. Phys. A* **29**, 1446012 (2014).

[485] ATLAS Collaboration (G. Aad *et al.*), «Observation of a new particle in the search for the Standard Model Higgs boson with the ATLAS detector at the LHC», *Phys. Lett. B* **716**, 1 (2012).

[486] CMS Collaboration (S. Chatrchyan *et al.*), «Observation of a new boson at a mass of 125 GeV with the CMS experiment at the LHC», *Phys. Lett. B* **716**, 30 (2012).

[487] P. Bechtle *et al.*, «Probing the Standard Model with Higgs signal rates from the Tevatron, the LHC and a future ILC», *J. High Energy Phys.* **2014**, 039 (2014).

[488] K. Černý, T. Sýkora, M. Taševský, R. Žlebčík, «Performance studies of Time-of-Flight detectors at LHC», *J. Instrum.* **16**, P01030 (2021).

[489] ATLAS Collaboration, «Calibrating the b-Tag Efficiency and Mistag Rate in 35 pb^{-1} of Data with the ATLAS Detector», ATLAS-CONF-2011-089, 2011.

[490] CMS Collaboration (S. Chatrchyan *et al.*), «Identification of b-quark jets with the CMS experiment», *J. Instrum.* **8**, P04013 (2013).

[491] ATLAS Collaboration (G.J.A. Brown *et al.*), «Trigger strategies for central exclusive $H \to b\bar{b}$ studies with the AFP detector», ATL-DAQ-PUB-2009-006, ATL-COM-DAQ-2009-062, 2009.

[492] E. Bagnaschi *et al.*, «MSSM Higgs boson searches at the LHC: benchmark scenarios for Run 2 and beyond», *Eur. Phys. J. C* **79**, 617 (2019).

[493] CMS Collaboration (A.M. Sirunyan *et al.*), «Search for a standard model-like Higgs boson in the mass range between 70 and 110 GeV in the diphoton final state in proton–proton collisions at $\sqrt{s} = 8$ and 13 TeV», *Phys. Lett. B* **793**, 320 (2019).

[494] S. Heinemeyer, T. Stefaniak, «A Higgs Boson at 96 GeV?!», *PoS* **(CHARGED2018)**, 016 (2019).

[495] ATLAS Collaboration (G. Aad *et al.*), «Search for Heavy Higgs Bosons Decaying into Two Tau Leptons with the ATLAS Detector Using pp Collisions at $\sqrt{s} = 13$ TeV», *Phys. Rev. Lett.* **125**, 051801 (2020).

[496] S. Fichet *et al.*, «Probing new physics in diphoton production with proton tagging at the Large Hadron Collider», *Phys. Rev. D* **89**, 114004 (2014).

[497] S. Fichet *et al.*, «Light-by-light scattering with intact protons at the LHC: from Standard Model to new physics», *J. High Energy Phys.* **2015**, 165 (2015).

[498] P. Azzi *et al.*, «Report from Working Group 1: Standard Model Physics at the HL-LHC and HE-LHC», *CERN Yellow Rep. Monogr.* **7**, 1 (2019).

[499] C. Baldenegro, S. Fichet, G. von Gersdorff, C. Royon, «Probing the anomalous $\gamma\gamma\gamma Z$ coupling at the LHC with proton tagging», *J. High Energy Phys.* **2017**, 142 (2017).

[500] E. Chapon, C. Royon, O. Kepka, «Anomalous quartic $WW\gamma\gamma$, $ZZ\gamma\gamma$, and trilinear $WW\gamma$ couplings in two-photon processes at high luminosity at the LHC», *Phys. Rev. D* **81**, 074003 (2010).

[501] ATLAS Collaboration (G. Aad *et al.*), «Observation of photon-induced W^+W^- production in pp collisions at $\sqrt{s} = 13$ TeV using the ATLAS detector», *Phys. Lett. B* **816**, 136190 (2021).

[502] C. Baldenegro, G. Biagi, G. Legras, C. Royon, «Central exclusive production of W boson pairs in pp collisions at the LHC in hadronic and semi-leptonic final states», *J. High Energy Phys.* **2020**, 165 (2020).